Planning and Design for Intelligent and Secure Integration of Electric Vehicles into the Smart Grid

Mohammad Ekramul Kabir

A Thesis
In
The Department
of
Concordia Institute for Information Systems Engineering

Presented in Partial Fulfillment of the Requirements
For the Degree of
Doctor of Philosophy (Information and Systems Engineering)
Concordia University
Montréal, Québec, Canada

February 2021
© Mohammad Ekramul Kabir, 2021

CONCORDIA UNIVERSITY

SCHOOL OF GRADUATE STUDIES

This is to certify that the thesis prepared

By: Mohammad Ekramul Kabir

Entitled: Planning and Design for Intelligent and Secure Integration of Electric Vehicles into the Smart Grid

and submitted in partial fulfillment of the requirements for the degree of

Doctor Of Philosophy (Information and Systems Engineering)

complies with the regulations of the University and meets the accepted standards with respect to originality and quality.

Signed by the final examining committee:

_____ Chair
Dr. John Xiupu Zhang

_____ External Examiner
Dr. Hany.E.Z. Farag

_____ External to Program
Dr. M. Zahangir Kabir

_____ Examiner
Dr. Jun Yan

_____ Examiner
Dr. Walter Lucia

_____ Thesis Supervisor
Dr. Chadi Assi

Approved by _____
Dr. Mohammed Mannan, Graduate Program Director

4/15/2021 _____
Dr. Mourad Debbabi, Dean
Gina Cody School of Engineering and Computer Science

ABSTRACT

Planning and Design for Intelligent and Secure Integration of Electric Vehicles into the Smart Grid

Mohammad Ekramul Kabir, Ph.D.
Concordia University, 2021

The transition to electric vehicles (EVs) is gaining momentum around the world and government initiatives to accelerate this transition range from major tax exemptions, lower insurance payments to convenient parking incentives at shopping malls. The major drivers for this acceleration are the rising awareness by the public for maintaining a clean environment, reducing pollutant emissions, breaking dependencies on oil, as well as tapping into cleaner sources of energies. EVs acceptance however is hindered by several challenges; among them is their shorter driving range, slower charging rates, and the ubiquitous availability of charging locations, collectively contributing to higher anxieties for EVs drivers. Governments of developed countries as well as major car manufacturers are taking solid steps to address these challenges and set ambitious goals to make EVs the major transportation mode within few years. Consequently, a significant number of EVs is going to connect to the existing smart grid and hence, the load pattern is expecting a paradigm shift. This immense load will challenge the generation, transmission and distribution sector of the grid along with being a potential cyber-physical attack platform. To attain a graceful EV penetration for curtailing GHG emission, along with the socioeconomic initiatives, an extensive research is required, especially to mitigate the range anxiety and ameliorate the load congestion on the grid. As a consequence, to reduce the range anxiety, we present a two-stage solution to provision and dimension a DC fast charging station (CS) network for the anticipated energy demand and that minimizes the deployment cost while ensuring a certain quality of experience for charging e.g., acceptable waiting times and shorter travel distances to charge. This solution also maintains the voltage stability by considering the distribution grid capacity, determining transformers' rating to support peak demand of EV charging and adding a minimum number of voltage regulators based on the impact over the power distribution network. We propose, evaluate and

compare two CS network expansion models to determine a cost-effective and adaptive CSs provisioning solution that can efficiently expand the CS network to accommodate future EV charging and conventional load demands. Though an adequate fast charging network may assist to reduce the range anxiety and propel the EV market, catering this large number of EVs using fuel based conventional grid actually shifts the carbon footprint from the transportation sector to the power generation sector. As a consequence, green energy needs to be promoted for EV charging. However, the intermittent behavior of renewable energy (RE) generation challenges to maintain a RE based stand alone CS. In order to address this issue, we consider a photovoltaic (PV) powered station equipped with an energy storage system (ESS), which is assumed to be capable of assigning variable charging rates to different EVs to fulfill their demands inside their declared deadlines at minimum price. To ensure fairness, a charging rate dependent pricing mechanism is proposed to assure a higher price for enjoying a higher charging rate. The PV generation profile and future load request are forecasted at each time slot, to handle the respective uncertainties. Whatever, the energy source is green or not of a CS, a static CS cannot offer the flexibility to charge an EV at any place at any time especially for an emergency case. Fortunately, the bidirectional energy transferring capability between vehicles (i.e., vehicle to vehicle (V2V)) might be a solution to charge an EV at any place and at any time without leaning on a stationary CS. Hence, we assume a market where charging providers each has a number of charging trucks equipped with a larger battery and a fast charger to charge a number of EVs at some particular parking lots. We formulate an integer linear program (ILP) to maximize the number of served EVs by determining the optimal trajectory and schedule of each truck. Owing to its complexity, we implement Dantzig-Wolfe decomposition approach to solve this. However, to build a prolific EV charging ecosystem, all its entities (e.g., EVs, CSs and grid) have to be connected through a communication link and that unveils a new cyberphysical attack surface. As a consequence, we exploit the abundance of Electric Vehicles (EVs) to target the stability of the power grid by presenting a realistic coordinated switching attack that initiates inter-area oscillations between different areas of the power grid and assess the dire consequences over the power system. Finally, a back propagation neural network (BPNN) technique is used in a proposed framework to detect such switching attacks before being executed.

Acknowledgments

I would like to express my gratitude to all of those people, without whose support, it was not possible to complete my Ph.D. thesis.

Firstly, I am expressing my sincere gratitude to my Ph.D. supervisor Prof. Dr. Chadi Assi for his continuous support to my Ph.D. study and research. With his enormous patience, motivation, and immense knowledge, Dr. Assi has directly taught me how to do research to accomplish the Ph.D. goal. I could not have imagined having a better advisor and mentor for my Ph.D. study.

Besides my supervisor, I would like to thank my committee members, Dr. M. Zahangir Kabir, Dr. Walter Lucia, and Dr. Jun Yan for their insightful comments to enrich my research from various perspectives. My sincere appreciation also goes to Dr. Mohsen Ghafouri for his insightful comments on my research.

I want to convey my sincere gratitude to all of my colleagues in the research lab at Concordia University for their insightful discussion, handy guidance and for those time, I spent with them, that really means a lot to me. I have to mention especially the name of Dr. Mosaddek Hossain Kamal Tushar, my colleague, mentor and friend; without his encouragement, this journey was not possible.

I also want to thank all of my friends in Canada and back in Bangladesh for their continuous kind support.

I am expressing my gratitude to my mother, my sisters and to all my family members and relatives. They sacrificed a lot to help me reaching my destination.

Last but not the least, I thank to my wife Moshfeka Rahman and to my daughter Onumegha Tanzeehi Ekram. My wife is the person who was continuously encouraging me to pursue my Ph.D. and tolerating all my hot temper for last four years. Even being a Ph.D. student and obviously a busy mother of a kid, I do not know how she can manage all!!! And to Onumegha, Baba is sorry for being unable to give you proper time; I hope that one day you could understand that I did everything for you.

To my mother, the strongest person I have ever seen
To my father, who could not see even my elementary school graduation

Contents

List of Figures

List of Tables

Abbreviations

ANN	Artifical Neural Network
AVR	Automatic Voltage Regulator
BEV	Battery Electric Vehicle
BPNN	Back Propagation Neural Network
CLSF	Cheapest Location Select First
CMS	Central Management System
CS	Charging Station
CSDP	Charging Station Dimensioning and Placement
CSDP-WA	CSDP Workload Assignment
DWDM	Dantzig-Wolfe Decomposition Model
ERA	Eigenvalue Realization Algorithm
ESS	Energy Storage System
EV	Electrical Vehicle
FACTS	Flexible Alternating Current Transmission System
FFT	Fast Fourier Transform
GHG	Green House Gas
HEV	Hybrid Electric Vehicle
ICE	Internal Combustion Engine
IEA	International Energy Agency
ILP	Integer Linear Programming

IPCC	Intergovernmental Panel on Climate Change
LLSF	Largest Location Select First
LP	Linear Programming
METI	Ministry of Economy, Trade and Industry
MILP	Mixed Integer Linear Programming
ML	Machine Learning
NiMH	Nikel Metal Hybrid
OCPP	Open Charge Point Protocol
PHEV	Plug-in Hybrid Electric Vehicle
PMU	Phasor Measurement Unit
PV	Photo Voltaic
RBF	Radial Basis Function
RE	Renewable Energy
RSU	Road Side Unit
SCADA	Supervisory Control and Data Acquisition
SDSPF	Shortest Deadline Shortest Path First
SoC	State of Charge
SVD	Singular Value Decomposition
SVM	Support Vector Machine
SWSPF	Shortest Window Shortest Path First
V2G	Vehicle to Grid
V2V	Vehicle to Vehicle
VR	Voltage Regulator

Chapter 1

Introduction

1.1 Overview and Objectives

The recent proliferation in the market of Electric Vehicles (EVs) has been a direct response to recommendations by the Intergovernmental Panel on Climate Change (IPCC) which suggested a reduction in carbon emission by 45% from 2010 immediately, and 100% by 2050 [83]. This is encouraging since the transportation sector contributes 14% of the total global greenhouse gases (GHG) emissions [42] and its electrification is an important and critical step in the right direction. Esteeming this preeminence of smooth penetration of EVs, cities around the globe have set ambitious goals along with a set of initiatives as offering rebate and tax exemptions in EV purchasing, permitting EV drivers in using emergency lane, providing toll free facility, spreading public charging stations etc. to propel the EV market at a remarkable pace. According to the International Energy Agency (IEA) Global EV Outlook 2019 report[150], the number of electric vehicles worldwide surpassed 5 millions, representing an increase of more than double from the year before. Analyzing the current trend of EV adoption, two different studies ("New Policies Scenario" and "EV30@30 Scenario") anticipated that by 2030 the number of EVs on the road would reach

more than 30 million globally. To achieve such ambitious target, many countries have already put plans to ban fossil fueled vehicles, including Norway by 2025, Ireland, Netherlands and Slovenia by 2030, France and UK by 2040[150]. Following the global trend, Canadian EV market is also burgeoning. The second quarter report of Electric Vehicle News monitors a 214% yearly growth [123].

Following the preset high ambitious goal, the EV market is expanding in every day. Now the question is that *"does the current EV adoption rate stipulate to attain such targets"*? Right now, this is not possible to provide a conclusive answer of such a question, especially when Oslo, the EV capital has already ensured one third of its newly registered cars are EVs [84] and this percentage is only 1.2% in USA [83]. On the other hand, China expected the EV share to be 12%–15% by 2020, while the IEA projected it to be only 11.0% by 2030 [172], when in Netherlands, EV took 30.4% of total market share [114]. This uneven acceleration is also found in auto mobile industry. It was reported by CNN on March, 2018 that Tesla had thousands of customers lined up ready to buy a Model 3, but kept missing its production targets. Tesla set a weekly target for its production of 2,500 for the end of the third quarter of 2018 [57]. Conversely, in the same year Chevy Bolt could sold only 41% of the target in USA [87]. Hence, it can be deduced that the EV market is not going in a linear fashion and an extensive research is required to understand the market growth to make it even for attaining the global target.

1.1.1 Technological Challenges

Though the philosophy of penetrating a large number of EVs is to mitigate the carbon and GHG emission to ameliorate the alarming global warming, a mass awareness regarding this issue cannot be expected from the majority of our population. As a ramification, the market has to rely on the incentive policies and attractive EV

features. But the existing EV technology and offered incentives seem still inadequate for its smooth adoption. The higher purchasing price of battery-powered vehicles is considered one of the major sticking points in markets where EVs aren't subsidized, with electric cars significantly more expensive than their conventional counterparts. In Australia, for example, the BMW i3 EV starts from almost $70,000, while the same money would purchase much of the larger 3 Series range, including the 330e hybrid. In Paris Motor Show, Klaus Frohlich, the head of research and development of BMW identifies the battery sell price as the main barrier of inexpensive EV production [30]. As a ramification, the average battery capacity is incompetent to provide significant mileage.

Consequently, this lower mileage of EVs increases the drivers' range anxiety and that incurs them to switch to EVs. As a revolutionary increment in battery capacity might not be possible (especially in cheaper price), a wide spread charging infrastructure can be treated as a solution to ameliorate the range anxiety. An adequate and strategical placement of public EV charging station (CS) can make opportunity to charge EVs at any where, when at present more than 80% of EVs have to charge at home [35]. But, spreading public CS network creates a chicken-egg dilemma due to the higher initial investment cost in terms of money and time. Should we expand the charging network to accelerate EV market or an expanded EV market encourages to spread the network?

Moreover, the availability of charging opportunity may not be able to invigorate the EV market due to the longer required time of EV charging. At present, three types of chargers are available e.g. level 1 & level 2 AC chargers and level 3 DC fast chargers (specification details will be discussed in section 2). Level 1 chargers require 8-16 hours to charge an EV battery when 4 to 8 hours is needed by level 2. Even, the fast charger needs 20-30 minutes to reach 80% SoC (state of charge) of an EV

battery. As a ramification, the charging time cannot be comparable with refuelling a gasoline based car and public CS network cannot replicate the widely researched gas station network. Hence, the average waiting time at a CS might be very long.

On the other hand, an enormous EV penetration asks for a mammoth energy demand and over burdens the power distribution network. A study made in Lisbon stated the concurrent attempt of 10% of current EVs at peak time may make a significant degradation in voltage level of Portuguese power distribution network [100]. Beside this, feeding EVs by fuel based electricity plant actually shifts the carbon foot print from the transportation sector to the power generation sector. Hence, incorporating green energy along with a smart charging mechanism might be an important key to accelerate the market.

The last but not the least major concern is that since, an interconnected EV charging ecosystem is inevitable for sharing information among all associated entities (e.g., EVs, CSs, central management system (CMS), grid etc.) for the smart and efficient management of EV charging, this communication link is going to unveil a new cyber-physical attack surface. By comprising the communication link, an attacker may deploy different attack strategies which might have dire consequences on EVs, CS providers or to the grid stability [16].

In order to address these issues, we overview the state of art and research challenges of introducing the avid, smart and secured mechanism of EV charging to reduce range anxiety, minimize waiting time and charging price and curtailing the burden over the power distribution network. An efficient and smart charging scheduling, demand based energy allocation and dynamic energy pricing policy, strategical placement of CSs, introducing renewable energy in EV charging, implementing bi-direction energy transfer capability of EVs etc. can be implemented to overcome these closely related barriers to ensure a graceful EV penetration.

1.1.2 Thesis Objectives

This research work will investigate and address significant hurdles which hinder the EV adoption rate and may impose a new cyber-physical threats to the smart grid. Consequently, the technical, commercial, and residential community will benefit significantly. In particular, this effort will:

- Study on the major obstacles which hinder people from adopting EV and determine the range anxiety as one of the major reasons.
- Design an adequate CS network to mitigate the range anxiety and propose its efficient expansion method.
- Investigate other auxiliary sources for EV charging to reduce the burden of the grid from catering a large number of EVs and curtail the GHG emission.
- Investigate the IoT enabled EV charging ecosystem as a possible cyber-physical attack surface mainly to create inter area oscillation in transmission link.
- Devise the vulnerability of widely used charging protocol, open charge point protocol (OCPP) and propose neural network based detection mechanisms to detect switching attack initiated from EV charging ecosystem.

This thesis work mainly starts to determine solutions for reducing the range anxiety while identifying this anxiety as the major hindrance of the smooth penetration of EVs. As a consequence, provisioning of a DC fast charging network for an urban area like Montreal is addressed to mitigate the range anxiety and an efficient expansion method is also proposed for this network to meet the future extended demand.

Though expanding the charging network might be a preliminary solution to attract user to switch to EVs, this will impose a huge load to the grid and actually shifts the carbon footprint from the transportation sector to the power generation sector.

As a consequence, auxiliary and green sources need to be integrated for charging EVs. Hence, a photovoltaic (PV) based stand alone charging station (CS) is assumed and a smart management system is proposed to handle the intermittent behavior of PV generation and EV arrival uncertainty, while an EV can enjoy quicker charge by paying more without violating others' deadlines.

Since, the bidirectional energy transfer capability of EV makes this attractive to compensate energy demand of grid (i.e., vehicle to grid (V2G)) or charge an EV at any place and in any time (vehicle to vehicle (V2V)), by exploiting the V2V capability, an EV can be charged at any time any place without depending on the static CS and that could be a solution for emergency charging requirement. Hence, a scheduling and routing problem is addressed for an assumed company which has a set of trucks equipped with larger battery and vehicle to vehicle (V2V) enabled fast charger to charge an EV.

However, the success of smart charging relies on the real time data sharing among the entities of the charging ecosystem (e.g., EVs, CSs, grid etc.). As a ramification, inter connected charging ecosystem could be a new attack surface to the grid, especially while the widely used charging protocol open charge point protocol (OCPP) is still not matured enough [16]. Hence, the EV charging ecosystem is investigated as a potential surface of switching attack to the transmission link and neural network based detection algorithm is proposed to detect such attack attempts even before the attack being executed.

1.2 Problem Statement and Motivation

To curtail the carbon emission from the transportation sector, a prompt transportation electrification has no alternative. Hence, to attain a large scale EV adoption, a DC fast charger network is provisioned to mitigate the EV drivers' range anxiety,

while to lessen the dependency on the conventional fuel based power grid for EV charging, auxiliary charging facilities are encouraged. As a consequence, a smart charging mechanism is proposed for a PV based stand alone CS, while to dispense a charging facility at any place at any time, an efficient routing and scheduling algorithm is developed for a set of V2V enabled charging trucks. Since, the success of a smart charging mechanism relies on an interconnected system, the cyber-physical vulnerability is assessed in term of switching attack and a detection methodology is proposed accordingly. The motivation and problem statements are as follows.

1.2.1 Demand-Aware Provisioning of Electric Vehicles Fast Charging Infrastructure

The concept of smart city strives for greener technology to reduce carbon emission to ameliorate the global warming. Following this footprint, the transportation sector is experiencing a paradigm shift and the transition to EVs has prodigious plausibility in reducing carbon emission. However, the anticipated EV penetration is hindered by several challenges, among them are their shorter driving range, slower charging rate and the lack of ubiquitous availability of charging locations, which collectively contribute to range anxieties for EVs drivers. Meanwhile, the expected immense EV load onto the power distribution network may degrade the voltage stability. To reduce the range anxiety, we present a two-stage solution to provision and dimension a DC fast charging station (CS) network for the anticipated energy demand and that minimizes the deployment cost while ensuring a certain quality of experience for charging e.g., acceptable waiting times and shorter travel distances to charge. This solution also maintains the voltage stability by considering the distribution grid capacity, determining transformers' rating to support peak demand of EV charging and adding a minimum number of voltage regulators based on the impact over the

power distribution network. We propose, evaluate and compare two CS network expansion models to determine a cost-effective and adaptive CSs provisioning solution that can efficiently expand the CS network to accommodate future EV charging and conventional load demands. We also propose two heuristic methods for this expansion method and compare our solution with them.

1.2.2 Optimal Scheduling of EV Charging at a Solar Power Based Charging Station

Though the transition to EVs has a prodigious plausibility in reducing GHG, EVs acceptance is however hindered by several challenges, among them is their avidity for quicker charging at lower price. Moreover, to attain the goal of curtailing GHG emission, renewable energy (RE) needs to be promoted in EV charging. As a consequence, we consider a photovoltaic (PV) powered station equipped with an energy storage system (ESS), which is assumed to be capable of assigning variable charging rates to different EVs to fulfill their demands inside their declared deadlines at minimum price. To ensure fairness, a charging rate dependent pricing mechanism is proposed to assure a higher price for enjoying a higher charging rate. The PV generation profile and future load request are forecasted at each time slot, to handle the respective uncertainty. An integer linear programming (ILP) based centralized system is first proposed to minimize the charging price per EV. Due to the larger computational time, we subsequently present two game theoretic algorithms, i.e., game 1 and game 2. In game 1, players are oblivious of upcoming charging requests, whereas in game 2, players consider the future anticipated load to select their charging strategies. The games are shown to converge to a Nash equilibrium and game 2 is capable of providing optimal solution.

1.2.3 Joint Routing and Scheduling of Mobile Charging Infrastructure for V2V Energy Transfer

Though an adequate charging infrastructure advocates to ameliorate the range anxiety to propel the disparaged EV market, the high initial installation cost, requirement of suitable places and the anticipated immense load on the grid during peak times hinder to elongate the CS network, especially in urban areas. Fortunately, the bidirectional energy transferring capability between vehicles (i.e., V2V) may act as an auxiliary solution to charge an EV at any place and at any time without leaning on a stationary charging infrastructure. Hence, we assume a market where charging providers each has a number of charging trucks equipped with a larger battery and a fast charger to charge a number of EVs at some particular parking lots. A provider intends to maximize the served number of EVs using its limited number of charging trucks, when an EV should be considered as served only if it would be fully charged during its declared charging window. All charging requests are assumed to be received by an agent which provisions a route and schedule for each charging truck and all trucks should return to the depot after serving EVs. We formulate this combinatorially hard problem as an integer linear program (ILP) to maximize the number of served EVs by determining the optimal trajectory of each truck. Owing to its complexity, we present a solution methodology by decomposing the problem using Dantzig-Wolfe decomposition approach; we divide the problem into one master problem and a set of pricing problems (one for each EV) and achieve the solution iteratively. Though the solution achieved from the decomposition might not be optimal, it is faster to be applicable in practice. We also compare the performance with two heuristic algorithms and report on the collected results.

1.2.4 Attack Model and Detection Methodology for a Coordinated Switching Attack Initiated from EV Charging Ecosystem

Since the inter connected EV charging ecosystem could act as a new cyber-physical attack platform, we exploit the abundance of EVs to target the stability of the power grid. Through a cyber attack that compromises a lot of available EVs and their charging infrastructure, we present a realistic coordinated switching attack that initiates inter-area oscillations between different areas of the power grid. The threat model as well as linearized state-space representation of the grid are formulated to illustrate possible consequences of the attack. Two variations of switching attack are considered, namely, switching of EV charging and discharging power into grid. Moreover, two possible attack strategies are also considered (i) using an insider to reveal the accurate system parameters and (ii) using reconnaissance activities in the absence of the grid parameters. In the former strategy, the system equations are used to compute the required knowledge to launch the attack. However, a stealthy system identification technique, which is tailored based on Eigenvalue Realization Algorithm (ERA), is proposed in latter strategy to calculate the required data for attack execution. The two-area Kundur, 39-Bus New England and the Australian 5-area power grids are used to demonstrate the attack strategies and their consequences. The collected results demonstrate that by manipulation of EV charging ecosystem and launching a coordinated switching attack to those portions of load, inter-area oscillations can be initiated. Finally, neural network based technique is used in a proposed framework to detect such switching attacks before being executed.

1.3 Thesis Contributions

The main contributions of the thesis are summarized as follows:

- To reduce the range anxiety, we design a DC fast charger network for an urban area at minimum installation cost (detail discussion in chapter 3). Our designed network ensures a minimum quality of service to EV users in terms of tolerable waiting time and shorter detour distance and this design is also capable in maintaining the voltage level of the distribution grid. Moreover, we also propose two different expansion models for this CS network to meet the upcoming EV growth and compare their efficiencies to determine the better one.

- To accelerate the pace of attaining the goal of zero emission transportation system, we design a smart management system for a PV based standalone CS (detail discussion in chapter 4). We propose a quadratic cost function, which ensures that an EV user can enjoy a faster charging only by paying more without violating the other EVs' deadline. A time slotted system is assumed and to minimize the aberration in PV generation and load prediction, the system predicts these two before every time slot. An ILP is formed and solved the problem centrally to minimize the charging cost. Due to the longer computational time of the centralized system, two types of non-cooperative game theory based algorithms are applied. This helps to attain a quicker and even optimal solution.

- To attain the flexibility in EV charging, we formulate an ILP to maximize the served number of EVs for an assumed company which has a number of charging trucks equipped with larger battery and V2V enabled fast charger to charge EVs at any time any place (detail discussion in chapter 5). The ILP decides the route and schedule of each trucks to maximize the served number of EVs.

However, this problem seems to be a multiple travelling salesmen problem and not computationally efficient for a large number of trucks. Hence, we implement Dantzig-Wolfe decomposition method to attain a quicker solution.

- Since, the success of smart charging relies on the inter connectivity among the entities of EV charging ecosystem, this becomes a new cyber physical attack surface to the grid. Hence, we investigate the competency of compromised EV charging ecosystem to mimic switching attack for generating inter area oscillation between two weakly tied power generation area (detail discussion in chapter 6). Two different types of attack strategies are studied on three different power system benchmarks to depict the competency of this ecosystem as a switching attack source.

- To detect the switching attack initiated from compromised EV charging network, we develop a neural network based algorithm in chapter 6. This algorithm would be hosted by a central management system (CMS) to observe the incoming charging/discharging requests' behavior and identify the malicious one. By implementing back propagation neural network (BPNN), a filter is designed to classify these incoming messages and identify coordinated switching attack attempts before being executed.

1.4 Thesis Outline

The remainder of the thesis is organized as following. Chapter 2 presents the related works. The design of a DC fast charger network for EV charging and its expansion procedures for being compatible with the upcoming increased EV load is described in Chapter 3. A smart management system is developed for a PV powered stand alone CS to minimize the charging price for EVs in Chapter 4, while a joint routing

and scheduling problem is addressed for a set of V2V enabled charging trucks to maximize the number of served EVs in Chapter 5. In Chapter 6, the competency of compromised EV charging infrastructures in mimicking switching attack to initiate an inter area oscillation on the transmission link along with a neural network based detection mechanism are presented. Chapter 7 concludes the thesis and depicts the future research directions.

Chapter 2

Literature Review and Preliminaries

In this chapter, we first highlight the preliminary ideas and technologies related with EV industry and then a detailed literature review is presented to depict the significance and novelties of the thesis objectives as mentioned in Chapter 1.

2.1 Preliminaries

2.1.1 History and Evolution of EV[1]

Gasoline based internal combustion engine (ICE) car has dominated the transportation sector for last one century. As a consequence, the concept of electric car seems a new idea; surprisingly this is not. Man intended to apply electrical energy to drive vehicles is pretty older than conventional gasoline based vehicles and it has started the journey since 1828. During this long journey, EV experienced a significant adaptability to get the modern form. In this subsection, we highlight the evolution process

[1]This subsection is based on [2].

of EV.

Figure 2.1: Thomas-Parker Commercial EV in 1895 [2].

Figure 2.2: Tesla Model 3 in 2020 [2].

- **Early rise of EV (1828-1883):** Since 1820, human started to introduce electrical energy to drive vehicles and at that very early age, most of the attempts were in too small scale. In 1828, Anyos Jedlik first invented an electric motor to drive a small car and Professor Sibrandus Stratingh designed a non rechargeable battery car in 1834. In 1837, Robert Davidson exhibited his galvanic cell powered car named Galvanic in the Royal Schotish Art Exhibition. Due to the non rechargeable battery, early stage cars needed battery replacement frequently and hence, failed to be popular. The invention of rechargeable battery cell in 1859 changed the scenario and finally people could think about the commercialization of battery driven vehicles.

- **First era of commercialization (1882-1920):**

  After a pile of unsuccessful attempts, finally in 1884, Thomas Parker successfully designed a practical electricity powered vehicle. He established his own company in 1882 at London and that Elwell-Parker company had launched its commercial product in 1888. Almost at the same time, France and Germany were also designing and modifying their own electric cars, but the intention of Thomas

Parker made him the pioneer. His intention was to find an energy efficient car accompanied with reducing environment pollution. After that, EV market got an enormous pace especially at Europe and USA. In 1990, London added her first electric taxi service named "Humming Bird" and by 1912, 32% of total cars in USA were electrified. Even, the world renowned scientist, Thomas Alva Edison designed a new car. This era was sustained till 1920 and after that the innovation of internal combustion engine (ICE) and the avidity of fossil fuel replaced electric car by gasoline based car.

- **Dark age of EV (1920-1960):**

  The innovation of internal combustion engine (ICE) opened a new door to design heavy and more powerful vehicles. And the same time oil was discovered in different parts of the world. Consequently, transportation sector experienced a paradigm shift and the rising of electric car faced a sudden declination. During this period, gasoline based vehicles became mammoth not only as the sense of market domination but also for environmental pollution. But the awareness to the environment and fossil fuel scarcity brought back the electric vehicle concept within few decades.

- **Revival of Interest (1960-2000):**

  The gasoline powered vehicles rapidly replaced EVs and expanded very quickly. Specially, after the second world war, the gasoline car market leaped incredibly and consequently raised the fuel scarcity. The political conflict for oil through the world also ignited the market. Hence, researchers began interested to curtail the oil dependency and in 1960, a hybrid car was modeled; that could recharge the battery from its own motion. By the same time, the plausibility of renewable sources were investigated and that created the concept of green transportation.

Even, Nasa sent a solar powered car at moon in 1973. These initiatives actually lead us to the modern era of EVs.

- **Modern age of EV (2000-):** In the new century, EV starts a new journey. The increasing interest in tapping green sources of energy to reduce GHG emission triggered the EV research and auto mobile companies grab the opportunity. Hence, again a paradigm shift is expected in the transportation sector. The modern EV started its journey with a hybrid concept where the primary energy source is gasoline, but it can use self generated electricity as a backup. The revolutionary improvement of battery technology by last few decades shifts the interest to pure EV. Fig.2.3 depicts the significant growth of EV market and full electric EV or battery EV (BEV) is increasing its share in the market in every day. Before discussing about the battery technology and related mileage of EVs, a brief description of major three classifications of EVs are presented below.

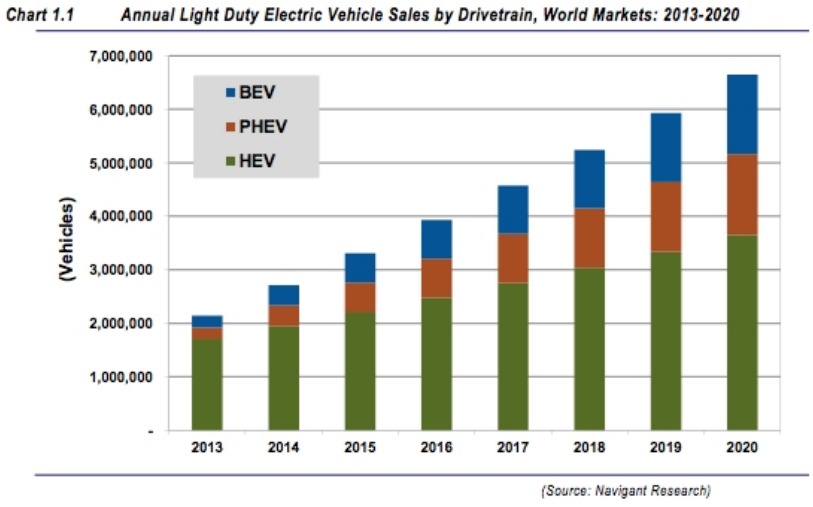

Figure 2.3: Global EV Market [101].

1. **Hybrid Electric Vehicle (HEV):** A total and sudden transition from fuel dependency to electricity was not expected and possible at the very beginning.

Hence, the first generation of EVs were mainly hybrid in nature. HEV consists of two types of engines. The primary engine is energized by gasoline and the backup one is driven by electricity. The main draw back of this sort of vehicle is not to charge the battery by any external source. The battery takes the charge from car's movement specially during the accelerating and breaking. Though this sort of EV is loosing its market share in every day, still it is significant in amount due to its good mileage. As an example, using one gallon of gasoline, Honda Accord HEV runs 47 mile, while it is just 30 mile for a pure gasoline Honda Accord.

2. **Plug-in Hybrid Electric Vehicle (PHEV):** For the first time, electric engine has become the primary engine in PHEV. The external charging capability of PHEV reduces the oil dependency. The gasoline engine kicks in only after the draining out the battery. A Chevy Bolt can run 38 miles before kicking in its gasoline engine. Moreover, the wide spread network of gas stations helps PHEV to overcome the range anxiety. But, obviously it does not serve the green transportation concept. As a consequence, full electric i.e. battery electric vehicle (BEV) should be the future of EVs.

3. **Battery Electric Vehicle (BEV):** BEV is the latest and the ultimate version of EVs. In many literature, the term EV actually stands for BEV. BEVs run exclusively on electricity via on-board batteries and those are charged by plugging into an outlet or charging station. Hence, BEV requires a comparatively large battery pack enabling of charging from external sources (power grid, renewable sources, other EVs etc.). The BEVs on the market today generally go around 60 to 80 miles per charge, though a Tesla can travel over 200 miles on a single charge. A recent UCS survey found that a BEV range of 60 miles would fit the weekday driving needs of 69 percent of U.S. drivers. As charging time is long

and charging facility through the locality is still in under progress, the main challenges of BEV is the driver's range anxiety along with a longer charging time. Moreover, the only dependency on electricity of a large number of EVs is going to challenge the power generation and distribution sector.

2.1.2 On-board EV Battery & Mileage

EV is struggling for the optimal choice of on-board battery since the very early age. Before inventing rechargeable lead-acid battery in 1859 [2], the early pilot projects required rapid replacement of batteries and that was not practical. Though lead-acid battery alleviated the rapid replacement problem, it was unable to provide a better mileage and higher speed. For a better mileage and higher speed, a larger battery pack needs to be installed and that causes to be the car over weighted and very expensive. These drawbacks mainly guided the ICE cars to grab the transportation market. And these challenges are still exist in the real.

The battery technology has experienced a revolutionary leap from the last two decades, especially when US Department of Energy invested 2.4 billion dollar in manufacturing and developing of batteries for EVs [28]. European Commission and governmental organizations in Europe and Japanese Ministry of Economy, Trade and Industry (METI) have also been continuously supporting the R&D activities in advanced batteries. BYD, Lishen, and Chunlan have obtained strong subsidy supports from the Chinese government for its research and manufacturing of advanced batteries and electric vehicles [167]. Currently, Li-ion and NiMH (Nikel metal hybrid) battery technology dominates the EV on board technology. The continuous development of battery industry shows her direct impact on EV evolution i.e. battery size is increased, price is decreased and hence EV becomes capable in providing more mileage.

- **Battery Capacity, Life Time and Price:** The rapid improvement of battery technology increases the battery capacity from few kWh to almost 100 kWh. Tesla provides a battery pack having 85 kWh capacity while Nisan Leaf provides up to 60 kWh . It is obvious that a larger battery pack can provide higher mileage. But as we mentioned earlier battery size is constrained by weight and expense. Tony Posawatz, the chief executive of Fisker Automotive indicated this fact and insisted to maximize the overall trade off instead of only emphasizing on the battery size [17]. Hence, regarding the updated technology, still the average on-board battery capacity lies between 16 kWh to 36 kWh. The regular charging and discharging causes a regular degradation of the performance and usually the manufacturers offer an average life span of 8 years having with a 100,000 mileage. The battery price depends on the capacity. According to the current market, Tesla battery requires $190 for each kWh while for Chevy Bolt, it is $205. The life span of a battery directly depends upon the charging mechanism and hence, chargers using in EV charging attracts the researchers' attention not only for charging time but also for battery performance.

- **Mileage of EVs:**

  From the very beginning of the journey, EVs are struggling to meet the preferred mileage. Obviously, there are few exceptions e.g. Tesla model s provides 265 mileage while it is 499 mile for model 3. This tremendous mileage is one of the major reasons of its higher price. Mass adoption of EVs by investing such large amount of money cannot be expected. Hence, to make EVs affordable, automobile companies cannot expand the battery capacity in a dramatic manner.

  According to a US research [86], an average trip length is not more than 65 miles and hence, 95% of users can complete their trip without recharging their

battery. But in reality, the potential consumers of EVs intend to compare the mileage with gasoline based cars. And most of the EVs are still far beyond the average mileage of an ICE car.

2.1.3 EV Battery Chargers

The utmost challenge of smooth EV penetration is the small EV battery size and shorter mileage. As a ramification, an EV needs a frequent charging and this charging procedure is a time consuming one. Here, we are going to elaborate the different types of chargers along with the charging behaviours of EV users and their consequences.

- **Type of EV Chargers**

Table 1 – Summary comparison of charging levels

	Level 1	Level 2	Fast charge
Voltage	120 V	208 or 240 V	200 to 450 V
Current type	AC	AC	DC
Useful power	1.4 kW	7.2 kW	50 kW
Maximum output	1.9 kW	19.2 kW	150 kW
Charging time[a]	12 h[a]	3 h[a]	20 min[b]
Connector	J1772	J1772	J1772 Combo, CHAdeMO and Supercharger

a. Charging time of a completely discharged 16-kWh battery at useful power.
b. Charging time to 80% charge, i.e., 12 kWh. Fast charging cannot be sustained to a full charge.

Figure 2.4: Different types of EV chargers [115].

Three types of chargers are now available for EV charging and a brief specification is depicted in Fig.2.4.

1. **Level 1 charger:** Usually auto mobile companies provide a level 1 charger as an on-board charger with the EV. This operates in a 120 V AC line. This sort of chargers takes average 12-16 hr to charge a battery. Hence, level 1 charger is popular as residential load. Most of the users plug in

their EVs with the installed level 1 charger after coming back at home with an intention of charging for the whole night.

2. **Level 2 charger:** To ameliorate the too long charging time taken by level 1 charger, a higher rating AC-DC charger is introduced known level 2. Level 2 can operate from 208 V to 240 V to ensure a full charge by 3-4 hr. This class is widely used in commercial places (e.g. parking lot, shopping mall, office house etc.), but due to the recent decreased cost, installing a level 2 charger at home is becoming popular.
3. **Level 3 charger:** This charger is operated with high voltage DC power. Using DC source eliminates the conversion step here and the higher power rating makes the charging very fast. That is why level 3 charger is also known as DC fast charger. Usually within 20 min a level 3 charger can charge 80% of the battery (after 80% the charging process gets slower).

- **Charging Behavior** In practice, most of the EV users charge their EVs at home. INSIDEEVs made an survey[1] among 3,247 EVs regarding their charging behavior and 81% of them usually do their charge at home. This finding is fairly close with the assumption of another research [35], where they claim more than 80% EVs charge at home. Their finding is that most of the EV users do not prefer charging at public CS for a higher uncertainty of outlets availability and higher waiting time even they prefer to charge at a quicker fashion.

  According to Fig.2.5, most of the EVs prefer to use level 2 charger. Still this level 2 charger is mainly used at public places. The lack of public charging infrastructure and the anticipated larger waiting time prevent them in using this facility in regular manner. Hence, strategical placement of adequate public charging infrastructure catches the attention to spread out the charging facility. On the other hand, the declining price of level 2 chargers insists to install this at

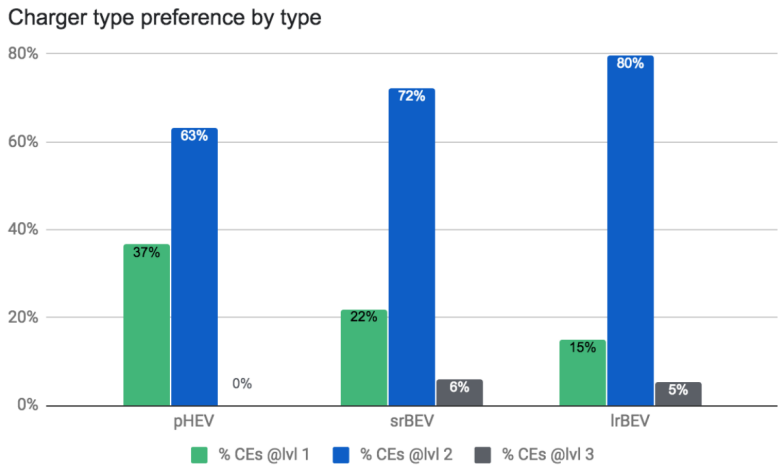

Figure 2.5: Charger preference [124].

home. As a ramification residential energy demand is supposed to be increased significantly to challenge the existing distribution network.

2.1.4 Bidirectional Energy Transfer Capability

On the other hand, the large penetration of EVs is supposed to be a burden for the power distribution network, especially when a study at Portugal stated that the concurrent attempt of charging by only 10% of total EVs at peak time may collapse the distribution network [100]. However, EV itself has the ability to mitigate this impact due to the bidirectional energy transfer capability. The concept is very straight forward; an EV can charge its battery at off peak time at lower energy price and sell it at peak hour to make some revenue. The concept of EV allows it to sell energy to any load that is called V2X. Here, we are going to introduce the vehicle to grid (V2G) and vehicle to vehicle (V2V) energy transfer.

- **V2G:** V2G allows an EV to sell energy directly to the distribution grid. The unprecedented load by EVs may create new peak demand too high to be attainable. Along with dynamic energy pricing, demand response resource allocation,

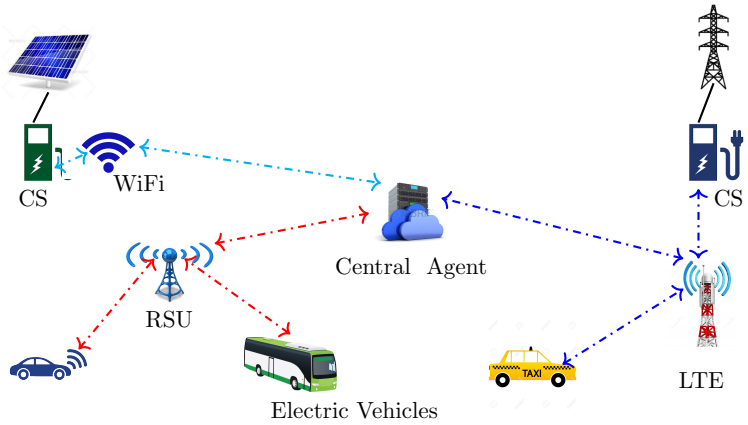

Figure 2.6: Communication Network for EV Charging.

day ahead energy management, V2G is becoming a popular solution for the peak shaving. Germany government has already permitted Nisan Leaf to sell energy in V2G environment commercially [141].

- **V2V:** The concept of V2V is the direct transfer of energy from one EV to other. Beside peak shaving, it may also help to ameliorate the range anxiety. An US company, AAA has already launched few trucks to recharge EVs on the road for emergency demand [26]. The major challenge of V2V is the V2V enabled charger and using the CHAdeMO standard, Anrdomeda has already invented a fast V2V charger [122].

2.1.5 An Adequate Communication Network

This is evident that a large scale penetration of EVs opens a free market of energy sharing which enlarges the energy generation and storage capacity. Consequently, the electricity market becomes more competitive and complex. However, for such users to participate in this market, an integrated reliable infrastructure (e.g., for communications, scheduling, payment, etc.) needs to be realized. Hence, beside the EV charging infrastructure, the energy network has also a demand of real time data sharing and

processing.

For sharing bulk data, all entities (EVs, charging stations, any sort of server, energy providers etc.) are expected to be connected through a reliable communication network for ensuring their participation either as consumer or as source. Fig 2.6 depicts a possible integrated networking system for the EV charging, encompassing LTE, WiFi, and IEEE 802.11p based RSU technologies which all can participate to achieve the required service. Though existing communication infrastructure is competent to handle the current entities, in near future, an enormous number of IoT devices will activate and may challenge this LTE based technology. We are fortunate enough that 5G is knocking our doors. The upcoming 5G network may connect any device from any place at any time and promotes inter vehicular communication [173]. 5G promises a very low end to end latency as well as 10 to 100 times higher data rates than LTE. 5G is expected to connect a massive number of devices, including vehicles, charging stations, and 100s of thousands of residential ones. 5G promises as well to virtualize wireless/radio resources and offer them in form of network slices to clients and other operators. Vehicles can access the information pertaining to charging place, charging time or price, while the charging station can broadcast their price, tentative waiting time, available space.

2.2 Related Works

A detailed literature review is presented here to highlight the motivations and novelties of the objectives, we set in this thesis.

2.2.1 Demand-Aware Provisioning of Electric Vehicles Fast Charging Infrastructure:

Following the EV adoption trend, researchers around the globe are investigating for a prolific CS network to assist the range anxiety reduction to propel the EV market. As an example, a profit maximization model was proposed in [171] to convert a parking lot into a solar powered CS. Two recent works [154] and [155] also encouraged to utilize parking stations as CSs. These sort of initiatives highlighted the immense necessity of the adequate charging facilities in public places and also reveal the challenges to adapt with the existing infrastructures. A remarkable amount of research works investigated the plausibility of the utilization of public places as CSs to support the burgeoning EV market.

The importance of introducing public CSs was analyzed in [131], where the intention of purchasing EVs was studied based on a proposed function, that takes the charging cost in consideration. The increasing EV adoption rate insists to replace conventional gas stations by CSs [144], but the EV charging pattern is different enough from conventional vehicles refuelling to prevent such solutions. Hence, a charging network needs to be provisioned in a different approach, especially when the anticipated cost is very high and ensuring a quality of service (QoS) to inspire people to shift into EV is inevitable. Ucer et al. [138] analyzed the EV user's experience in DC fast charging station using real life data of Columbus, OH. Though this work [138] did not deal with the locations of CSs, this analyze the impact of size (e.g., number of poles and power capacity) over queuing delay of EVs in urban, sub-urban and rural areas.

To reduce the range anxiety, considering existing road network and driving behavior for CS deployment problem are noteworthy. In [108], an ILP was proposed to place a number of CSs to cover route between any two consecutive nodes of the

road network. To achieve the same goal, Michigan university did an extensive work [45], where they considered the variation in charging behavior from season to season for Michigan and a meta-heuristic algorithm was introduced to solve this. Similarly, in [50], for road networks for Boston and Dublin, a minimum number of CSs were determined to confirm a reachable CS for each EV. Tao et al. [133] selected a set of locations for CSs to minimize the time of over discharging of EVs' batteries using genetic algorithm. In [85], a CS citing problem was proposed for an urban area to minimize the installation cost, where the authors analyzed the complexity of such problem and compared different solution algorithms. To minimize the cost, [107] optimized the suitable locations for CSs based upon the traveling behavior.

A sustainable charging facility also has to maintain socio-economic values and consequently energy stabilization [53]. To mitigate the impact of EV charging on power grid, relying on battery swapping or V2G [7] or incorporation with community microgrid [8] backed by a smart energy management system to minimize the charging cost might be an auxiliary solution, especially when EV charging demand is rising on a daily basis. Mahnoosh et al. [11] analyzed the impact of large scale EV penetration on both road and power network, while in [103], the distribution of traffic flow was represented by a semi-dynamic traffic assignment model to assess the impact of charging behavior over power network. Considering the inter dependency between power and road network, a holistic framework of power systems and electrified transportation network were introduced to enhance the operational performance of these systems as a network-of-networks, and explain the required information exchange via coupling agents (e.g., EVs and CSs) [14]. Though these works ([11] - [14]) highlighted the consequences of EV charging over power network, strategical placement of CSs were not proposed to minimize such consequences. To mitigate such consequences,

Lam et al. [85] considered the total capacity of the power grid instead of the variation from one bus to other while the waiting time at CS was not taken into account. Using swarm optimization, [99] searched for the optimal positions of CSs where the authors assumed that the grid capacity could be increased as required, where [158] proposed to add more transformers. Maintaining voltage stability was also taken in to consideration in [39],[59] and [171] to find out the optimal positions for the CSs without taking the waiting time or the comfortable detour distance to CS in consideration. Cui et al. [34] proposed to minimize the installation cost for an urban area, where they also considered the required protective device cost to maintain the power quality. As the mass integration of fast chargers may add a remarkable degradation in power quality [71] and hence, in [72], authors proposed strategical placement of fast chargers backed by alternative energy sources (e.g., renewable energy, V2G) to reduce the harmonic distortion. However, they did not propose any solution to cope with the upcoming increased demand, while the growth rate of EV penetration encourages to take physical actions (e.g., expansion of power network, deploying more voltage regulators) along with strategical one to maintain the voltage stability.

In [23], maintaining voltage level was considered before a strategic deployment; that might force EVs to travel too long to reach the CSs. Almost a similar approach was shown in [27], where the real travel data of Beijing city was used to find the optimal locations, however, energy limitation was ignored. Minimization of power loss was presented in [143], where traffic pattern was considered to maximize the charging service. However, they do not consider the waiting time and no adaptation process was given to handle the increased demand of upcoming years. In [160], though both transportation and power network constraints were taken into account before deploying CSs, they also did not consider any further increment of EV load.

However, most of these research did not consider the users' preferred QoS (quality

of service), maintaining power quality and adaptability with the upcoming EV load all together and hence, considering the importance of the integration of all these features in CS network provisioning, dimensioning and expanding, we propose our own solution in Chapter 3.

2.2.2 Optimal Scheduling of EV Charging at a Solar Power Based Charging Station:

For user's convenience, today, the concept of a micro grid has inspired many organizations to equip their parking lots with charging facilities by installing renewable energy (RE) system along with energy storage system (ESS), especially when the commercial roof top photovoltaic (PV) energy has already reached several MW. Permacity has already installed a 16.4 MW roof top solar system in a single roof at Los Angeles, the largest roof top solar energy production system at present [3]. Meanwhile, at Oman, a 6.4 MW system is installed for supporting EV parking lot by Solar Car Park to support EV charging [3]. In Canada, a 1.14 MW roof top system is installed at Leduc Recreation Center, Alberta [5]. As another example, the Swedish home furnishings giant IKEA is going to establish free electric car-charging stations at all 12 of its stores in Canada [4]. Solar panels in Ontario and Quebec are installed, while wind turbine is in Alberta [4]. Such stand alone CSs have been examined as feasible as well [91], [163].

Whatever the energy source is, ensuring the user satisfaction should be one of the major concerns of EV charging algorithms. Usually an EV user expects to recharge the battery quickly at minimum price. For example, in [136], a Stackleberg game was introduced to maximize the profit of a grid, while EVs played another game to choose their charging time slot to avoid excessive price, but here the charging rate was either maximum or zero, as no intermediate value was in their consideration. In

decentralization systems [161] and [145], temporal coordination was used for making the decision of charging by the EV owners themselves on the basis of declared price. Mixed integer linear program (MILP) was used in [149] to minimize the charging cost for EV owners and a moving horizon methodology [104] was used not only for the cost minimization of EVs, but also to balance the load for CSs. To balance the load, a web based day-ahead scheduling mechanism was proposed in [116] to minimize the charging price. Along with the day-ahead market, dynamic pricing is also becoming popular for peak shaping. Foster et al. [48] proposed a scheduling mechanism, where each EV received the real-time charging price after each 5 min and based upon that, decided their charging profile to minimize the price. A Fuzzy logic based algorithm was proposed in [9] to schedule a set of EVs in a parking lot based CS to maximize the EV owner's satisfaction. A similar approach was shown in [44] to maximize the quality of service. And in both the works of [9] and [44], no RE source was considered for EV charging.

In [29], [102], [157], [162] and [174] the penetration of RE and their integration with conventional grid was considered for charging EVs. Renewable sources were used as the primary source and CSs can purchase energy from the grid as it was required. In some works ([102], [145], [146], [157]), ESS was considered in CS. The main challenge of RE penetration is its production uncertainty and hence, considering the grid connection as a secondary source, these works mitigate the consequences of production uncertainty. Further, although the production cost of RE is zero, however these energy sources come with a sizable installation cost. In [162], renewable energy could be purchased by a service provider from neighboring infrastructures, but they assumed this energy was cost free. In [162] and [174], the overall pricing of production and purchasing of renewable energy was not considered at all.

As a consequence, in chapter 4, we present a smart management system for a PV

based standalone CS to handle the uncertainty of both PV generation and upcoming EV load and propose a charging rate dependent pricing mechanism to offer the opportunity of enjoying fast charging by paying more.

2.2.3 Joint Routing and Scheduling of Mobile Charging Infrastructure for V2V Energy Transfer:

EV's bidirectional energy transfer capability makes them a mobile energy server which can store energy at off peak and release at peak hours. Thus far, in most cases, only V2G (vehicle to grid) is considered as the operational mode of energy seller EVs for peak shaping of the load demand over distribution grids [122], [153]. Germany has already given the commercial permission of energy exchange via V2G to Nisan Leaf [141]. Comparing with the trend of V2G, V2V is still a new concept. Nevertheless, the feasibility and opportunity of V2V technology are widely tested and V2V is a potential candidate for mitigating range anxiety and energy scarcity [95], [105], [111]. Researchers in [132], [147], [165] considered V2V to reduce the burden of distribution grids, while others ([26], [166], [170]) examined V2V charging use to mitigate range anxiety. Kim et al. designed a model, where an EV could charge either from a CS or from another EV [75]. They concluded that EVs and CS cooperation is the better approach rather than just relying on CSs or V2V.

Whatever the purpose of V2V, two major problems need to be addressed. One is to determine the efficient energy transferring process and the other is to match the seller-buyer EV pair or schedule of charging/discharging in the best way. Nasr et al. has achieved the energy transfer efficiency up to 98% in an aggregator based V2V system [111], while Sousa et al. suggested to rely on direct V2V energy transfer to attain more efficiency [129]. V2V-enable on board charger was considered in [117] and a DC-DC converter was designed for V2V energy sharing in [137], which was faster

than level 2 charger. Such quicker charging rate along with an achievable higher efficiency could assist V2V of being a potential solution of the range anxiety.

On the other hand, few works proposed different methods to attain the buyer-seller pair or charging/discharging schedule. Li et al. first determined a parking spot and then found the optimal pair to maximize the satisfaction level [92] and Zhang et al. proposed a bipartite graph method to find out the optimal pair [170]. Daily travelling pattern was analyzed to determine the energy exchange place and EV pairing in [13], [26]. On the other hand, the authors in [80] designed a Markov chain model to charge a set of EVs in a parking lot using a mobile robot like charger, where energy was directly transferred from the mobile charger to EVs through V2V. On the other hand, Wang et al. [152] assumed a power lane on the road, where a set of EVs were allowed to exchange their energy through wireless technology, while a game theoretic approach was used to determine the buyer-seller pair. However, most of the literature aims at maximizing the revenue of EV sellers to encourage them to participate in V2V. As an example, real time energy pricing was used as the decision maker of starting V2V [81], [148], [166].

However, due to the mobility of both the load and source in V2V technology, finding an appropriate communication network to connect them is another preliminary interest for researchers. Wang et al. proposed a heterogeneous network to exchange information for V2V operation [147], while a VANET network may be considered for the same purpose [92], [121]. Beside establishing an appropriate communication network, energy transfer protocols were also investigated to identify the buyer and seller along with a smooth energy transmission [117], [132]. All these very recent research works underlined the feasibility and potential of V2V charging. This gives rise to the need to develop algorithms to schedule and route mobile V2V charging while capitalizing on mobile energy supplier goals and satisfying EV charging requests.

As a consequence, we design an algorithm to select the route and schedule of a set of charging trucks to charge a maximum number of EVs inside their declared deadline. Though for EV charging, as per as our best knowledge, no prior work deals such problem, this problem can be compared with a well known NP-hard problem, i.e., multiple travelling salesmen problem having service window. Aircraft routing and scheduling or school bus routing problem are such type of popular problem having service time window [37], [127]. Beside different heuristic approaches, decomposition methods were also implemented to attain the solutions of such routing and scheduling problems. As an example, Desrosiers et al. [38] applied Lagrangian relaxation method to determine minimum fleet size to reach a set of destination within a predefined time window, while in [36] modeled an aircraft routing and scheduling problem in two models; a column generation technique was applied to solve the linear relaxation of the first model and a Dantzig-Wolfe decomposition approach was used to solve the linear relaxation of the second model. However, as per as our best knowledge, no prior work addressed such problem for EV charging. Moreover, most of these works mainly focused to minimize the fleet size to serve a particular amount of demand, while we intend to maximize the served number of EVs using a limited number of trucks and along with time window constraints. Our model considers the energy constraints for each truck and forces them to return back to the depot before fully depleted. We solve the problem using Dantzig-Wolfe decomposition method and compare this with two proposed heuristic algorithms. The detailed justification of applying this method will be mentioned in chapter 5.

2.2.4 Attack Model and Detection Methodology for a Coordinated Switching Attack Initiated from EV Charging Ecosystem:

On the other hand, the EV charging ecosystem and IoT-connected high wattage devices have recently received much attention from the research community. Indeed, [10], [16], [49] and [52] investigated plausible cyber attacks and threats in an IoT-enabled EV charging infrastructure especially when the widely used message protocol open charge point protocol (OCPP) is still not secured and matured enough [16]. These works demonstrated that the manipulation of the EV ecosystem is possible through compromising the communication protocols and technologies, and eventually creating sizeable consequences on the grid performance. OCPP has been found vulnerable to a wide range of MitM attacks [10] and that might provide the opportunity to an attacker to initiate the switching attack. In the work, Alcaraz et al.[10] depicted a detailed theoretical and simulated vulnerabilities of OCPP, while they depicted three types of vulnerabilities: 1) disclosure, which corresponds to illicit reading and/or copying of information; 2) distortion, any (fake) data insertion, spoofing or modification action (data, processes or configurations); and 3) disruption that comprises the deleting or dropping of messages, processes or actions. As a ramification, by manipulating OCPP messages, an attacker can initiate denial of service (DoS), energy theft or man in the middle (MitM) attack.

Moreover, Wang et al. [151] reported that two types of attacks, i.e., load altering attack or rate alternation, can be initiated from load side to make the grid vulnerable in terms of voltage or frequency degradation, or even load congestion. A load altering attack is an attempt to control a set of unsecured controllable load within a very short period of time in order to damage the grid through circuit overflow or other adverse effects [15], while in rate alternation attack is mainly initiated by fabricating

the pricing messages for inspiring load shifting to make load congestion [109]. Furthermore, the authors in [128] introduced an IoT Botnet that exploited vulnerabilities in high wattage IoT devices to cause disturbances to the grid in terms of frequency instability, cascading failures, and increasing the operational costs, while [6] identified EV charging infrastructure as a potential surface for same kind of attacks using publicly available data. More recently, Khan et al. [70] demonstrated how a botnet of compromised EVs and EV charging infrastructures can be used to launch cyber attacks on the power grid.

On the other hand, the impact of the switching attack in introducing inter-area oscillation and its consequences over power system was first formulated by Kundur et al. [78] who examined a two-area system to analyze the inter-area oscillations. Furthermore, a coordinated switching attack was modeled in [96] to demonstrate how an attacker can compute and apply a coordinated switching sequence through a successful cyber intrusion and local knowledge of the grid. To increase the stealthiness of a switching attack, in [55], this attack was modeled just by comprising a 2% of total load, where the switching frequency was determined through measurement-based analysis of the frequency deviation at a selected bus. The loads in [55] were assumed to be fixed and the variation of system operation point was achieved by connecting/disconnecting a fixed percentage of load. They assumed that due to low frequency of disconnecting, the attack was stealthy. However, such an attack was performed by imposing a three-phase fault to the system which may result in operation of protection devices, such as relays, and changes the system topology. They examine the consequences to the four-machine two-area power system and the Northeast Power Coordinating Council 68-bus system for both a single attack and a coordinated attack. On the other hand, a state dependent switching rule was implemented in [97] to model a coordinated switching attack to create a massive disturbance in the power system.

Farraz et al. [47] utilized the knowledge of local generators rotor speed to initiate a switching attack, while Liu et al. [98] implemented Luenberger-based state estimation technique when they assumed that the knowledge about rotor angle and frequency was not accurate. After analyzing the impact of switching attack, [47] proposed a game theoretic approach to mitigate the consequences, while a proposed parametric game theoretic controller was also applicable during the attack. An automatic inter area oscillation detection method based on phase angle measurement was presented in [159]. However, none of these works considered EVs or their charging ecosystem as a potential attack surface for switching attacks and hence, they only could make change in load, while vehicle to grid energy transfer capability of EV provides an opportunity to create an increase in generation in the form of discharging energy.

Since switching attack initiated from EV charging network is a new concept, works aiding the mitigation for OCPP vulnerabilities do not provide any kind of direction to detect switching attack attempt. As an example, Morosan et al. proposed a back propagation neural network only to detect the distributed denial of service (DDoS) attack [110], while in [119], authors suggested to add an encapsulation for the future versions of OCPP to avoid the man in the middle (MitM) attack. For a secure charging environment, Vadiya et al. [139] proposed private keys for authentication while to ensure the integrity, Khodari et al. [73] designed a decentralized firmware attestation scheme for each EV. However, none of these works focused on detecting switching attack attempt and for the sake of secured charging, all of these work except [110] mainly proposed additional features or suggestions for upcoming versions of charging protocol. In [110], using a back propagation neural network, authors analyzed the time span between two successive incoming requests from the same CS and compare this with a threshold and previous three requests to make a validation. A deep learning algorithm was designed in [169], to detect malicious attempts over controller

area network (CAN). Since, OCPP is a message protocol like CAN, we intend to do feature extraction of requested messages using neural network to design a cyber detection layer hosted by the CMS after proposing a coordinated switching attack from a set of compromised CSs in Chapter 6.

Chapter 3

Demand-Aware Provisioning of Electric Vehicles Fast Charging Infrastructure[1]

In this chapter, we provision a DC fast chargers network (i.e., determine the maximum number of CSs, their best locations and capacities) along with an efficient expansion methodology for an urban area, while the objective is to minimize the installation cost. The design considers the demand of EV charging and predicts the future growth of the demand in the expansion plan and ensures a minimum quality of service (QoS) in terms of a tolerable waiting time or tolerable detour distance to a CS. Moreover, to maintain the voltage stability, an optimal number of tap changing voltage regulators are placed at optimal position of the distribution grid, while the grid capacity is taken in consideration.

[1]This chapter is published in IEEE Transactions on Vehicular Technology [63] and partially presented in IEEE SmartGridComm'2019 [62]

3.1 Motivation

To propel the EV market, an adequate charging facilities is essential to reduce the EV drivers' range anxiety. Due to the relatively small EV battery size, there is a frequent need for charging. This need, combined with the relatively slow charging process, necessitates a smart and adequate distribution of charging facilities at strategic locations in order to ensure the convenience for drivers to reach a CS within comfortable distance along with a tolerable waiting time there. Since deploying CSs is an expensive project, the strategical placement and capacity provisioning of such a CS network should be compatible with the increasing demand of the upcoming years.

Furthermore, prior to any mass deployment, a significant factor to consider is the consequence of the large penetration of EVs and their asynchronous connection on the power grid, which may destabilize the grid especially at peak times. As a consequence, an effective deployment of CSs has to maintain the voltage stability of the distribution network as well.

As discussed in section 2.2.1, though a number of works investigated the design of a prolific CS network to reduce the range anxiety, no one of them considered users' preferred QoS (e.g., tolerable waiting time and detour distance), power quality maintenance and grid capacity all together. Moreover, since, deploying a CS network is an expensive project, an efficient expansion methodology also needs to be in consideration to support the upcoming increased EV load even during the present installation. Considering these issues, we propose a DC fast charger provisioning and expanding method in this chapter.

3.2 Problem Definition and Contributions

In order to address the above challenges, we present our Charging Station Dimensioning and Placement (CSDP) framework for provisioning fast charging infrastructure at minimum cost to accommodate the charging demand of the incremental integration of EVs. Namely, our framework concurrently considers making decision on the placement (and capacity) of CSs and the allocation of the EV charging workload and that ensures a maximum tolerable waiting time at CSs (i.e., quality of experience) as well as a maximum driving distance to reach a CS. Our workload allocation is also sensitive to the voltage level at the power distribution network and hence at design time, we have to decide whether a minimum number of voltage regulators (to minimize the overall cost) opt to be provisioned to maintain the voltage at acceptable level. We also determine the transformer size to support the maximum capacity of a CS and we consider the maximum capacity of each power distribution network. Finally, two different types of expansion models are proposed and analyzed to meet the future increased energy demand and the results are compared with two proposed heuristic algorithms.

The main contributions of this work are:

- A fast charging stations deployment and sizing problem is addressed, where an EV has not to wait more than a predefined time before the charging session and has not to drive more than a predefined distance to reach a CS.

- The strategical placement of these CSs considering both the required number of voltage regulators and the transformer capacity help to keep the voltage level stable through the distribution grid.

- We formally show that the solution of the CSDP problem that accounts for only

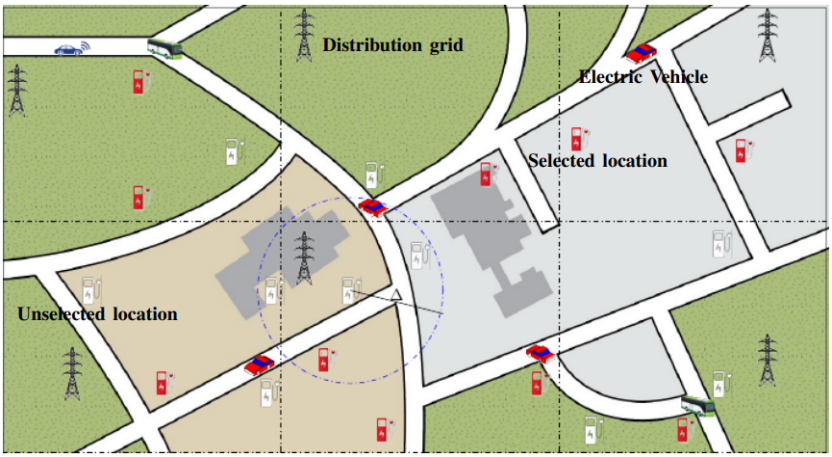

Figure 3.1: An example of potential locations of CSs in an urban area.

the current demands may lead to a high expansion cost of the existing infrastructure in the future. Hence, we examine two planning methods to determine a cost-effective solution of the CSDP problem with increased demands: 1) CSDP forward design which assumes the current load to solve the CSDP problem and updates the infrastructure as the load increases; 2) CSDP backward design which accounts for the future demands in order to decide the present deployment strategy.

3.3 CSDP Model

We consider a metropolitan city powered by a single power grid having a determined number of radial distribution networks. We aim at studying the CSDP problem to determine an optimal deployment of CSs to reduce the range anxiety and simultaneously ensure the voltage stability at each bus of the distribution network. The optimal number and positions for voltage regulators are determined and we also determine the transformer rating for each CS to support its peak demand considering the distribution grid capacity. Fig.3.1 depicts the demand zone and potential locations, whereas

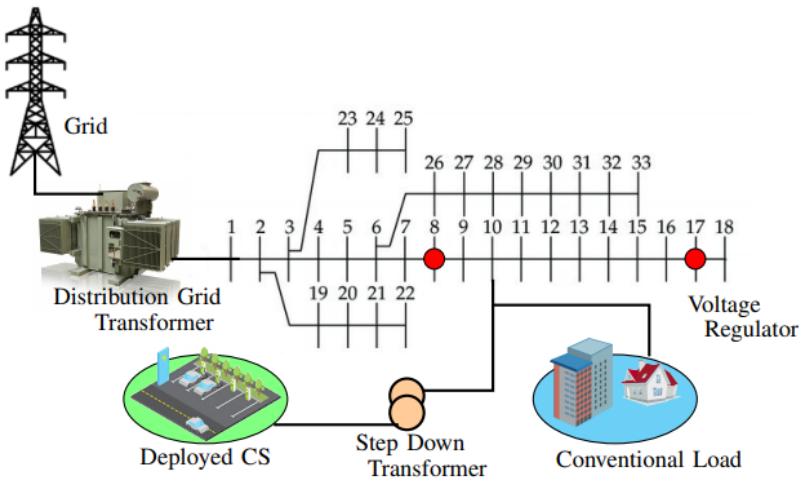

Figure 3.2: An example of power distribution network.

Fig.3.2 depicts an example of a power distribution network.

3.3.1 Charging Request Model

We assume $|\mathcal{E}|$ types of EVs which are available in the city and the EV type is determined based upon the battery size [58] (as an example, $e = 1$ represents a small size EV, $e = 2$ means mid size and large EV is presented by $e = 3$). Now the city is supposed to be divided into a set of demand zones, $\mathcal{Z}$ (each square in Fig.3.1 indicates a zone $z \in \mathcal{Z}$). We consider that each zone $z \in \mathcal{Z}$ has an average EV charging request rate σ_z every hour, which follows a Poisson distribution [19]. And this σ_z is actually the summation of a number of independent Poisson distribution such that $\sigma_z = \sum_e \sigma_z^e$ [19]. σ_z^e is the charging request rate of e type EVs from zone z. The energy demand of each class of EV is supposed to follow a truncated Gaussian distribution [74] with a mean of ω_e kWh. Moreover, due to residential buildings and industries, each zone z has a conventional energy demand and that can be predicted based on historical data [43].

3.3.2 Charging Station Model

A set of locations, $\mathcal{L}$ has been assumed to be primarily selected by the municipality as the potential locations for CSs deployment (both red and white colored CSs depicted in Fig.3.1). If a location is selected for deploying a CS (red colored CSs shown in Fig.3.1), we need to determine the number of charging poles p_l to be deployed at location $l \in \mathcal{L}$. Each pole is considered as a level 3 fast charger and the charging rate is assumed as α. In order to minimize the EV driver's range anxiety, we set a predefined comfortable distance Δ, that an EV should not be forced to exceed to charge its battery. In addition, we set a maximum allowed waiting time τ as queuing delay before starting the charging at the CS. This waiting time is dependent on the EV arrival rate (λ_l) at CS l and on the service rate (the number of EVs which are served by unit time) μ_l of the CS deployed at l. $\mu_l = f(p_l, \mu_l^p)$ is dependent on the number of charging poles p_l and their respective service rate of each of the pole μ_l^p. Each CS is abstracted as a queuing system with multiple servers to determine the waiting time (each server models one charging pole). Hence, we assume an $M/M/p_l$ queue for each CS l and we calculate the average queuing delay W_{lq} as depicted in Eq. (3.1) [134] where N_{lq} indicates the number of EVs at the queue of a CS, deployed at l and λ_l represents the EVs arrival rate (arrived from different zones z) to the mentioned CS.

$$W_{lq} = \frac{N_{lq}}{\lambda_l}; \forall l \in \mathcal{L} \tag{3.1}$$

where N_{lq} can be calculated by the following equation [134]:

$$N_{lq} = \frac{P_{lo}(\frac{\sum_{z \in \mathcal{Z}} \lambda_{zl}}{\mu_l})^{p_l} \Gamma_l}{p_l(1-\Gamma_l)^2}; \forall l \in \mathcal{L} \tag{3.2}$$

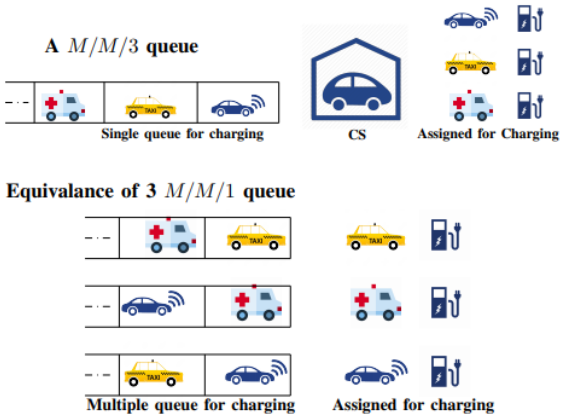

Figure 3.3: One $M/M/3$ system is approximated as 3 $M/M/1$ system.

where λ_{zl} is the fraction of EVs in zone z that are assigned to the CS deployed at l. Γ_l is the probability of having that CS busy (i.e., cannot serve an EV immediately) and P_{lo} is the probability of this CS having no EV to serve. Both Γ_l and P_{lo} depend on the EV arrival rate λ_l, service rate μ_l and the number of charging poles p_l as defined in Eqs. (3.3) and (3.4):

$$\Gamma_l = \frac{\sum_{z \in \mathcal{Z}} \lambda_{zl}}{p_l \mu_l}; \forall l \in \mathcal{L} \tag{3.3}$$

$$P_{lo} = 1/[\sum_{m=0}^{p_l-1} \frac{(p_l \Gamma_l)^m}{m!} + \frac{(p_l \Gamma_l)^{p_l}}{p_l!\,(1-\Gamma_l)}]; \forall l \in \mathcal{L} \tag{3.4}$$

The load distribution λ_{zl} should conform to the comfortable distance Δ used to minimize the drivers' range anxiety. Hence, we represent the distance from zone z to the location l of the CS by δ_{zl} and we use the Euclidean distance from the center of z to the center of l to calculate it.

Note that, considering the $M/M/p_l$ model to determine the optimal location and size for each CS will include a set of non-linear, non-convex constraints (Eqs. (3.1)-(3.4)) to maintain a minimum waiting time and hence, the solution of the problem may become computationally intractable to achieve the optimal solution. Hence, for the sake of simplicity, we approximate a $M/M/p_l$ queuing model as a p_l number of $M/M/1$ queuing system as shown in Fig. 3.3 to determine the location first and

then return back to $M/M/p_l$ queuing system to figureout the required number of poles for each system. Hence, we solve the model in two stages- i) CSDP Workload Assignment (CSDP-WA) model, ii) CSDP-sizing model. These CSDP-WA and CSDP sizing models will be discussed in the next Section.

3.3.3 Power Distribution Network Model

We also assume a set $\mathcal{F}$ of radial distribution Power Network (i.e., medium voltage feeders) that covers the city. Each network $f \in \mathcal{F}$ has a set $\mathcal{N}_f$ of buses and these buses can support the EV load along with the conventional load as depicted in Fig. 3.2. The CSs will be supported by the existing distribution networks. As $\mathcal{L}$ is determined by the municipality, we can assume that the possible allocation of CS l to bus n of the distribution network f is known. Now, to support the load, a set of actions need to be taken for a smooth distribution of power.

- First to operate a fast charging station, line voltage needs to be stepped down to a range of 200 V to 600 V [118]. Fig. 3.2 shows a step down transformer is connected with bus 10 for the deployed CS. The power rating of this transformer should be dependent on the peak demand of the connected CS. No transformer is shown in Fig. 3.2 to support conventional load, as we assume that the required infrastructure for conventional load is already present.

- Establishing a CS at l which is supported by bus $n \in \mathcal{N}_f$ of the radial network should decrease the bus voltage level and that also affects the subsequent buses downstream in the network. Each EV at a CS is regarded as an active load as the reactive load of battery charging is small enough to be ignored. Hence, using the flow branch equation [21], we can determine the voltage of any bus n of any distribution network f. The voltage level of each bus n of the distribution network should be maintained in a tolerable range. Additional voltage

regulators need to be installed at some buses to maintain the voltage level [120]. The red solid circle at bus 8 and bus 17 in Fig. 3.2 represents installed voltage regulators to maintain the voltage level.

- Each of the distribution grid transformer has a maximum capacity to serve the assigned load. As a ramification, only a limited number of CSs should be permitted to draw power from a particular distribution grid to obey its maximum capacity.

3.4 CSDP-WA and CSDP sizing model

To avoid the computational complexity, instead of $M/M/p_l$, the CSs are considered as a total of p_l number of $M/M/1$ systems before designing an ILP of CSDP-WA model to determine the locations for CSs. After determining the locations of CSs and their assigned load, a heuristic algorithm is applied in each location to figure out the required number of charging poles in CSDP sizing model. The overall process is illustrated in Fig. 3.4 and both CSDP-WA and CSDP sizing model are described in following subsections in detail.

3.4.1 CSDP-WA Model

To overcome the intractability of $M/M/p_l$, mainly for location selection and EV assignment to that location, we model each pole of a CS as an $M/M/1$ queue (i.e. $M/M/p_l$ is approximated as p_l number of $M/M/1$ as shown in Fig. 3.3) to be able to get a more tractable expression for the acceptable average queuing delay. This method also provides an upper bound of the required number of poles to maintain the predefined waiting time at each CS (shown in Fig. 3.5) and the charging request rate from different zones, σ_z should be distributed among the installed poles of the

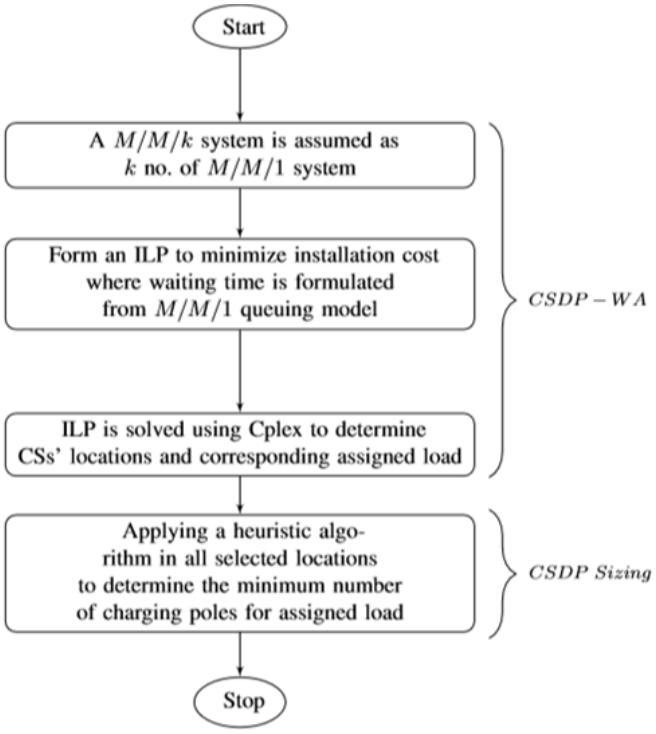

Figure 3.4: The proposed two stage solution method of CSDP model.

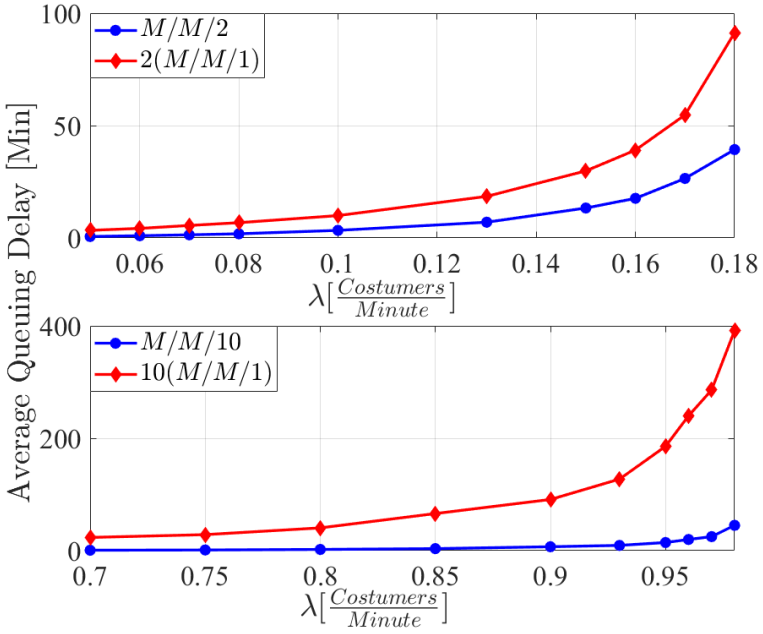

Figure 3.5: Average waiting time comparison between k number of $M/M/1$ with a $M/M/k$.

Table 3.1: List of input parameters

Input symbols	Description & (Unit)
$\mathcal{L}$	set of potential locations l to deploy CS
$\mathcal{Z}$	set of zones z, from where EV load would be assigned to different poles
$\mathcal{F}$	set of distribution network f
$\mathcal{N}_f$	set of buses n of distribution network f
$\mathcal{P}$	set of charging poles p
$p^l_{max} \in Z^+$	maximum number of poles at CS l
$\sigma^e_z \in R^+$	Charging request rate of type e EV at zone $z \in Z$ (rqst/hour)
$\sigma_z \in R^+$	EV charging request rate at zone $z \in Z$ as $\sigma_z = \sum_e \sigma^e_z$ (rqst/hour)
$\delta_{zl} \in R^+$	distance from zone z to location l (km)
$\Delta \in R^+$	the maximum distance an EV travels for charging (km)
ζ_{zl}	is a binary constant as, if $\delta_{zl} \leq \Delta$, $\zeta_{zl} = 1$, otherwise 0
q^{fn}_l	is a binary constant as, if location l is powered by bus n of network f, $q^{fn}_l = 1$, otherwise 0
$P^c_{fn} \in R^+$	conventional active power supported by node $n \in N_f$ (kW)
$Q_{fn} \in R^+$	conventional reactive power supported by node $n \in N_f$ (kV A)
$\tau \in R^+$	tolerable waiting time for an EV in a queue at a CS (min)
$\omega_e \in R^+$	average energy demand by an e type EV (kWh)
$\alpha \in R^+$	charging rate of the pole (kW)
$\alpha_e \in R^+$	maximum charging rate of an e type EV (kW)
$a_l \in R^+$	land cost of location l (\$)
$b \in R^+$	cost of a charging pole (\$)
$c_k \in R^+$	cost of a transformer having rating of T_k (\$)
$\beta \in R^+$	cost of a voltage regulator (\$)

deployed CSs.

The input parameters for the model are listed in Table 3.1.

Objective:

Minimize the total deployment cost.

$$min(\sum_{l \in \mathcal{L}} C_l + \sum_{f \in \mathcal{F}} \sum_{n \in \mathcal{N}_f} C'_{fn}) \tag{3.5}$$

where C_l stands for the CS deployment cost at location l and C'_{fn} is the cost of the additional voltage regulators that need to be installed at bus n of distribution network f. We discuss this cost function in details after describing the constraints.

CSs and poles deployment constraints:

To determine the location of CSs, a binary decision variable γ_l is defined as $\gamma_l = 1$ if location l is chosen for deploying a CS, and 0 otherwise.

If a location $l \in \mathcal{L}$ is selected for deploying a CS, a number of charging poles need to be provisioned. We assume that a set of poles $\mathcal{P}$ are available and we define a decision binary variable ρ_p^l to decide whether pole $p \in \mathcal{P}$ will be installed ($\rho_p^l = 1$) at CS l or not ($\rho_p^l = 0$).

Another decision variable λ_{zp}^e is defined to indicate the arrival rate of type e EVs from zone z to pole p. Eq. (3.6) ensures that a pole is installed at location l, only if that l is chosen for deploying a CS.

$$\gamma_l \geq \rho_p^l; \forall p \in \mathcal{P}, \forall l \in \mathcal{L} \tag{3.6}$$

The following constraint prevents a charging pole from being installed at multiple locations.

$$\sum_{l \in \mathcal{L}} \rho_p^l \leq 1; \forall p \in \mathcal{P} \tag{3.7}$$

Each location l has a space capacity to deploy and Eq. (3.8) ensures that the total number of charging poles at location l should not exceed its maximum capacity.

$$\sum_{p \in \mathcal{P}} \rho_p^l \leq p_{max}^l; \forall l \in \mathcal{L} \tag{3.8}$$

Service rate constraint:

Recall, each pole p_l is abstracted as an M/M/1 queue and to measure the service rate of a charging pole, the weighted average demand, ω_p and charging rate of assigned EVs, α_p are considered. These weighted values depend upon the ratio of each class of EVs.

$$\omega_p = \frac{\sum_e (\omega_e \sum_z \lambda_{zp}^e)}{\sum_e \sum_z \lambda_{zp}^e}; \forall p \in \mathcal{P} \tag{3.9}$$

$$\alpha_p = \frac{\sum_e (\alpha_e \sum_z \lambda_{zp}^e)}{\sum_e \sum_z \lambda_{zp}^e}; \forall p \in \mathcal{P} \tag{3.10}$$

where ω_e is the average energy demand of e type of EV and α_e is the average charging rate of type e EV. And λ_{zp}^e indicates type e EV arrival rate from zone z to pole p.

$$\mu_p \leq \frac{\alpha_p \sum_{l \in L} \rho_p^l}{\omega_p}; \forall p \in \mathcal{P} \tag{3.11}$$

where μ_p is the service rate of charging pole p.

EV load assignment constraints:

We should provision sufficient charging infrastructure to support all EV loads of all zones.

$$\sum_{p \in \mathcal{P}} \lambda_{zp}^e \geq \sigma_z^e; \forall z \in \mathcal{Z}, \forall e \in \mathcal{E} \tag{3.12}$$

We assume the distance from zone z to any pole p of CS deployed at a location l is uniform and denoted by δ_{zl}. Hence, a fraction of EV load in zone z can only be assigned to pole p of CS at l when the distance δ_{zl} does not exceed Δ. The following

constraint avoids long driving distance by EV owners only to charge their EVs.

$$\lambda_{zp}^{e} \leq \sum_{l \in \mathcal{L}} (\rho_p^l \zeta_{zl}) \sigma_z^e; \forall p \in \mathcal{P}, \forall z \in \mathcal{Z}, \forall e \in \mathcal{E} \tag{3.13}$$

where ζ_{zl} is input binary coefficient where $\zeta_{zl} = 1$ for $\delta_{zl} \leq \Delta$ and 0 otherwise. δ_{zl} indicates the distance from z to l.

Delay constraints:

We consider the allowable waiting time τ for any EV at any pole p; hence, each pole is modelled as a $M/M/1$ queue. Our model ensures that at every pole p, the maximum waiting time for EVs should not exceed the value τ.

$$\frac{1}{\mu_p - \sum_{z \in Z} \sum_e \lambda_{zp}^e} \leq \tau; \forall p \in \mathcal{P} \tag{3.14}$$

To maintain a stable queue, we consider that the service rate must be greater than the EV arrival rate.

$$\mu_p - \sum_{z \in \mathcal{Z}} \sum_e \lambda_{zp}^e \geq 0; \forall p \in \mathcal{P} \tag{3.15}$$

Voltage regulator placement and tap positioning constraint:

The voltage at each bus n of any radial distribution network f should be maintained in a tolerable range as Eq. (3.16) .

$$V_{min} \leq V_{fn} \leq V_{max};\ \forall f \in \mathcal{F}, n \in \mathcal{N}_f \tag{3.16}$$

The voltage V_{fn} of any bus n of network f can be calculated based on Eq. (3.17)[21]:

$$V_{f(n+1)}^2 = V_{fn}^2 - 2(r_{fn}P_{fn} + x_{fn}Q_{fn}) + \frac{(r_{fn}^2 + x_{fn}^2)(P_{fn}^2 + Q_{fn}^2)}{V_{fn}^2};\ \forall n \in \mathcal{N}_f, \forall f \in \mathcal{F} \tag{3.17}$$

where $r_{fn}+jx_{fn}$ is the line impedance from bus n to $n+1$ of network f, Q_{fn} represents the reactive power flow and P_{fn} accounts for the active one. Due to the deployed CSs, the active power P_{fn} at bus n of radial network f might increase and can be calculated by Eq. (3.18).

$$P_{fn} = P_{fn}^c + \sum_{l \in \mathcal{L}} q_l^{fn} (\sum_{p \in \mathcal{P}} \rho_p^l)\alpha;\ \forall f \in \mathcal{F}, n \in \mathcal{N}_f \tag{3.18}$$

Since Eq. (3.17) is non-convex, the solution of the model becomes intractable. We are inspired by [164] to make an approximation to estimate the bus voltage of the radial distribution network. This approximation is based upon two conditions [164]:
1) the power loss is small enough in compare with active and reactive power flow, i.e., $\frac{(r_{fn}^2+x_{fn}^2)(P_{fn}^2+Q_{fn}^2)}{V_{fn}^2} = 0$.
2) the voltage deviation is very small as $1-\epsilon \leq V_{fn} \leq 1+\epsilon$ to assume $(V_{fn}-V_0)^2 = 0$.
Hence, the following linear form can be achieved from Eq. (3.17).

$$V_{f(n+1)} = V_{fn} - \frac{(r_{fn}P_{fn} + x_{fn}Q_{fn})}{V_{f0}};\ \forall n \in \mathcal{N}_f, \forall f \in \mathcal{F} \tag{3.19}$$

where V_{f0} is the source voltage of network f and it is assumed to be known. This linear form of flow equation was first introduced in [20]. Now, as we assume a metropolitan city, the line loss is expected to be very smaller in compare with the CS load [69] and the model maintains a voltage level lies between an acceptable range ($[V_{min} = 0.95\ p.u.,\ V_{max} = 1.05\ p.u.]$), hence, we can adopt this approximation.

Now, once a CS is provisioned at node n of network f, the load will increase and the voltage level will drop. Hence, a voltage regulator needs to be installed whenever the additional load of the installed CSs drops the voltage level of a bus n or subsequent buses of a network f below a minimum tolerable level V_{min}. For this purpose, a binary variable y_{fn} determines the decision of installing a voltage regulator i.e., $y_{fn} = 1$ when a voltage regulator is required to install at bus n of network f and 0 otherwise.

A voltage regulator is actually a tap changer transformer and usually each of the tap makes a certain amount of changes in voltage level (e.g., in a regular voltage regulator there are 32 taps; 16 positive and 16 negative [79]. Hence, for each of the tap makes a change of 5% to 8% in voltage level [79]). To determine the tap position of the installed voltage regulator, a discrete variable $t_r \in [-t_{max}, t_{max}]$ is declared. Now for maintaining the voltage level, the model follows the following constraint.

$$V_{min} \leq V_{fn} + y_{fn}(\frac{t_r}{t_{max}})V_{f(n-1)} \leq V_{max};\ \forall f \in \mathcal{F}, n \in \mathcal{N}_f \tag{3.20}$$

CS transformer rating constraint:

To support, a new deployed CS at location l, a step down transformer needs to be deployed to match the required voltage level. The power rating of this transformer is dependent on the peak demand of the CS at l. Hence, the power rating of an installed step down transformer:

$$\alpha \sum_{p \in \mathcal{P}} \rho_p^l \leq \sum_k \eta_k^l t_k; \forall l \tag{3.21}$$

where η_k^l is a decision binary variable such that $\eta_k^l = 1$ when the power rating of the step down transformer is $t_k \in T_k = \{3kVA, 6kVA, 9kVA, 15kVA\}$[118] for CS at l and otherwise 0, where $k \in \{0, 1, ..., |T_k|\}$. Now, to prevent multiple ratings of a

certain transformer, the model obeys the following constraint.

$$\sum_{k} \eta_k^l = 1; \forall l \in \mathcal{L} \tag{3.22}$$

Distribution grid transformer constraint:

Each of the distribution grid transformer has a maximum capacity to serve CS demand along with conventional power demand and for simplicity, we assume this quantity is identical as D_{max} . As a ramification, the total demand (conventional load and CS load) is not allowed to exceed the value of D_{max}.

$$\sum_{n} (P_{fn} + Q_{fn}) \leq D_{max}; \forall f \in \mathcal{F} \tag{3.23}$$

Cost function:

According to Eq. (5), the objective is to minimize the total cost. C_l represents the installation price of a CS at l. This depends on the location price a_l, the number of charging poles $\sum_{p \in \mathcal{P}} \rho_p^l$ and the cost of each charger, b. This C_l also depends on the price of the installed step down transformer and this price depends on the power rating t_k. Eq. (3.24) expresses the value of C_l.

$$C_l = \gamma_l a_l + \sum_{p \in \mathcal{P}} \rho_p^l b + \sum_{k} (\eta_k^l c_k); \forall l \in \mathcal{L} \tag{3.24}$$

where c_k is the cost of installing a step down transformer having a power rating of t_k. On the other hand, the voltage regulator installation cost can be expressed as:

$$C_{fn}^{'} = y_{fn} \beta; \forall n \in N_f, \forall f \in \mathcal{F} \tag{3.25}$$

where β presents the cost of a voltage regulator.

Some of the constraints are non-linear and we have to make them linear. As Eqs. (3.9), (3.10) and (3.11) are non-linear due to the product of two continuous variables, we apply McCormick envelopes approximation [106] to make them linear. On the other hand, Eq. (3.20) is non-linear due to the product of a binary and a continuous variable and hence, can be linearized as [32].

3.4.2 CSDP-sizing Model

As discussed earlier, in order to overcome the complexity of the delay constraint expression, we approximated the $M/M/p_l$ model of the CS by p_l number of $M/M/1$ systems where each $M/M/1$ models the single pole per CS. This allows us to model the charging latency by Eq. (3.14) which is simpler to work with. In practice, however, the CS is expected to have a single queue. Hence, a $M/M/p_l$ is a more realistic model. We should note here that our design based on p_l number of $M/M/1$ queues yields a CS design with over provisioned resources (poles) since, the latency of p_l number of $M/M/1$ is an upper bound for $M/M/p_l$ as shown in Fig. 3.5. To mitigate this, we develop a method that provisions at each CS sufficient (just enough) poles to accommodate the assigned workload. In other words, we take the solution of assigning load and selected locations for the CSs from CSDP-WA model, and we start incrementally adding poles at each CS to meet the demand of the workload, while satisfying the charging latency, τ. The details are presented in algorithm 3.1.

3.5 Expansion Model

As the EV load demand is expected to increase in the upcoming years, the provisioning of public CSs should accommodate this anticipated increment. Indeed, we can predict the future EV load (e.g., over 10-20 years), however installing all CSs

Algorithm 3.1 CSDP-sizing model

1: Set $p_l^{max} = p_l, \forall l \in \mathcal{L}$ (p_l got from CSDP-WA model)
2: Set $l = 1$
3: If $\gamma_l = 1$,go to Step 5; else $l++$
4: If $l \leq |\mathcal{L}|$, go to Step 3; else go to Step 10
5: Set $p_l = 1$
6: Calculate the new delay time $\tau^{'}$ using $M/M/p_l$ queuing system
7: If $\tau^{'} \leq \tau$, take p_l as the required number of poles and go to Step 9; else p_l++
8: If $p_l \leq p_l^{max}$, go to Step 6
9: $l++$ and go to Step 4
10: Exit

based on future demand may not be cost effective as many of those would remain idle when handling the current demand. Hence, it would be wise to expand the charging facilities gradually. Thus we propose two different designs: CSDP forward design and CSDP backward design to handle the expansion of CSs.

3.5.1 CSDP Forward Design

Assume that a gradual CS deployment is taken from year i to year j and the resolution set as k year (i.e. new deployment would be done after each k year). Now, in CSDP forward design, we select a set of locations $\mathcal{L}_i \subset \mathcal{L}$ to install the CSs based on the current demand of year i without accounting for the future growth using our proposed model. Then, in year $i+k$, the EV load demand would be too large to serve with this infrastructure. Hence, we use the CSDP-WA and CSDP-sizing model to decide on the additional number of CSs to deploy at $l \in \{\mathcal{L} - \mathcal{L}_i\}$ and redetermine the capacity of CSs deployed at $l \in \mathcal{L}_i$. This approach would be continued till year j. The design is elaborated in algorithm 3.2. This approach is quite straight forward and though the initial installation cost is expected to be lower here, it cannot guarantee a lower cost in the long run.

Algorithm 3.2 CSDP forward design

1: Initialize the year m=i
2: Determine the location and capacity for required number of CSs, $\mathcal{L}_m \subset \mathcal{L}$ based on the demand of year m
3: If k years elapsed, set $m = m + k$
4: If $m \leq j$, determine the new CSs set $\mathcal{L}_m \subset \{\mathcal{L} - \mathcal{L}_{m-k}\}$, recalculate the capacity of $\{\mathcal{L}_{m-k}\}; \forall k$ and go to Step 3; else go to Step 5
5: Exit

3.5.2 CSDP Backward Design

The future demand of upcoming years are taken into consideration in this design. First, we select a set of locations $\mathcal{L}_j^{'} \subset \mathcal{L}$ based upon the predicted load of year j. After that, demand prediction and locations selection are made for year $j-k$ in such a way that $\mathcal{L}_{j-k}^{'} \subset \mathcal{L}_j^{'}$. This process is also made for $j-2k$, where $\mathcal{L}_{j-2k}^{'} \subset \mathcal{L}_{j-k}^{'}$ and is going as long as $j - nk > i$. Now, we select the location set $\mathcal{L}_i^{'} \subset \mathcal{L}_{j-nk}^{'}$ for handling the present demand of year i. After k years, we can deploy new CSs on $l \in \{\mathcal{L}_{j-(n-1)k}^{'} - \mathcal{L}_i^{'}\}$ and hence, it is expected to be more compatible with future demand and cost effective for the long run. Algorithm 3.3 elaborates the design.

Algorithm 3.3 CSDP Backward Design

1: Initialize the year $m = j$
2: Predict the demand of year m
3: Determine the locations and capacity of a set of locations $\mathcal{L}_m^{'} \subset \mathcal{L}$ based on the demand of year m
4: Set $m = m - k$ and predict the demand of year m
5: If $m \geq i$, determine CSs set $\mathcal{L}_m^{'} \subset \mathcal{L}_{m+k}^{'}$ and go to Step 4;else go to Step 6
6: Exit

3.6 Empirical Evaluations and Discussions

3.6.1 Data Analysis

To evaluate the performance of CSDP method, we consider an EV equipped city like Montreal. The total area of Montreal is 431 square km and the population is 1.78 million. Now to determine the EV charging demand, an extensive analysis is required, especially when CS deployment problem is still not investigated for Montreal. According to our model, the city is assumed to be divided into 19 different zones (e.g., $|\mathcal{Z}|= 19$) as similar as those 19 boroughs of Montreal [33]. Each of these boroughs has different area size along with different population density. To determine the number of EVs of each borough and their corresponding mobility, we replicate a research work [22], which analyzed the EV penetration and its consequences over power grid for an area of Montreal. To estimate the EV penetration, they considered all 21 types of EVs available in Montreal and moreover, based upon the socioeconomic status of the people of this area, they assumed that the penetration level of each type of EVs. According to their finding, in Montreal, the overall EV penetration is 10% and it will reach up to 86% if any drastic change will not occur in the city's economic sector. Hence, we can assume a total number of EVs in Montreal as 90900 (assume 10% penetration) and nearly 42% of them are BEV having different size of batteries [22]. As we are planning to deploy a number of fast chargers, in this work we should focus only on BEV (which is named as EV here) not on any PHEV. Now, based upon the battery size, we classify these EVs into three major groups [138] as EVs having a battery capacity more than 85 kWh are considered in large category, while EVs having battery capacity from 24 kWh to 60 kWh are considered as small EVs. In between these two categories, there are mid size EVs having the capacity from 60 kWh to 85 kWh.

Based on the population density, we can assume the number of each category of EVs for all 19 zones and hence, in Montreal, the small EVs are approximately 14,500 where mid size EVs are 3,000 and the rest are big size EVs [22]. In addition to determine the distribution of EVs through the whole city, travelling behavior and charging habit are also to be investigated to estimate the charging demand of each zone. Now, such type of behavioral analysis is done in [60], where Stockholm city is taken to evaluate their proposed algorithm to deploy a number of fast chargers. Though Stockholm (231 square km) is almost half of the size of Montreal and they divide the city into 12 zones, the population density is almost same. Moreover, there is a lot of similarity in climate and socioeconomic condition between these two cities, hence, we adopt their approach to determine the charging demand in our work. Almost 40% of EVs are expected to be charged at public charging infrastructure [60] and the average departure and return time of EVs at home in Montreal are 8 am and 6 pm respectively [22]. Hence, we expect 4,560 EVs may attempt to charge from 8 am to 6 pm in Montreal at public CSs and they are assumed to be uniformly distributed through all 19 zones of the city.

We also assume that the energy demand by each EV follows a truncated Gaussian distribution [74] having a mean of ω_e kWh for e type of EVs (where $e = 1$ means small size, $e = 2$ means mid size and $e = 3$ means large size EV). We consider that the municipality has primarily selected 40 potential locations ($|\mathcal{L}|= 40$) for deploying CSs, a maximum of 200 charging poles ($|\mathcal{P}|= 200$) are going to be installed and maximum allowed waiting time at any CS should not be more than τ min.

A normalized value is used to express the installation cost. To normalize the value of the prices, \$ x is set as the price of a single voltage regulator and the other entities' prices are demonstrated as proportionally to \$ x. As an example, land cost varies from one place to other and is assumed to follow a Gaussian distribution having a

mean of \$ $20x$ and a variance of \$ $5x$. For the conventional active and reactive power, we consider the values from IEEE 33 bus system. Now based upon these assumptions, we evaluate the impact of these parameters on the two stage CSDP solutions (CSDP-WA and CSDP-sizing) and we assess two planning methods to determine a cost-efficient solution of the CSDP problem with the increased demand. We also propose two heuristic approaches; 1) Largest Location Select First (LLSF) and 2) Cheapest Location Select First (CLSF) and compare them with the CSDP. The model is solved with IBM Cplex optimizer using C++ platform on an Intel(R) Core(TM)i7-6700 CPU having a speed of 3.40 GHz. Finally, a custom built PYTHON-based discrete event simulator is built to evaluate the solutions.

3.6.2 Performance evaluation of CSDP-sizing model

To evaluate the performance of CSDP-sizing method in cost reduction, we determine the optimal locations for CSs and their assigned EV load for $\tau = 9$ min and $\Delta = 3$ km. Upon obtaining the solutions of EV workload assignment and location selection from the CSDP-WA model, the CSDP-sizing method is applied at each selected location. CSDP-sizing problem significantly reduces the required number of poles to maintain this queuing delay. Fig. 3.6 illustrates that 9 locations are selected through the CSDP-WA problem and the CSDP-sizing reduces the required number of poles for all CSs. Upto 45% of charging poles can be reduced for a particular CS and consequently, the total installation cost is reduced by 27%. To asses the competency of our proposed model, a custom built PYTHON-based discrete event simulator is developed. Following the given solution, 1 million sample EVs were distributed among those 9 CSs and the simulator provides the average waiting time for all. The results shown in Table 3.2 shows that all CSs would be able to maintain that predefined maximum waiting time ($\tau = 9$ min).

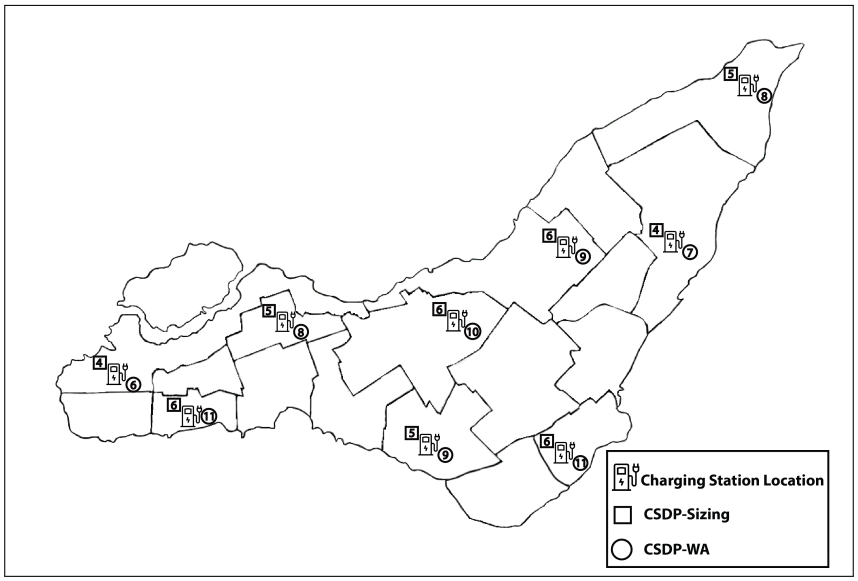

Figure 3.6: CSs' capacity comparison for CSDP-WA & CSDP-sizing method.

Table 3.2: Evaluate the performance of CSDP-sizing method

Selected location	No. of poles from CSDP-WA	No. of poles from CSDP-sizing	Avg. queuing time (min) for CSDP-WA	Avg. queuing time (min) for CSDP-sizing
0	6	4	4.05	1.53
12	11	6	4.25	3.61
13	8	5	4.22	1.67
15	9	5	4.21	3.79
17	10	6	4.23	1.8
23	11	6	4.23	3.7
27	9	6	6.07	2.96
32	7	4	4.16	4.09
36	8	5	4.24	1.81

3.6.3 Empirical evaluation of different parameters

As a charging facility provisioning model, maintaining a stricter waiting time requires installing more CSs with higher capacity. Fig. 3.7 depicts that for $\Delta = 3$, the required cost is \$ $678x$ when the maximum allowed waiting time is 7 min and that becomes \$ $478x$ for 9 min. Alternatively, a slower service rate is enough to maintain the same energy demand while a waiting time is increased to 9 min and consequently, a

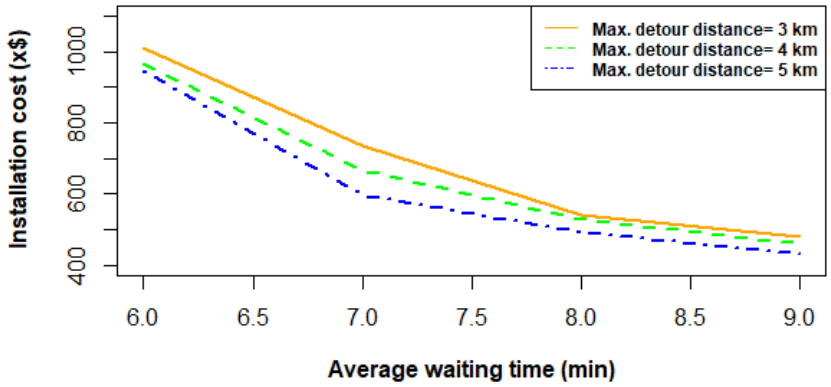

Figure 3.7: Cost variation with waiting time.

fewer number of CSs would be sufficient. Fig. 3.8 depicts that 11 locations need to be selected for guaranteeing τ= 7 min while 9 locations are adequate for τ= 9 min (for simplicity, only the selected locations are indicated in Fig. 3.8 without showing their capacity). As a consequence, 29.8% of the installation cost can be reduced by increasing the allowed waiting time just by 2 min. But this reduction rate does not show a linear relation with the increased value of waiting time. As an example, increasing the waiting time from 6 min to 7 min can save about 40% of the total cost. This cost reduction becomes smaller with the further increment of waiting time and such finding is significant to determine an acceptable maximum waiting time which is cost effective and tolerable to the consumer as well. Fig. 3.7 also depicts that the installation cost is supposed to be influenced by the detour distance (Δ) needs to be traveled by an EV to reach a CS.

According to Fig. 3.7, a shorter distance causes a higher installation cost for maintaining a fixed waiting time. For instance, Fig. 3.9 depicts that for a waiting time of 6 min, the total deployment cost decreased from \$ $1010x$ to reach \$ $990x$ with an increasing maximum travelling distance from 3 km to 3.5 km. This is because 19 CSs are sufficient to serve all EVs instead of 20 while EVs travel a maximum distance of 3.5 km instead of 3 km. The installation cost reduction rate is almost linear with

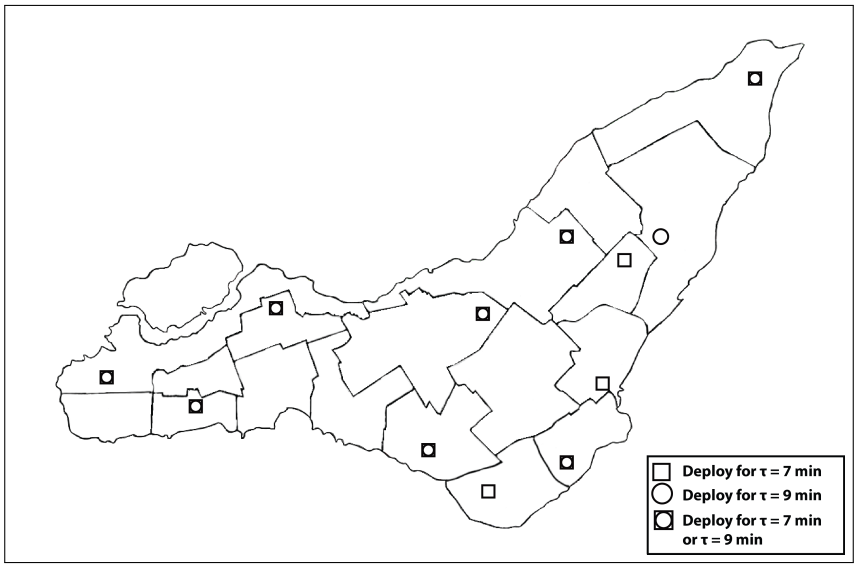

Figure 3.8: No. of CSs variation with waiting time.

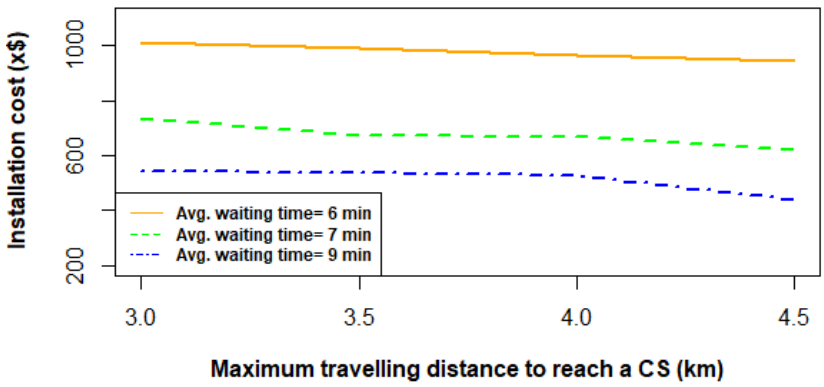

Figure 3.9: Cost variation with maximum detour distance.

the increased value of detour distance, but this variation is not so steeper as that with waiting time.

Installation price is also influenced by the average energy demand by each EV. The average energy demand is dependent on the ratio of different types of EVs and on the mean demand of each type of EVs. As the average charging time increases with the increase of the average energy demand, more CSs need to be deployed for guaranteeing the predefined waiting time and hence, the installation cost increases as well. For instance, Fig. 3.10 depicts that for a waiting time of 9 min, the total

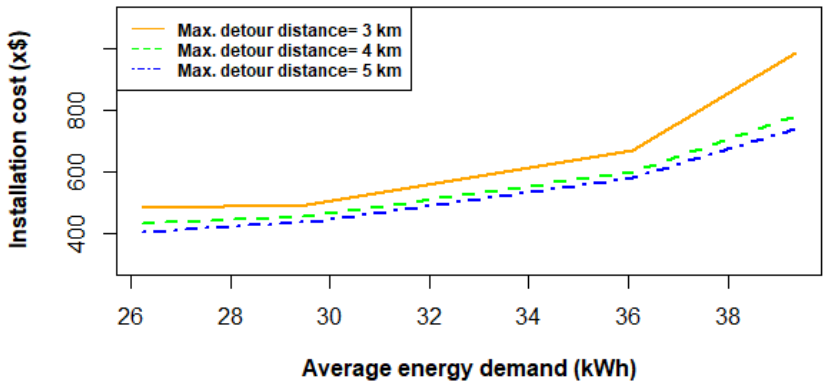

Figure 3.10: Cost variation with average energy demand.

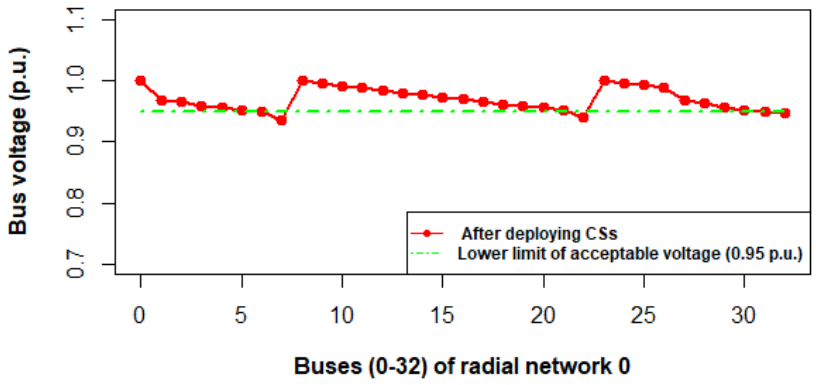

Figure 3.11: Voltage variation due to EV load.

deployment cost increased from \$ $404x$ to reach \$ $439x$ with an increasing average energy demand from 26.2 kWh to 29.5 kWh while the maximum detour distance to reach a CS is 5 km.

Our model also considers the impact of CSs installation on the existing power distribution network and determines the optimal number of voltage regulators at optimal positions to minimize the overall cost. This also determines the corresponding tap position of the voltage regulator. Now, the deployed CSs may degrade the voltage level of the distribution network. A strategic placement of CSs may help to dwindle the impact over bus voltage level and reduce the required number of additional voltage regulators to curtail the deployment cost. Fig. 3.11 presents the voltage level of all 33

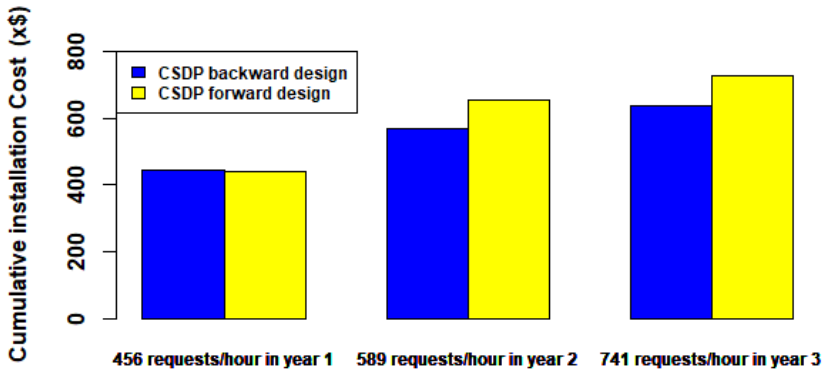

Figure 3.12: Yearly cumulative cost comparison.

buses of radial network 0 ($f = 0$) for such a scenario that 2 CSs are connected with bus 2 and another one is connected with bus 4 of this same radial network (considering the maximum demand of each CS). As the network has to serve more load due to the provisioning of these CSs, the voltage level of bus 7 and 22 drop to below 0.95 p.u. (0.95 p.u. is the minimum required voltage and indicated by a green dotted line in Fig. 3.11). Hence, for the voltage stability, we have to install voltage regulators at these buses. The voltage regulator installed at bus 7 sets the tap position at 2 while tap position is 1 for the other one.

3.6.4 Analyzing the charging infrastructure expansion methods

For a gradual expansion of CS network, we provide two different designs as CSDP forward design and CSDP backward design. To compare these two designs, we assume a 25% of increment in EV adoption from year 1 (current year) by year 2 and another 25% by year 3. We also assume a 5% increment in conventional load by year 2 and this is assumed as 10% by year 3. For simplicity, we consider constant values of $\Delta = 3$ km and $\tau = 9$ min. For handling the initial demand, the initial installation cost in CSDP backward design is slightly higher (Fig. 3.12) due to the enforcement

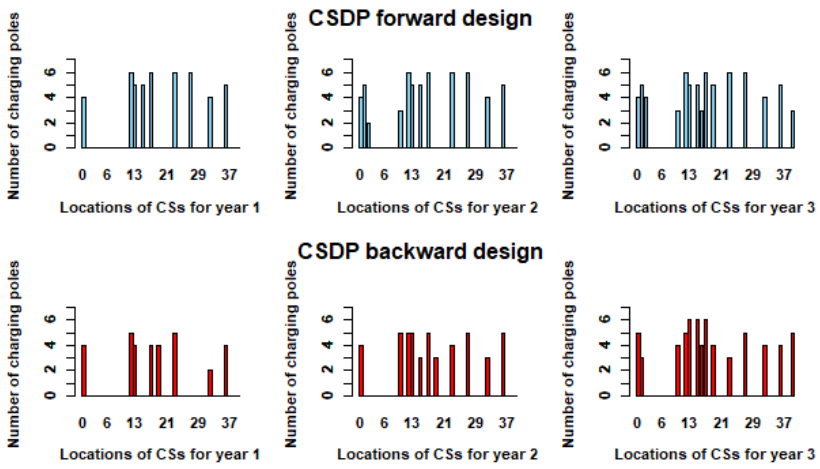

Figure 3.13: Year wise CS deployment.

of selecting 8 expensive locations instead of cheaper options (Fig. 3.13 depicts the selected locations and their respective size). This CSDP backward design gradually proves itself cost effective. In fact for the demand of year 2, it can reduce almost 14% by deploying 11 CSs , while CSDP forward design suggests for 12 locations due to consider all installed CSs of year 1. And for year 3, this cost reduction is almost 11%. Hence, considering future load does not seem to be efficient initially, but in the long run, it is more cost effective.

3.6.5 Comparative analysis

Finally, we compare the performance of our CSDP model with two heuristic methods; largest location select first (LLSF) and cheapest location select first (CLSF). The concept of LLSF is to select the larger locations (i.e., more poles can be installed) to deploy sufficient number of CSs. As a consequence, the location l for which p^l_{max} is maximum gets the highest priority for selecting to deploy a CS. On the other hand, the CLSF selects the cheapest location first. That means the location l having the minimum price a_l should be selected first. Fig. 3.14 illustrates the cost variation for three different average waiting times. Our CSDP model shows better performance

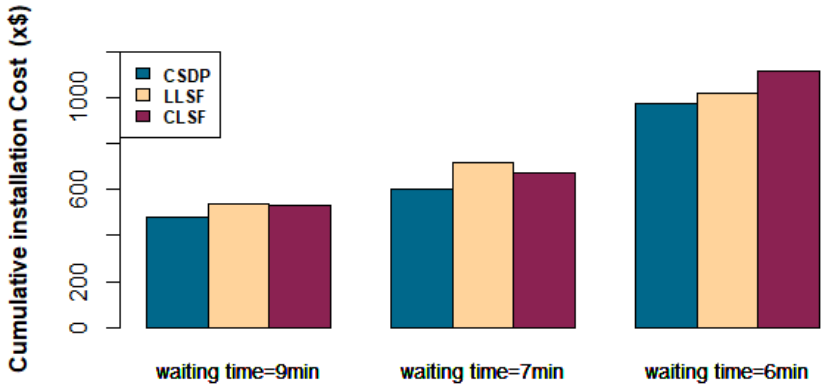

Figure 3.14: Comparing the deployment cost of CSDP with LLSF & CLSF

over both heuristic methods. As an example, for maintaining $\tau = 6$ min, CSDP selects 20 locations while LLSF also selects 20 different locations (but it selects two costly locations 5 and 8 instead of a cheaper option of 4 and 32). On the other hand, CLSF has to choose 24 locations.

3.7 Conclusion

In this chapter, a two stage model is proposed to tackle a charging infrastructure design problem which is capable of determining the optimal locations and capacity (number of poles) at minimum deployment cost. Considering the comfortable distance to travel for charging and an acceptable maximum waiting time make the model appealing for EV drivers. To determine the waiting time at a CS, we model each charging pole as a server and we use queuing theory to estimate the waiting time for charging EVs. CSDP-WA method applies M/M/1 queuing theory to estimate the waiting time to figure out the optimal locations of CSs and after deciding the locations, CSDP-sizing method implements M/M/c queuing over the allocated EVs to determine the required number of charging poles. Given that the mass deployment of CSs may degrade the voltage level at any bus of the power distribution network. To

make it stable, we consider installing voltage regulators (if required). The strategical CS deployment is capable of reducing the required number of voltage regulators to minimize the cost and IEEE 33 bus system is tested here. We also examine two different designs of expanding CSs facility to meet the increasing anticipated demand. Though CSDP backward design costs higher initially, in the long run, it shows better performance in cost minimization over CSDP forward design.

Chapter 4

Optimal Scheduling of EV Charging at a Solar Power Based Charging Station[1]

In the previous chapter, a DC fast charger network was designed to mitigate the range anxiety and an expansion procedure was depicted to manage the anticipated upcoming EV load. Though maintaining voltage stability even after catering this large number of EVs was ensured, this would provoke the power generation sector in emitting more GHG. As a consequence, to curtail the GHG emission, green energy needs to be incorporated for EV charging. Hence, in this chapter, we assume a PV powered standalone CS, while by implementing a charging rate dependent pricing mechanism a set of EVs are scheduled for charging inside their deadlines at minimum price.

[1]This chapter is published in IEEE Systems Journal [64].

4.1 Motivation

Many governments around the world are providing subsidies to the EV market in order to stimulate the awareness of the general public for the need of clean energy. Such subsidy programs accelerate the EV penetration. Nonetheless, the predominant hindrance in the development of EVs is their requirements to have to be charged frequently and this is exacerbated by the fact that the charging time can be quite long as opposed to gasoline based vehicles. Further, one should stress that the majority of people may not switch to EVs just because they are environmentally sustainable and safe. Therefore, to ameliorate the acceptability of EVs, there needs to be a quicker and cheaper green charging facility.

Moreover, if electricity continues to be generated from non-renewable, to cater for the added EVs demand, more energy needs to be supplied and hence shifting the problem from one side of the spectrum to another, i.e., the carbon footprint shifts from transportation sector to the power sector. Hence, alternative energy sources need to be exploited together with intelligent demand response and scheduling schemes. But intermittent energy sources, e.g., wind or solar, need to be accurately predicted. Another challenge in load scheduling is the demand side uncertainty. Namely, given the mobility of EVs, it is difficult for a charging station (CS) to know the energy demand of upcoming time slots. Consequently, without considering future demand, scheduling the present load at a CS may fail to provide optimal operation and hence revenue for the operator. While it is not possible to know the future demand of EVs, historical data may be used to predict that.

As a consequence, we present a smart management system for aPV based standalone CS to handle the uncertainty of both PV generation and upcoming EV load and propose a charging rate dependent pricing mechanism to offer the opportunity of enjoying faster charging by paying more.

4.2 Problem Definition and Contributions

Figure 4.1: A PV powered CS.[112]

We consider a PV based CS (as shown in Fig.4.1) equipped by an ESS. As a self-harvested CS, this standalone CS does not rely on the power distribution grid and consequently, does not cause any load congestion to the grid and also, it contributes in GHG reduction. Moreover, the usage of ESS helps to store the surplus energy to manage the higher demand, while a conventional CS needs to consume more energy from the grid at a higher price. We also consider a smart DC-DC charger, which is assumed to be capable of providing variable charging rate to all EVs. Now, though the production cost of RE is zero, these energy sources come with a sizable installation cost. As a consequence, we propose a charging price and that is directly dependent on the enjoyed charging rate. Hence, the charging rate per EV is determined such that the declared deadlines must not be exceeded and would be able to minimize the charging price for all EVs. PV is considered as the only source and a time slotted system is assumed; to handle the intermittent behavior of PV, a short term prediction [135] is used and this prediction is revised after each time slot. The future load is also predicted and the EVs are scheduled for charging, based on the current charging request and load forecast. According to our model, an EV having a strict deadline has the option to enjoy faster charging rate. Hence, others have to consume at a

slower rate due to the limited amount of energy. To ameliorate this differentiation, a charging rate dependent price function is proposed. The price function adopted here is quadratic and convex, which ensures higher price for higher charging rate and vice versa. The installed ESS is used for storing any excess of energy, for future use. The ESS maximum capacity and maximum charging and discharging rate are also taken in account. The major contributions of the work are as follows:

- Though the designed ILP provides an optimal solution, due to its larger computational time (especially for a large number of EVs), two game theoretic decentralized models, i.e., game 1 and game 2 are proposed to make the decision making process faster. The purpose of modeling two different types of game is to verify the importance of load prediction.

- The PV generation is predicted at the beginning of each time slot to avoid the aberration, rather than relying on a long term prediction at the onset of the scheduling horizon. The importance of this continuous assessment in charging price minimization is examined here.

- A charging rate based quadratic price function is proposed to ensure the fairness among the EVs. Now, as a non-cooperative game (both game 1 and game 2), no EV is interested to give opportunity to other for charging without any incentives and consequently many EVs having stricter deadline might fail to achieve the target even after willing to pay a higher price. To ameliorate this problem, our proposed cost function makes the price very high when the demand is higher than the supply. As a consequence, the EVs which have longer deadline abstain themselves from charging to avoid the higher price. This not only helps to accommodate the EVs, but also brings the price back to a normal range.

4.3 A Centralized Model for EV Charging

4.3.1 System Model

We assume a PV energy based charging station as shown in Fig.4.1 and we assume the CS has enough facilities to connect every assigned EVs instantaneously and provides charge according to the determined schedule only. PV energy is considered as the only source of energy and an ESS is maintained to store the excessive production for future use.

The main challenge of using PV is its production uncertainty. Though the production of solar energy is totally dependent on nature, i.e. random, it is possible to predict it on the basis of historical data. For example, at the beginning of time slot 1, the PV generation for all upcoming slots can be predicted. The PV prediction model applied in [135] is adopted here. As Markov models, based on solar radiation (using historical data) have been successfully used in climatology, a Markov model with the impact of cloud intensity on solar radiation [113] is considered in [135]. The following Markov first order transition probability matrices were used to express the solar radiation:

$$\Psi = \{\psi_{ij}; 0 \leq i \leq k \ \& \ 0 \leq j \leq k\}; \tag{4.1}$$

$$\Psi_I = \left[\ \lambda_0, ..., \lambda_i, ..., \lambda_k \ \right] \tag{4.2}$$

where k represents the number of states of radiation e.g., $i = 0$ the sky is fully clouded and $i = k$, solar radiation is maximum, λ_k. $\psi_{i,j}$ of Ψ indicates the transition probability from λ_i to λ_j in Ψ_I, where matrices Ψ and Ψ_I denote the transition probability matrix among solar radiation states and intensity of the solar radiation

(W/m^2) , respectively.

Under the assumption that the cloud size is exponentially distributed with mean c_i, the solar radiation state is λ_i. Assuming that transitions among solar radiation states are sequential and circular, the transition matrix for solar radiation is expressed as a continuous time Markov chain to estimate the radiation variation [175].

$$\Psi_c = \begin{bmatrix} -\frac{S_w}{c_0} & \frac{S_w}{c_0} & & \\ & -\frac{S_w}{c_1} & \frac{S_w}{c_1} & \\ & \cdots & \cdots & \\ \frac{S_w}{c_k} & \cdots & \cdots & -\frac{S_w}{c_k} \end{bmatrix} \tag{4.3}$$

$\frac{S_w}{c_i}$ denotes the variation rate between solar radiations. Now, the power generation E_h of any slot h is directly dependent on solar radiation λ_h. To calculate the power generation, the size of PV panel (number of PV cell, ξ), efficiency (e_c) and critical radiation (K_c) beyond which an increase of radiation results in a smaller increase inefficiency are considered. The relation is shown below:

$$E_h = \xi. \begin{cases} \frac{e_c}{K_c}\lambda_h^2; 0 \leq \lambda_h \leq K_c \\ e_c\lambda_h; \lambda_h > K_c \end{cases} \tag{4.4}$$

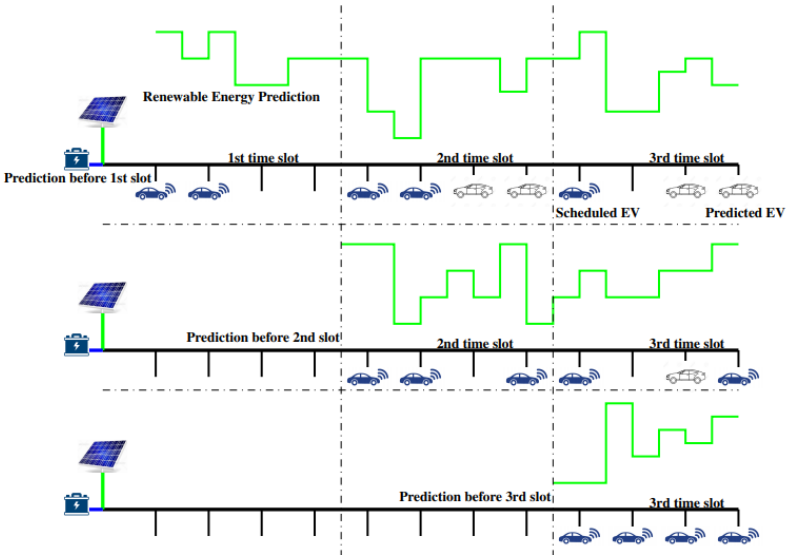

Figure 4.2: The prediction of PV generation and load demand.

This can again be predicted for upcoming slots (as shown in Fig. 4.2) before time slot 2, and this process should be done for all upcoming slots before the starting of any time slot till to the end of the horizon to ensure a proper handling of the intermittent PV generation.

Now, at the beginning of any time slot, m, two sets of EVs, $I(m)$ and $I^{'}(m)$ are considered. $I(m)$ indicates the set of those EVs which have already arrived at the CS for charging. Hence, all the parameters, e.g., demand, deadline, etc. of each EV $i \in I(m)$ are known. $I^{'}(m)$ denotes the expected/estimated arrival of EVs for future time slots, i.e., future load; a Poisson process is assumed for these EVs to determine the rate of their arrivals per time slot [19], and a truncated Gaussian distribution is used for their respective charge demand and deadlines [74]. Fig.4.2 depicts the load prediction where the solid blue cars indicate EVs $i \in I(m)$ and $i \in I^{'}(m)$ are presented by the dotted cars. For simplicity only 3 time slots are shown in Fig.4.2. A CS having a PV system along with ESS is represented, where at the beginning of slot 1, the PV power output for all three upcoming time slots is predicted and we get the charging requests of EVs attempting charging in slot 1. Based upon the

requirement and deadlines of these EVs, few of these cars have to charge even in slots 2 or 3. Meanwhile, using historical data [130], the EV arrivals for slot 2 and 3 also can be predicted. The charge demand and deadlines are assumed to follow a truncated Gaussian distribution. Using this information, all EVs (existing and predicted) in time slot m ($\forall i \in I(m) \cup I^{'}(m)$) are scheduled in such a way that the charging price will be minimum. The overall model is explained in Fig.4.3.

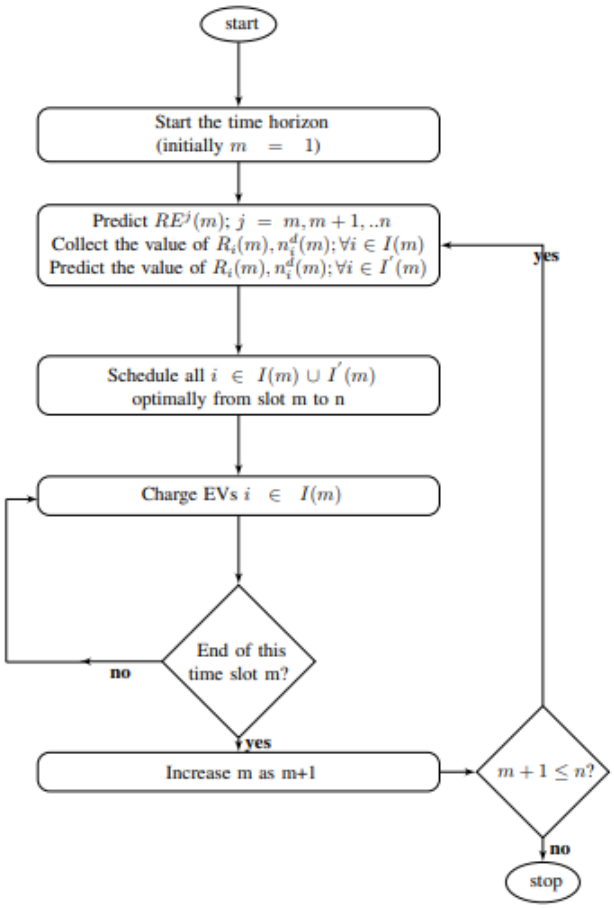

Figure 4.3: Flow chart of the centralized model.

Since we cannot predict accurately the energy and load, we proceed as follows; at the very end of time slot m, we predict the PV for the remaining slots $(m+1, m+2, ..., n)$, we also predict the load for slots $(m+2, m+3, ..., n)$. This time, the accurate load for slot $m+1$ is known: $I(m+1) = I(m) + A(m+1) - D(m+1)$, where

$A(m+1)$ is the newly arrived EVs to be charged and $D(m+1)$ is those EVs that have completed their charging at slot m. After revising the energy and load profile, the optimizer again schedules all EVs for all upcoming slots to ensure minimum charging price. This is repeated for every time slot along the scheduling horizon. Hence, some assumptions are taken at the beginning of any time slot m as-

- $RE^j(m)$ is the predicted PV energy of any slot $j \in \{m, m+1, ..., n\}$. Due to very short time span, $RE^m(m)$ is assumed to be accurate.
- The initial value of ESS is assumed to be constant and known as ESS^1.
- EV^m, the number of EVs, which attempt to charge at slot m is known. The departure slot, i.e. deadline, $n_i^d(m)$ and required amount of energy $R_i(m)$ for $\forall i \in I(m)$ are assumed to be known as well.
- $EV^j(m)$, the number of EVs, which may arrive at any future slot $j \in \{m+1, m+2, ..., n\}$ can also be predicted.
- The expected departure slot i.e. deadline, $n_i^d(m)$ and required amount of energy $R_i(m)$ for any $i \in I^{'}(m)$ are assumed to follow a truncated Gaussian distribution.
- The maximum value of $n_i^d(m)$ (expressed in time slot) for any EV $i \in I^{'}(m)$ can be n and its minimum is $j+3$ if it would arrive at slot $j \in \{m+1, m+2, ..., n\}$. Our assumption is that an EV has at least 1 hour to spend at the CS (less than 1 hour can also be managed by this model), where each 15 min is considered as a slot.

A smart DC-DC charger is assumed to be incorporated at the CS that can charge any EV $i \in (I(m) \cup I^{'}(m))$ at a rate $\theta_i^j(m)$, $\theta_i^j(m) = f_q(m) \times \theta^{max}$, where, $f_q(m) \in F = \{0, 0.25, 0.5, 1\}$ and $q = 1, ..., |F|$. $f_q(m)$ indicates the fraction of maximum charging

Table 4.1: List of input parameters

Input symbols	Description
I	set of actually presented EVs at CS
$I^{'}$	set of anticipated EVs may arrive at future at CS
RE^{j}	predicted PV energy of any slot j
Ess^{j}	stored amount of energy at any slot j
Ess^{cap}	storage capacity of ESS
n_i^d	departure slot of EV i
n_i^a	arrival slot of EV i
R_i	required energy of EV i
θ^{max}	maximum charging rate for any EV
θ_i^j	charging rate of EV i at slot j
C_i^j	charging price of EV i at slot j
γ^{max}	maximum charging rate of ESS
γ^j	charging rate of ESS at slot j
β^{max}	maximum discharging rate of ESS
β^j	discharging rate of ESS at slot j
S	strategy set of the game
S_i	strategy set of EV i
μ	payoff function set of the game
μ_i	payoff function of EV i

rate, which an EV can enjoy at any time slot j. For example, when $f_q(m) = 0.25$, the charging rate of the EV is the quarter of its maximum and if the EV is not scheduled to charge at that time slot, $f_q(m) = 0$. Here, for simplicity we assume all EVs have the same maximum charging rate, θ^{max}.

Considering these assumptions and making the predictions, we seek to determine an optimal charging schedule.

4.3.2 Problem Formulation

We seek to schedule all EVs for charging to fulfill their demand inside the deadline at minimum price. At the beginning of any time slot m, $I(m)$ and $I^{'}(m)$ should be revised. After that $RE^{j}(m)$; $\forall j \in \{m, m+1, ..., n\}$ and $R_i(m), n_i^d(m); \forall i \in I^{'}(m)$ are predicted. $R_i(m)$ and $n_i^d(m)$ for any EV $i \in I(m)$ are known. Hence, at each slot m,

the optimizer minimizes the charging price for any EV $i \in (I(m) \cup I^{'}(m))$. At time slot m, the model can be formulated as follows:

Objective:

$$min \sum_{j=m}^{n} C_i^j(m); \quad \forall i \in (I(m) \cup I^{'}(m)) \tag{4.5}$$

At time slot m, $C_i^j(m)$ is the charging price for EV i for any time slot $j \in \{m, m+1, ..., n\}$.

Constraints:

According to our model, an EV may enjoy a variable charging rate. Hence, we introduce a binary decision variable $x_i^{j,q}(m)$. For any EV $i \in (I(m) \cup I^{'}(m))$, the value of $x_i^{j,q}(m)$ must be zero before its arrival slot, $n_i^a(m)$, and after the departure slot, $n_i^d(m)$. Eq. (4.7) ensures that $x_i^{j,q}(m) = 0$ for any $j \in \{\{j < n_i^a(m)\} \cup \{j > n_i^d(m)\}\}$. As mentioned earlier, $f_q(m)$ indicates the fraction of maximum charging rate and by determining the value of $x_i^{j,q}(m)$, the optimizer picks the suitable value of f_q which is sufficient for completing the charge for EV $i \in (I(m) \cup I^{'}(m))$ inside the deadline $n_i^d(m)$ at minimum price. For a particular time slot, $f_q(m)$ should have a fixed value. Considering these assumptions, Eqs. (4.6) to (4.8) explain this decision binary variable.

$$x_i^{j,q}(m) = \begin{cases} 1;\ i \text{ is charging at } f_q \text{ th rate at slot } j \\ 0; \text{otherwise} \end{cases} \tag{4.6}$$

$$(n_i^a(m) - j)(n_i^d(m) - j)x_i^{j,q}(m) \leq 0; \forall i \in (I(m) \cup I^{'}(m)); \forall j \tag{4.7}$$

$$\sum_{q} x_i^{j,q}(m) = 1;\ \forall i \in (I(m) \cup I^{'}(m))), \forall j \tag{4.8}$$

For Eqs. (4.6) to (4.8), $j \in \{m, m+1, ..., n\}$.

At slot m, the charging rate $\theta_i^j(m)$ of all EVs $i \in (I(m) \cup I^{'}(m))$ for any time slot $j \in \{m, m+1, ..., n\}$ are as:

$$\theta_i^j(m) = \sum_q (\theta^{max} f_q x_i^{j,q}(m)); \ \forall i \in (I(m) \cup I^{'}(m)), \forall j \tag{4.9}$$

$$\sum_{j=m}^{n} \theta_i^j(m) \geq R_i(m) - \sum_{j=1}^{m-1} \theta_i^j; \forall i \in (I(m) \cup I^{'}(m)) \tag{4.10}$$

Eq. (4.9) expresses the value of the variable charging rate while θ^{max} depicts the maximum charging rate. Eq. (4.10) ensures that EV i will be charging until fulfilling its requirement. $\sum_{j=1}^{m-1} \theta_i^j$ is known at time slot m and for $m = 1$, this value is assumed as 0.

Hence, our model offers a variable charging rate to different EVs. Even for a particular EV $i \in (I(m) \cup I^{'}(m))$, this charging rate may be varied from one slot to another according to the total available energy and total demand. To ensure equity, the price should be directly related with the charging rate and at time slot m, the charging price of EV $i \in (I(m) \cup I^{'}(m))$ for any slot $j \in \{m, m+1, ..., n\}$ can be expressed with the following equation.

$$C_i^j(m) = a(\theta_i^j(m))^2 + b\theta_i^j(m) + c \ ; \forall i, \forall j \tag{4.11}$$

here, a, b and c are constants. The CS can set the values of a, b and c, but a regulatory board should have the authority to declare the maximum range of these values to ensure the social welfare [2]. Moreover, no EV is allowed to start charging in the middle of any slot and the EV has to pay for the whole slot it is assigned to.

[2]NREL report states that the tariff of micro grid electricity is monitored by a regulatory board [126]

At any time slot $j \in \{m, m+1, ..., n\}$, any EV $i \in (I(m) \cup I^{'}(m))$ has to take its charge from either real time PV generation or from the ESS. This ESS stores the excess energy which is not used in EV charging at that time slot j. Our assumption is that for a particular time slot j, the ESS might either charge or discharge (but not both concurrently). To determine the charging or discharging of ESS at slot j, another decision binary variable $\alpha^j(m)$ is declared. Let, γ^{max} and γ^{min} be the maximum and minimum rates of charging per slot for the ESS and β^{max} and β^{min} be the maximum and minimum rates of discharging. $\gamma^j(m)$ and $\beta^j(m)$ represent the charging and discharging rate of the ESS for slot j and $Ess^{(j)}(m)$ expresses the amount of energy storage after slot j. Ess^{cap} is assumed as the maximum capacity of the ESS. Hence, Eqs. (4.12) to (4.16) explain the charging or discharging decision of ESS and the amount of ESS after any slot j.

$$\alpha^j(m) = \begin{cases} 1;\ \text{ESS is charging at the } j\text{th slot} \\ 0;\ \text{otherwise} \end{cases} \tag{4.12}$$

$$\gamma^{max}\alpha^j(m) \geq \gamma^j(m) \geq \gamma^{min}\alpha^j(m)\ ;\forall j \tag{4.13}$$

$$\beta^{max}(1-\alpha^j(m)) \geq \beta^j(m) \geq \beta^{min}(1-\alpha^j(m))\ ;\forall j \tag{4.14}$$

$$Ess^{cap} \geq Ess^{(j-1)}(m) + \gamma^j(m) - \beta^j(m) \geq 0\ ;\forall j \tag{4.15}$$

$$Ess^j(m) = \sum_{j=1}^{j-1}(\gamma^j(m) - \beta^j(m))\ ;\forall j \tag{4.16}$$

At $j = 1$, ESS^1 is assumed to be constant and known. And at time slot m, $\theta^j(m)$ is calculated to determine the amount of total energy which should be allocated for the all EVs in j^{th} slot . This amount must not exceed the value of $RE^j(m) + \beta^{max}$. These scenarios are expressed for any $j \in \{m, m+1, ..., n\}$ by Eqs. (4.17) and (4.18)

$$\sum_i \theta_i^j(m) \leq \theta^j(m); \forall j \tag{4.17}$$

$$\theta^j(m) \leq RE^j(m) - (\gamma^j(m) - \beta^j(m)); \forall j \tag{4.18}$$

4.4 Game-theoretic Decentralized System

Our proposed centralized solution might be time consuming, as it involves solving the ILP (derived before); particularly, when the number of EVs is high, the processing time becomes prohibitively expensive and that renders the model less significant in practice. Hence, we present a game theoretic methodology where each EV acts as a player in a non-cooperative game. Our problem is solved in a decentralized manner and each of the players tries to achieve its goal simultaneously; as a result, such decentralized solution is expected to be much faster than the centralized system.

Let, $G =< I(m), S(m), \mu(m) >$ be the game model, where at time slot m, G has its all three major components: the player set $I(m)$, the strategy set $S(m)$ and the respective payoff function $\mu(m)$.

Each EV $i \in I(m)$ acts as a player and selects its own strategy to get the required energy inside the deadline at minimum price. Here, the charging rate of a particular EV for a particular time slot depends on the energy availability from PV and ESS as well as the charging strategies of other participating EVs. Hence, this game is actually a mixed strategy game [18]; every player informs the CS about the arrival time $n_i^a(m)$, the energy requirement $R_i(m)$ and the deadline $n_i^d(m)$. The CS will not take any decision about scheduling, it will simply convey the total demand and predicted amount of PV power generation of each time slot $j \in \{m, m+1, ..., n\}$ to all participating EVs. Each player has its own action set and it takes a strategy to

minimize its charging price as much as possible. We propose two different algorithms (game 1 and game 2) to play this non-cooperative game.

In game 1, EVs start their game at the beginning of any time slot m without considering $I^{'}(m)$, i.e. without looking ahead for upcoming demand, that means only EV $i \in I(m)$ participates in the game and $I^{'}(m) = \emptyset$. The CS predicts the $RE^{j}(m)$ generation for all remaining time slots as well. And due to the arrival of new EVs $i \in A(m)$ and departure of $i \in D(m)$, set $I(m)$ is revised at the beginning of each slot, consequently all players need to play the game again. The strategies taken by the players are depend on the predicted amount of PV energy and other players' strategies. Algorithm 4.1 explains the procedure of game 1.

Algorithm 4.1 Game 1

1: Revise the set $I(m)$ and assume $I^{'}(m) = \emptyset$
2: Predict $RE^{j}(m)$; $\forall j \in \{m, m+1, ..., n\}$
3: Declare $R_i(m)$,$n_i^a(m)$ and $n_i^d(m)$; $\forall i \in I(m)$
4: Play $G =< I(m), S(m), \mu(m) >$ to select $s_i^*(m); \forall i \in I(m)$
5: Increase m to $m+1$
6: If $m \leq n$ repeat steps 1 to 6, else go to step 7
7: End of scheduling

On the other hand, in game 2, the set $I^{'}(m)$ is not considered as empty, that means we predict the arrival rate of EVs for all upcoming slots $j \in \{m, m+1, ..., n\}$ and also predict their associated demand and deadlines just like the centralized system. In

Algorithm 4.2 Game 2

1: Revise $I(m)$ and predict $I^{'}(m)$
2: Predict $RE^{j}(m)$; $\forall j \in \{m, m+1, ..., n\}$
3: Declare $R_i(m)$, $n_i^a(m)$ and $n_i^d(m)$; $\forall i \in I(m)$
4: Predict $R_i(m)$, $n_i^a(m)$ and $n_i^d(m)$; $\forall i \in I^{'}(m)$
5: Calculate $L^{j}(m)$; $\forall j \in \{m+1, m+2, ..., n\}$
6: Play $G =< I(m), S(m), \mu(m) >$ to select $s_i^*(m); \forall i \in I(m)$;
7: Increase m to $m+1$
8: If $m \leq n$ repeat steps 1 to 8, else go to step 9
9: End of scheduling

the game theoretic model, each EV has to take its own decision, as a ramification we cannot expect that an EV $i \in I^{'}(m)$ participates in the game at slot m. Therefore, only EVs $i \in I(m)$ play the game, but an average future load ,$L^{j}(m); \forall j \in \{m+1, m+2, ..n\}$ is taken into account. This demand can be calculated from $R_i^j(m); \forall i \in I^{'}(m)$. As a result, in game 2 (explained in algorithm 4.2), all players select their strategies based on the predicted RE, average future demand and other players' strategies.

Assume that at slot m, the game has a strategy set $S(m)$ which depends on the strategy set of all EVs $i \in I(m)$:

$$S(m) = \{S_1(m) \times S_2(m)..... \times S_i(m)..... \times S_k(m)\} \tag{4.19}$$

where k is assumed to be the total number of players and $S_i(m)$ indicates the strategy set of EV $i \in I(m)$ at time slot m. Here, the strategy means the value of the variable charging rate for a particular time slot and this value is directly influenced by the other players' charging rates.

$$S_i(m) = \{\theta_i^j(m); \forall j\}; \forall i \in I(m) \tag{4.20}$$

This $\theta_i^j(m)$ is defined by Eq. (4.9) and it is applicable $\forall j \in \{m, m+1, ..., n\}$. The game is a mixed strategy game. The charging rate of EV i is varied from iteration to iteration and depends on others' strategies. By picking a value of $f_k(m) \in F$, the EV sets its charging rate and the probability of selecting any value of $f_k(m)$ at any time slot $j \in \{m, m+1, .., n\}$ can be expressed by Eqs. (4.21) and (4.22).

$$P_i^j(f_k(m)) < 1; \forall i \in I(m), f_k(m) \in F, \forall j \tag{4.21}$$

$$\sum_k P_i^j(f_k(m)) = 1; \forall i \in I(m), \forall j \tag{4.22}$$

The payoff function determines the impact of the selected strategy. At every

iteration, EV $i \in I(m)$ calculates the payoff for its every possible strategy and selects the best one. Definitely, the payoff of EV i is also dependent on others' strategies. Now during every iteration, each EV calculates this payoff by considering the possible strategies of all others:

$$\begin{aligned} \mu_i(m)(s_i(m), s_{-i}(m)) = M - min \sum_j C_i^j(m) \\ ; \forall s_i(m) \in S_i(m), \forall i \in I(m) \end{aligned} \tag{4.23}$$

At time slot m, $\mu_i(m)$ is the payoff of EV i, $s_i(m)$ is the strategy taken by the EV $i \in I(m)$ and $s_{-i}(m)$ indicates the strategies of all EVs except this EV i. M is a large positive constant and here the price function needs to be slightly modified from Eq. (4.11) of the centralized system.

As a non-cooperative game, no EV would change its strategy for other players' benefit even for the same payoff. At slot m, it might be happened that the first p players set their best strategies in such a way that all available energy of slot j, $RE^j(m)+\beta^j(m)$ is consumed or almost consumed. If the $(p+i)^{th}$ player has no option other than taking $\theta_{p+i}^j(m)$ amount of energy from the jth slot, then none of the players give the $(p+i)^{th}$ EV the opportunity of charging without getting any incentive. Hence, we consider the charging price to be dependent not only on the individual's charging rates, but also on the total demand. If the total demand of a slot becomes larger than the available energy for the taken actions of the players, an additional price will be added. As a result any EV having options to get charge at a lower price from other subsequent slots will make free (vacate) slot j for the $(p+i)^{th}$ EV. To add this additional price, we declare a binary variable $y^j(m)$ and the price

function becomes as Eq. (4.27).

$$y^j(m) = \begin{cases} 0; \text{if} \sum_i \theta_i^j(m) > RE^j(m) + \beta^{max}; \forall j \\ 1; \text{otherwise} \end{cases} \tag{4.24}$$

$$\sum_{i=1}^{p} \theta_i^j(m) + \theta^{max} \geq y^j(m)(RE^j(m) + \beta^j(m)); \forall j \tag{4.25}$$

$j \in \{m, m+1, ..., n\}$ and Eq. (4.25) will be slightly changed for game 2. If the average future demand is $L^j(m)$ for slot j at m, the equation would be as follows:

$$\sum_{i=1}^{p} \theta_i^j(m) + L^j(m) + \theta^{max} \geq y^j(m)(RE^j(m) + \beta^j(m)); \forall j \tag{4.26}$$

$$C_i^j(m) = a(\theta_i^j(m))^2 + b\theta_i^j(m) + c + (1 - y^j(m))\Gamma \\ ; \forall i \in I(m), \forall j \tag{4.27}$$

where Γ is a large positive number. To avoid this extra price, all EVs try to set their charging pattern in such a way that the total consumption by all EVs from a particular slot always maintains a gap of θ^{max} with the available energy of that slot. Finally all the other constraints of centralized systems are also applicable here. Now using Eq. (4.27), EV $i \in I(m)$ determines its best strategy $s_i^*(m)$ only when it considers the best strategies of other EVs:

$$s_i^*(m) = arg\ min\ \mu_i(m)(s_i(m), s_{-i}^*(m)) \\ ; \forall s_i(m) \in S_i(m), \forall i \in I(m) \tag{4.28}$$

where at slot m, $s_i^*(m)$ is the best strategy for EV $i \in I(m)$ because its payoff is

at least as good as all other possible strategies which might be taken as a response of the best strategies of all other players, which is expressed as

$$\begin{aligned} \mu_i(m)(s_i^*(m), s_{-i}^*(m)) \geq \mu_i(m)(s_i(m), s_{-i}^*(m)) \\ ; \forall i \in I(m), \forall s_i(m) \in S_i(m) \end{aligned} \tag{4.29}$$

The players are continuously trying to improve their payoff by changing their strategies over others' best responses from one iteration to another in the game. This game goes on until any change in the strategy of any EV has no impact over the payoff of all other EVs. This means, no further improvement in payoff is possible by selecting a new strategy and this scenario is true for all players as well. This procedure achieves a stable value of payoff functions for all EVs using the corresponding best strategies from the following equation:

$$\mu_i^*(m)(s_i^*(m), s_{-i}^*(m)) = M - min \sum_j C_i^j(m); \forall i \in I(m) \tag{4.30}$$

By this way, all the participating EVs set their charging profile to get the required charge at the least possible price inside the deadlines by taking their own decision. But at the beginning of next time slot $(m+1)$, $I(m+1)$ should be revised, consequently $\forall i \in I(m+1)$ shall play the same game to select their charging rate for all upcoming time slots j. This process is going till the end of scheduling horizon.

Lemma 1 (Nash Equilibrium) In this mixed strategy non-cooperative game, the $I(m)$ players having a compact, non-empty, convex strategy set $\{S_i(m)|i \in I(m)\}$ play a game to maximize their payoff individually as in Eq. (4.23). $S_i(m)$ contains a finite number of strategies. According to [168], the objective function converges to at least one Nash equilibrium in this case if the payoff function is convex and continuous.

Proof As a strategy, each player $i \in I(m)$ takes a value from set F to set the charging rate while the EV $i \in I(m)$ is charging. By definition, this set can be covered by a collection of open sets $\{H\}$, where each H is also compact. The strategy set is obviously non-empty as well. As a compact and non-empty set, $S_i(m)$ shows the completeness.

Now $S_i(m)$ is also a convex one. Any value of $s_i(m) \in S_i(m)$ belongs to the real number set R. To prove this convexity, we assume A,b,C and d as real value such that $As_i(m) \leq b$ and $Cs_i(m) = d$ for both $s_i(m) = x$ and $s_i(m) = y$, where $s_i(m) \in S_i(m)$. Now any value of κ is chosen as $0 \leq \kappa \leq 1$ and it can easily be shown that $A(\kappa x + (1-\kappa)y) \leq b$ and $C(\kappa x + (1-\kappa)y) = d$ are also true. Hence, our strategy set is convex.

For a finite strategy set, to get a Nash equilibrium the objective function needs to be convex and continuous [168]. Our payoff function (Eq. (4.27)) is a quadratic one and all its coefficients are real. Hence, as per the definition it is continuous for any real value and it is proven that every continuous function shows semi-continuity [140]. For the positive coefficients of the payoff function, it acts like a parabola, which means it is strictly convex as well. All the properties of our game match with the mentioned properties of [168]. Hence, the game must converge to at least one Nash equilibrium.

4.5 Empirical Evaluation and Discussions

This section solves both the centralized and decentralized models derived earlier. The objective of our model is to minimize the charging price for all EVs. The impact of deadline over the charging pattern and the corresponding charging price is analyzed in this section. Charging price is also expected to be influenced by demand and the impact of energy demand over charging price is examined. The contribution

of the ESS on handling the shortage of energy in a particular time period is also deduced here. Recall for handling intermittency, the energy profile is revised after each time slot using a short term prediction algorithm. The importance of this revision is analyzed along with the load forecast. Then the performance of the proposed model is compared with a published work [136]. Finally the performance of the centralized and decentralized methods are compared in terms of computational time. Randomly generated data is used for simulation and for each case, the simulator runs for different data sets and their average is taken. For EV arrival, the parameter of the Poisson distribution is set to a certain value e.g. 10 EVs/time slot. And if each EV having a minimum range of 4 slots and a maximum range of 12 slots (end of the horizon), a truncated Gaussian distribution is used to generate the respective deadline. Finally, the energy requirement of EV i was generated by using a truncated Gaussian distribution for the whole set of EVs. Finally for simplicity, we assume the maximum charging rate is fixed for all EVs of 10 kWh/slot and we also assume that the length of each time slot is 15 min.

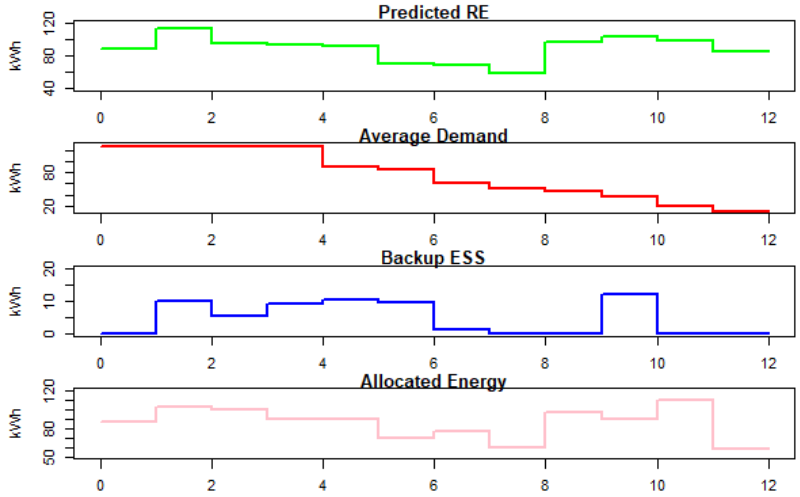

Figure 4.4: Energy allocation based on RE, ESS and demand.

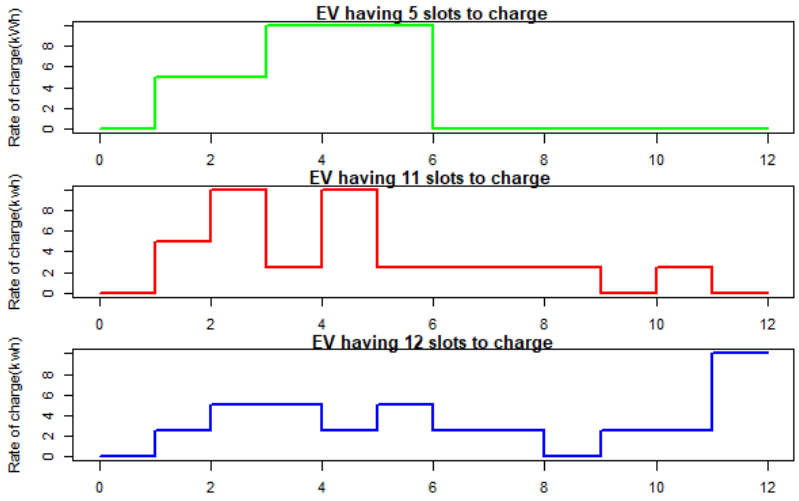

Figure 4.5: Charging pattern variation due to different deadlines.

Consider a total of 40 EVs having different energy demand and deadlines; Fig. 4.4 shows the total energy generated by PV and the average demand of each slot for 12 consecutive time slots. The figure clearly shows that in some time slots, e.g., slot 0 and between slots 2 and 4, the demand is more than the energy predicted from PV. After running the centralized model with this input, the charging schedule is determined for all EVs. It is evident from the figures, that although the demand of energy from EVs can exceed the available energy from PV, the model makes informed decision to store excess energy in the ESS in times of high demand to use it for allocation for EVs. It is also clear that there is a shift in the charging of EVs to future time slots, e.g., compare the average demand for energy with the allocated energy by the model, in particular for those EVs with less strict deadlines.

Shifting the schedule of EVs having less strict deadlines to later time slots is more clearly depicted in Fig.4.5, where three different EVs are taken, which start their charging at slot 1 having the same demand of 40 kWh. We assume that one of them has to finish its charging by slot 5, another has to finish by slot 10, and the last one has enough time to finish its charging by slot 11. Fig.4.5 depicts that, the EV having the most strict deadline charges at a faster rate while others have the opportunity to

charge at a slower rate to avoid higher price.

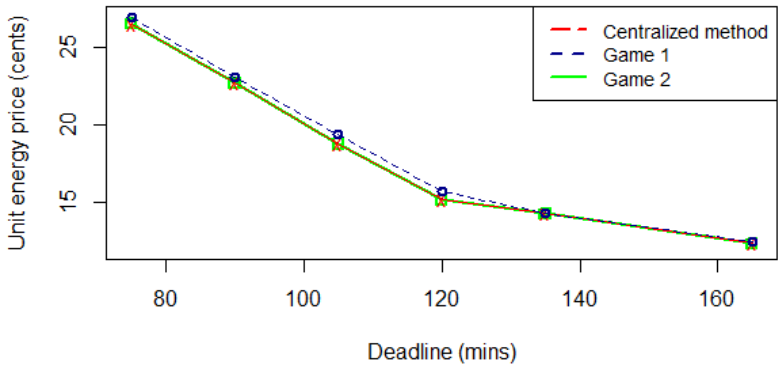

Figure 4.6: Unit price variation with deadline.

By shifting the demand to the less congested time slots, the EV having less strict deadline actually creates the opportunity of higher charging rate for those EVs whose deadlines are tight. Hence, the charging price should be varied with respect to deadline to ensure equity, i.e., an EV needs to pay more for charging at a higher rate. A set of EVs having same demand but different deadlines is considered. Fig.4.6 shows that, in the centralized model, the unit price is decreasing almost linearly as the deadline increases and this solution is optimal one. It is evident that, an EV can reduce its unit energy price by almost 50% by increasing its deadline by 1 hour. In the decentralized method, the average unit price also seems to be behaving in the same fashion, where each EV tries to minimize its price after playing a non-cooperative game. We observe that the relation between unit price with deadlines in game 2 is identical with the centralized model, which proves that the solution of game 2 is optimal. On the other hand, though game 1 also shows the tendency of decreasing price with the increment of deadline, the solution is slightly deviated from the optimal solution.

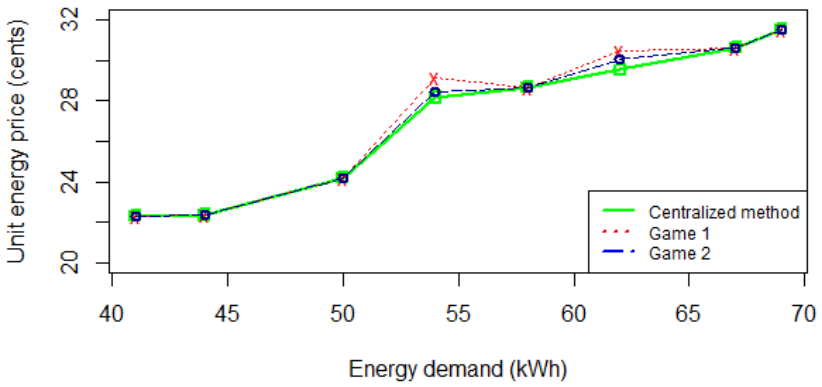

Figure 4.7: Unit price variation with demand.

Next, intuitively the unit energy price should also be influenced by the aggregated energy demand. We depict the relation of the charging price with the respective aggregate demand in Fig.4.7 to analyze this influence. We assume a set of EVs having different amount of energy requirement, which start their charging at slot 0 and finish by slot 6. All three algorithms show that the unit energy price increases with the demand. For all three algorithms, the unit price increases slowly at the beginning and then suddenly spikes when the demand increases from 50 kWh to 55 kWh; this increment in the demand for energy may force the particular EV to charge at a higher rate for certain period of charging time to be able to meet its deadline, which implies a higher price of charging. The centralized method shows that the optimal solution and the output of both game theoretic models are almost identical with that. The deviation from optimal solution is slightly higher in game 1 in comparison with game 2. This sort of deviation of game 1 from optimal solution was also found in Fig.4.6, where unit price variation was analyzed with respect to deadlines. Actually a slight variation in charging pattern of the same EV in the two games causes the deviation, as mentioned above. To explain this phenomenon, we choose an EV having energy requirement of 45 kWh from a fixed set of EVs. This particular EV intends to charge between slot 0 to slot 6. Now this set of EVs was scheduled using both games. Fig.4.8

depicts the charging pattern of this particular EV for both game theoretic models. It is evident that, charging pattern is slightly varied from game 1 to game 2; in game 1 the EV charges at maximum rate in three time slots, where in only two time slots using game 2. This difference in charging pattern helps to understand the variation in pricing between game 1 and game 2 for few of the EVs, which was already shown in Fig.4.6 and Fig.4.7.

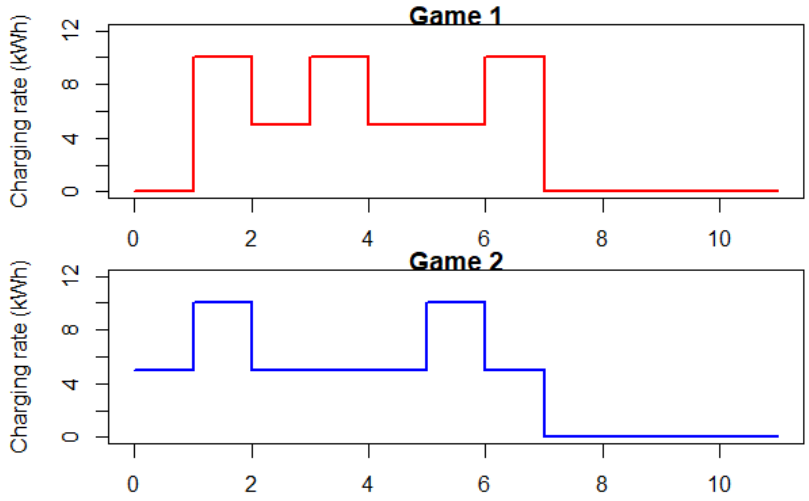

Figure 4.8: Charging pattern comparison between game 1 and game 2.

Another important feature of our model is its prediction of PV energy profile at the beginning of each time slot to avoid the aberration, rather than relying on a long term prediction at the onset of the scheduling horizon. To analyze the impact of this continuous assessment, we run game 2 for 80 EVs with different deadlines in two different scenarios. In one condition, we just predict the PV generation for all upcoming slots at the beginning of time horizon and in the other, we revised it after each time slot m. The results are presented in Fig.4.9 where we show the unit price vs. the deadlines only of those EVs which start their charging at slot 0 having same energy requirement but different deadlines. It is shown that for EVs with deadlines that are lower than 105 min, the price under both conditions is the same. This is true since for a shorter time period, the deviation between the expected predicted

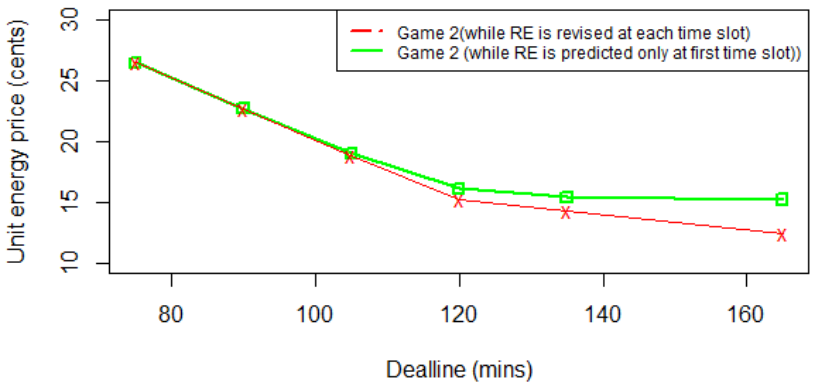

Figure 4.9: Unit price variation with PV generation.

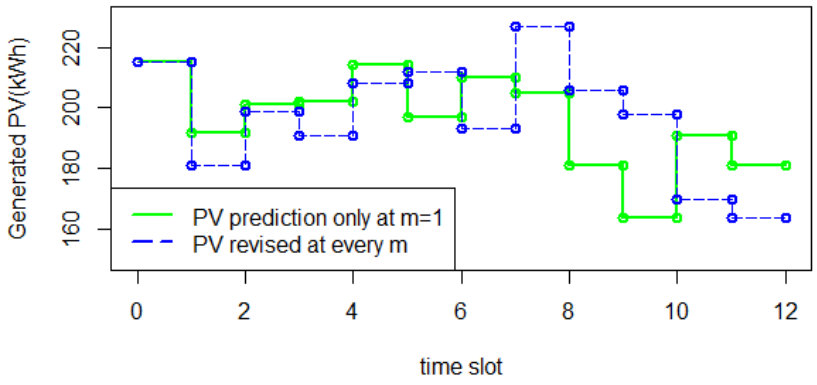

Figure 4.10: PV energy profile.

energy and the one that is generated at each time slot is not very high. To validate this scenario, we may check Fig.4.10, where the deviation from predicted value of PV energy is clearly much smaller for shorter time period rather than longer one. As per example, at slot 2, the real generation of PV is deviated by 5% from the predicted value, where this deviation is increased as almost 10% for slot 7 and more than 10% for slot 11. Hence, for EVs staying longer in the system, i.e. with higher deadlines, when PV energy is not corrected, the error or deviation with the actual becomes higher, and ultimately affects more on price. Whereas, if the PV is predicted at each time slot, the error with actual is smaller, and hence scheduling decisions made by the EVs are more informed.

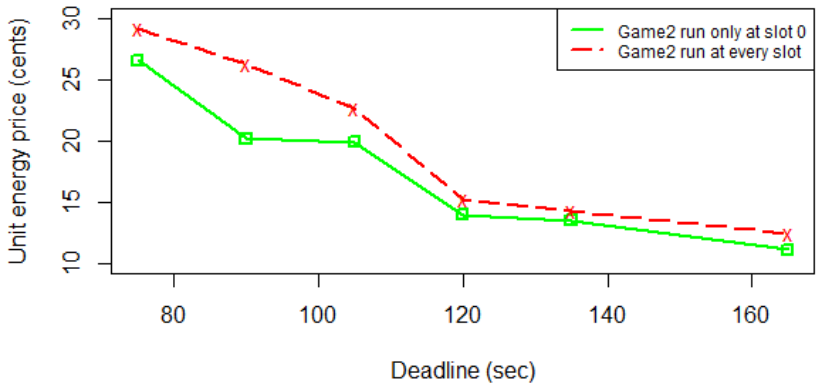

Figure 4.11: Comparison with super idealistic assumption.

Throughout our discussions, we assumed that at each time slot m, in addition to knowing the set of vehicles currently in the system $I(m)$, we also assume an anticipated incoming load $I^{'}$(m), and at each time slot $I^{'}$(m) is re-evaluated (only in centralized method and game 2); at each m, both EVs in $I(m)$ and $I^{'}$(m) will be used to determine the charging schedule as well as the unit price. The objective of this is to be cautious in scheduling currently available EVs, since current actions would affect future actions as the state of the system changes in the future with new arrivals and changing energy generation. To evaluate the effectiveness of this approach, we assume a somehow idealistic scenario where at the onset of the horizon, i.e., slot 0, we have a complete knowledge of the exact set of EVs at each time slot. We compare game 2 under both the realistic and idealistic scenarios, and the results are shown in Fig. 4.11. We assume all EVs have the same demand, but their deadlines are different. The figure shows the charging unit price for different deadlines. Clearly, both exhibit a decreasing price with longer deadline, which is expected since EVs with larger deadlines may be more flexible in shifting their charging to other time slots where either demand is lower or sufficient energy is available either from PV or from the ESS. However, EVs with stricter deadlines are less flexible and end up requesting higher charging rates to meet their deadlines, but at higher price indeed. Now, when the

exact load is known throughout the scheduling horizon, i.e., idealistic scenario, a more informed decision is made by the game to globally optimize the schedule of all EVs. Thus, not surprisingly this method exhibits a lower unit price in comparison with the realistic scenario where the estimate of $I^{'}(\mathrm{m})$ may not be accurate. In particular, the results show that EVs with stricter deadlines are more affected by the uncertainties in demand prediction, i.e., larger price deviation with ideal scenario, since those players of the game may not have enough time to compensate for decisions they have made in the few time slots they had to charge. EVs with larger deadlines have only slightly higher unit price, because they are in the system for a longer period and have more opportunities to modify their strategies for selecting suitable charging rates.

Now, to assess the performance of our model, we have taken Tushar et al. [136] as an example, where they design a Stackleberg game among a set of EVs which try to determine their charging rates for each time slot as either zero or maximum, while the grid changes the price to make its revenue higher. As the objective [136] is different than ours, instead of making a direct comparison, we have just taken their strategy set (i.e., an EV charges its battery either at maximum rate or restrain itself from charging) and test our model maintaining the same utility function. Fig.4.12 depicts that though unit energy price is increasing with the average demand of the set of EVs for both strategy sets, our one is more capable to minimize the price. As an example, for an average energy demand of 40 kWh, according to our model, the unit price is \$0.20 where it is almost \$0.26 for the other, i.e., our model reduced the unit price by almost 23% than demonstrated in [136]. By considering two more intermediate charging rates between zero and maximum, our model actually provides more flexibility to EVs to charge at lower price. On the other hand, EVs have to charge at maximum rate to fulfill their demand in [136] and experience a higher unit price. The unit price difference between these two strategy sets is becoming lower

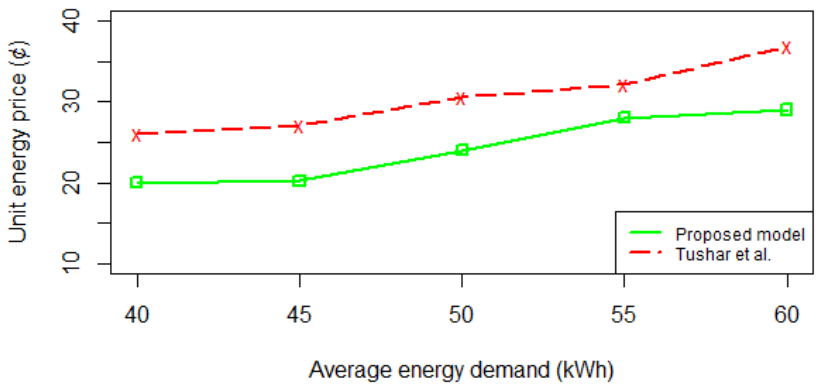

Figure 4.12: Performance comparison with a published model [136].

with the increasing average energy demand, e.g., for a 55 kWh of average energy demand, the unit price difference is decreased to $0.04, when it is almost $0.06 for a 40 kWh average energy demand and the reason behind this is that for a higher energy demand, even our model forces a larger number of EVs to select maximum charging rate for a higher number of slots to maintain their deadline.

Finally, all three models are compared in terms of their computation times. Using C++ platform, IBM Cplex optimizer was run to solve all three models for different set of EVs on an Intel(R) Core(TM)i7-6700 CPU having a speed of 3.40 GHz to examine their scalability. Table 4.2 shows that the decentralized method is much faster than the centralized method as we expected earlier. In the decentralized method, all EVs play simultaneously to select their charging strategies, while in the centralized system, the optimizer solves an ILP to make decision for all EVs. As a consequence, game based models are much faster than the centralized model, e.g. for 40 number of EVs, the centralized method took 998 sec while the decentralized method took just almost 3 sec. The run time would be increased with the number of EVs in both methods. But the finding shows that the decision making time is not varied a lot by the total number of players in the decentralized method, e.g. 2.2 sec is required when total players are 20 and this time is 2.9 sec for 40 number of total players. On

the other hand, the centralized method takes more time for higher number of EVs, e.g. 168 sec is required by the optimizer for scheduling 20 EVs while it would be 998 sec for 40 EVs. Another important observation is that both game methods almost require the same time for making the decision in identical conditions. Hence, it can be concluded that game 2 algorithm performs best among all; not only for providing optimal solution but also for moderate decision making time.

Table 4.2: Comparison on Computational Time

No. of EVs	Centralized Method	Game 1	Game 2
10	72 sec	2.0 sec	2.4 sec
20	168 sec	2.2 sec	2.5 sec
30	441 sec	2.3 sec	2.4 sec
40	998 sec	2.9 sec	3.7 sec
100	1496 sec	7.3 sec	7.6 sec
200	–	12.6 sec	13.1 sec
500	–	15.1 sec	15.7 sec

4.6 Conclusion

Users' satisfaction should get most priority to promote the EV market. Getting required energy inside targeted deadlines at minimum price, rather than the cleanliness of the energy source, is a major key to satisfy EV owners. However, green energy sources need to be incorporated for achieving the anticipated benefits of EVs in mitigating global warming and energy scarcity. Hence, a smart CS is assumed here, which uses a PV system integrated with an ESS to charge EVs at variable rates. A quadratic price function is proposed, that ensures the equity among the EVs, i.e., an EV can enjoy a higher charging rate only by paying more. As PV is the only energy source, when few EVs are charging at higher rates, others have to charge slowly at lower price. This load shifting mechanism together with an ESS help accommodate the EV charging. Moreover, to avoid sudden load congestion, upcoming load forecast

is considered during scheduling of current EVs and a short term PV prediction is applied to predict the energy profile. To handle the uncertain behavior of both the load request and PV generation, a frequent prediction is made. Actually both are predicted after each time slot of 15 min and the significance of this frequent prediction over charging price minimization is analyzed. The model is examined in both centralized and decentralized methods. Though the centralized method is capable of providing optimal solution, it takes a very long time in making a decision, specially for a large number of EVs. To mitigate this computational problem, two different types of game theoretic algorithms are proposed here, game 1 and game 2. The only difference between them is that in game 2, players consider the upcoming load requests while they select their strategies for minimizing the price. In both algorithms, each player makes her own decision simultaneously after playing a non-cooperative game and as a consequence decision making time is very fast here. Nash equilibrium is proven for both methods and game 2 is shown to attain the optimal solution.

Chapter 5

Joint Routing and Scheduling of Mobile Charging Infrastructure for V2V Energy Transfer[1]

In chapter 4, a set of EVs were scheduled for charging at minimum price in a PV based standalone CS to depict a management system of handling a green CS to curtail the dependency over the grid and consequently, reduce the carbon emission. But whatever the energy source of a CS, an EV has to reach there before depleting the battery and as a ramification, an auxiliary solution is required to support EVs for emergency energy scarcity. Hence, in this chapter, a company is assumed which has a set of V2V enabled charging trucks to charge a set of EVs to provide the flexibility of EV charging in terms of place and time. A joint routing and scheduling problem is addressed and solved here for those trucks to maximize the number of served EVs.

[1]This chapter is accepted in IEEE Transactions on Intelligent Vehicles [68] and partially presented in IEEE PESGM'2020 [67]

5.1 Motivation

The higher upfront installation cost or their geographical placement may make the CS network expansion challenging and somehow non-profitable. For example, the Ontario, Canada government has taken a 20 million dollar project to deploy 500 fast chargers in public places and 55% of them are already in service [54]; unfortunately, users' feedback indicate that most of the established CSs are under utilized. Beside this, a massive CS deployment may also have a substantial impact on power distribution grids in terms of imposing new peak and degrading the power quality [100]. As a ramification, power utility companies also need to invest a lot to enhance their network and generation capacity. Hence, a set of auxiliary technologies need to be elaborated to support such grid connected CS network to mitigate the range anxiety; a contender solution would be to explore the bidirectional energy transfer capabilities of EVs (especially vehicle to vehicle (V2V)) for energy transfer between vehicles' batteries.

V2V offers an opportunity when a vehicle is unable to reach a CS, whereby a *mobile charging station* is dispatched to serve an EV charging request at its location; this model for electric charging service breaks the dependence on a fixed charging infrastructure, by bringing the service closer to the end user. Being independent from the charging infrastructure, and hence the grid connection, V2V promotes a new business at commercial scale, especially where installing a permanent infrastructure might not be profitable.

AAA, a US company, has already converted this concept into reality by launching a number of trucks to charge EVs [26]. All these trucks are equipped with generators and level two chargers. In fact, few of them are equipped with CHAdeMO fast chargers. Meanwhile, Rivian, another automobile company, introduces V2V charging to transfer energy from one Rivian car to another to ameliorate the range anxiety [125],

while Hyundai provides this service for its Kona electric cars in some selected cities such as Delhi, Mumbai, Chennai, and Bengaluru in India [82]. The lack of charging infrastructure in India makes the initiative of Hyundai significant and indicates the prospect of V2V in EV charging.

Since, the V2V enabled technology is still very new as we discussed in Section 2.2.1, as per our best knowledge, still no one has designed a V2V enabled service for commercial purpose. As a consequence, we design a strategical scheduling and route selection of charging EVs/trucks of a V2V energy provider company to maximize the served number of EVs.

5.2 Problem Definition and Contributions

Accelerating the acceptance of EVs by the public mandates facing the growing demands to address range-anxiety issues and an adequate charging infrastructure would help in improving customers' experience. While much work has been done on provisioning, deployment and management of fixed charging infrastructure, this chapter considers a parallel, but integrated, approach for dealing with range anxiety, namely exploring the usability of mobile charging service which is enabled by the emerging technology of V2V.

A number of EV users sends their requests to the company to receive charging service; each request contains a time window (start and finish times) as well as a demand. Users also declare their locations (any one of the parking spots advertised by the company) at the beginning of the charging window. The company intends to dispatch trucks to satisfy EV users charging requests while satisfying the battery capacity restrictions of each truck. Hence, a dispatched truck has to return to the depot before fully depleting its battery after charging the assigned EVs. The objective is to maximize the number of served EVs to fulfill their energy demand inside their

charging windows using the available number of trucks. We assume a mobile EV charging company owning a set of charging trucks to recharge EVs through V2V technology. The company has a depot where the trucks park and charge their batteries (e.g., off peak or through a third party energy trader). Each of these trucks is assumed to be equipped with a very large battery pack to store energy along with an on board fast chargers.

The contributions of this work are listed below:

- We determine routes and schedules for a set of charging trucks to charge a number of EVs through V2V energy transfer.
- Considering the deadlines of EVs and the battery capacity of each truck, we design a mathematical model to optimize the routes and the schedules of charging trucks to maximize the served number of EVs. We formally prove that such combinatorial problem is NP-hard.
- To reduce the computational complexity and time of the designed NP-hard model, we apply a Dantzig-Wolfe decomposition method to separate the problem in a master and a set of pricing problems (one for each EV instead for each truck to avoid a multiple travelling salesmen scenario which is a well known NP-hard problem). Our proposed decomposition method is compared with two other heuristic approaches.

5.3 Mathematical Model and Formulation

5.3.1 System Model

We consider a city where a mobile charging service is provided by company which operates to charge EVs (through V2V technology) by dispatching a limited number

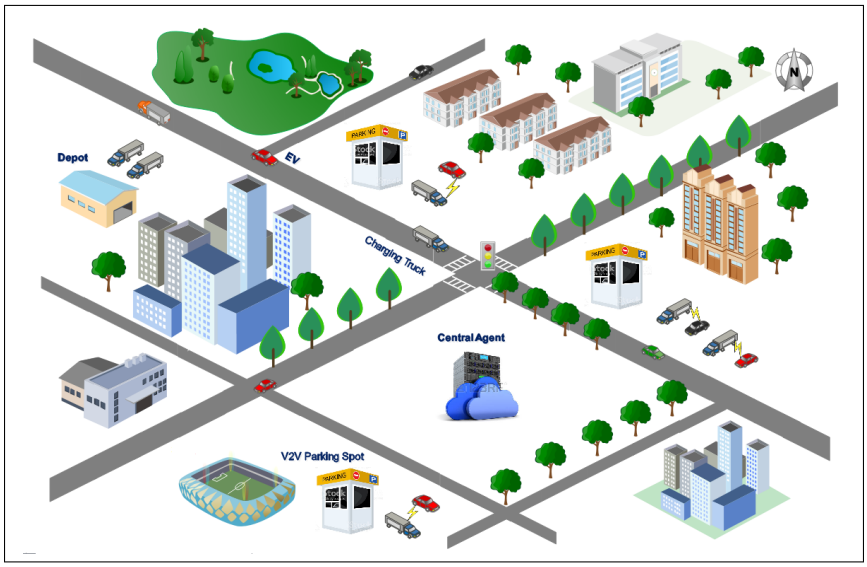

Figure 5.1: V2V enabled EV charging model.

of charging trucks as shown in Fig. 5.1. This company has a depot, where trucks are parked and charged. We assume that the company has a set of charging trucks T and each truck $t \in T$ has an equal battery capacity of C kWh. The company has a central agent which receives charging requests from buyer EVs $v \in V$ (V denotes the set of buyer EVs) to purchase energy. We assume a time horizon and at the beginning of the time horizon, all buyers EV submit their requests to the central agent along with the energy demand E_v and the time window w_v to purchase the energy. The time window of EV $v \in V$, w_v starts at δ_v (time when the EV v is available to charge its battery) and finish at Δ_v (after Δ_v, EV v is assumed to be unable to receive charging services). Each EV v reports its position (x_v, y_v), which should be one of the predefined parking lots by the company. On the other hand, from the depot, a charging truck $t \in T$ starts its journey with the full battery capacity C to serve a number of EVs and should return back to the depot before its battery is fully depleted. For simplicity, we assume an average speed m for all charging trucks during their travel and e amount of energy is assumed to be required by any truck to travel each kilometer. All entities (e.g. depot, seller trucks and buyer EVs) are assumed to be connected with a central

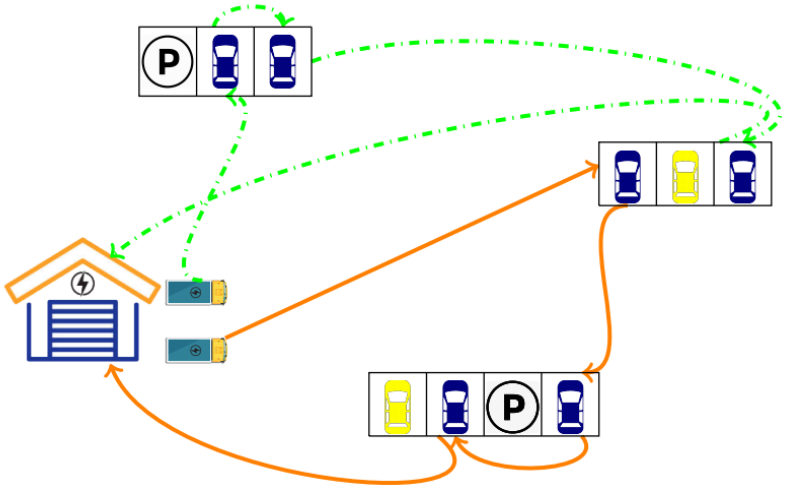

Figure 5.2: Load allocation & trajectory selection for seller trucks.

agent as shown in Fig. 5.1.

The central agent gathers all requests (submitted by EVs) and subsequently, the central agent decides how to dispatch a number of trucks to meet the maximum number of buyers' energy demand. As an example, in Fig. 5.2, the central agent receives 8 charging requests, while it has two charging trucks at its depot. Each request is assumed to have different energy demand and charging window. The central agent allocates these two trucks to maximize the number of served EVs. There are a number of combinations to dispatch these two trucks to charge EVs and only an optimal combination can ensure to charge maximum number of EVs. As an example, Fig.5.2 depicts a route selection of these two trucks where each truck serves 3 EVs (blue color EVs are served) in the shown order and before battery depletion, each truck also goes back to the depot. Other two EVs (yellow colored EVs in Fig. 5.2) cannot be served with this decision. The objective is then to determine the optimal route and schedule of trucks to maximize the served number of EVs (an EV should be charged up to the declared demand inside the declared charging window).

Table 5.1: List of input parameters

Input symbols	Description
T	set of charging trucks t
$C \in \mathcal{R}^+$	battery capacity of any truck t
$m \in \mathcal{R}^+$	speed of any truck t
$e \in \mathcal{R}^+$	energy required by any truck t to cross 1 km distance
$\zeta \in \mathcal{R}^+$	charging rate offered by any truck t
$l_d \in \mathcal{R}$	location of the depot as (x_d, y_d)
V	set of buyer EVs v
$E_v \in \mathcal{R}^+$	energy demand of buyer EV v
$l_v \in \mathcal{R}$	location of buyer EV v as (x_v, y_v)
w_v	charging window of EV v as $w_v = [\delta_v, \Delta_v]$

Theorem 5.3.1. *The problem described above is a strong NP-Hard problem.*

Proof *Consider an instance of the well known NP-Hard scheduling problem $P|r_i|\sum U_i$ where we want to schedule jobs $J = \{j_i : i \leq J_n\}$ each with a release time r_i, deadline d_i and processing time p_i over a multiple machines to maximize the throughput. This problem can be reduced to our problem in polynomial time as follows. Each job j_i can be mapped into a vehicle $v \in V$ with starting (available for charging) time δ_v equals to r_i and the deadline Δ_v equals to d_i. The required charging time (E_v/ζ) of an EV v can be mapped to p_i, the capacity of a truck can be considered as the capacity of a machine. This reduction takes only polynomial time. And, hence the defined problem is NP-hard.*

5.3.2 Mathematical Formulation

An ILP (Integer Linear Program) is designed here to determine trucks' optimal routes and service order of EVs in order to maximize the served number of EVs using a limited number of charging trucks .

Parameters: The input parameters for the model are listed in Table 5.1.

Decision variables: A binary decision variable γ_{vto} is declared to decide whether

EV v would be charged or not.

$$\gamma_{vto} = \begin{cases} 1 & \text{if EV } v \text{ is charged by truck } t \text{ in an order of } o \\ 0 & \text{otherwise} \end{cases} \tag{5.1}$$

Here, service order o is a positive integer to indicate the order for an EV by which that is served by a particular truck. As an example, a truck t serves the EV v at an order o means, this truck t has served $(o-1)$ number of EVs before serving this EV v. As the total number of vehicle is $|V|$, the maximum value of o can be $|V|$.

The other decision variable $\tau_v \in \mathcal{R}^+$ is declared to determine the charging starting time of EV v.

Objective: The objective of our model is to maximize the number of served EVs.

$$max \sum_{v,t,o} \gamma_{vto} \tag{5.2}$$

Job allocation and service order constraints: An EV v only can be charged by only one truck t in a particular order o or not to be charged at all:

$$\sum_{t,o} \gamma_{vto} \leq 1; \forall v \in V \tag{5.3}$$

The following equation ensures that a truck t can serve only one EV v at a particular order o:

$$\sum_{v,o} \gamma_{vto} \leq 1; \forall t \in T \tag{5.4}$$

A truck t can serve EV v in order $o \geq 2$ if and only if this truck serves another

EV v' with an order of $(o-1)$:

$$\gamma_{vto} \leq \sum_{v'} \gamma_{v't(o-1)}; \forall v, o \geq 2, t \tag{5.5}$$

Charging window constraints: The charging process of an EV v cannot be started before its declared window $w_v = [\delta_v, \Delta_v]$:

$$\tau_v \geq \delta_v; \forall v \tag{5.6}$$

here, τ_v is the starting time of charging for EV v.

And the charging process of EV v should be finished by the deadline Δ_v:

$$\tau_v + \frac{E_v}{\zeta} \leq \Delta_v; \forall v \tag{5.7}$$

here, $\frac{E_v}{\zeta}$ is the required service time to charge EV v.

Trucks trajectories constraints: Eq. (5.8) confirms that to serve the EV v having the order $o = 1$, truck t should leave the depot and reach to EV v by τ_v.

$$\gamma_{vt1}\tau^t_{dv} \leq \tau_v; \forall t, v \tag{5.8}$$

here, τ^t_{dv} indicates the required time for truck t to reach EV v from the depot.

After serving EV v' in an order $o-1$, a truck t needs to maintain the following constraint to serve EV v in an order of o.

$$\sum_{o} (\gamma_{vto}\gamma_{v't(o-1)})[\tau_{v'} + \frac{E_{v'}}{\zeta} + \tau^t_{vv'}] \leq \tau_v; \forall t, v, v', o \geq 2 \tag{5.9}$$

here, $\tau^t_{vv'}$ is the required time by truck t to reach EV v after charging EV v' and $\frac{E_{v'}}{\zeta}$ is the time required to charge EV v'.

Energy constraint of trucks: A truck t cannot spend more than C amount of energy for travelling and charging EVs. The following constraint ensures this.

$$\tau_T^t me + \sum_{v,o} \gamma_{vto} E_v \leq C; \forall t \tag{5.10}$$

where, the total travel time τ_T^t of truck t can be calculated as follows:

$$\begin{aligned} \tau_T^t = & \sum_v (\gamma_{vt1} \tau_{dv}^t) + \sum_{v,v',o\geq 2} (\gamma_{vto} \gamma_{v't(o-1)} \tau_{vv'}^t) \\ & + \sum_{v,v',o\geq 2} ((1-\gamma_{vto}) \gamma_{v't(o-1)} \tau_{dv'}^t); \forall t \end{aligned} \tag{5.11}$$

where τ_{dv}^t is the distance from depot to vehicle v and $\tau_{vv'}^t$ is the distance between vehicle v and v'.

5.4 Dantzig-Wolfe Decomposition Model

As indicated earlier, the defined problem is NP-hard and is expected, as will be also shown later, to be computationally very complex. The objective of the program is to maximize the number of served EVs by determining the optimal route and schedule of a set of trucks; this might be viewed as a multiple number of travelling salesman problems having service windows for customers. Hence, solving the designed ILP might be time consuming especially for realistic instances (i.e., a larger number of charging requests and charging trucks) and might not be applicable in practical purposes. As a ramification, we seek a more scalable methodology, which provides a good (optimal or closer to optimal) solution as well. To attain such a good and quick solution, we decompose our problem by using the Dantzig-Wolfe decomposition

approach. We design our Dantzig-Wolfe decomposition model (DWDM) where the original problem (formulated as an ILP) is divided into a master problem and a set of pricing problems (one for each EV). However, a similar decomposition approach that can be used to solve this problem is the Lagrangian relaxation. Such approach is efficient when there is an easy way to derive an efficient solution from the infeasible relaxed solution. Obviously, our problem does not have this property due to the complex set of constraints it has.

Now, by inspecting the ILP formulation, we find that there are several ways to decompose the problem. The very direct, but naive, way of decomposing it is the per-truck decomposition. Such a decomposition will end up with multiple salesman problems (one for each truck). This might lead into a gain in the speed of the computation, but still may not be scalable enough. Instead, we propose to decompose the problem through an EV-wise decomposition which leads, as we will see later, into a very simple pricing problem which is solvable by a simple greedy fashion. The challenge in the proposed decomposition lies in how to break down the original problem into the master problem variables/constraints and the pricing problems variables/constraints as well as the integration between the pricing problems solutions, as columns, and the master problem. This is a consequence of the considerable linearization amount required and the tidy number of constraints/variables that bind the EVs together (e.g., Eq. (5.5), Eq. (5.9) and Eq. (5.10)).

As stated, after the decomposition, we end up with one master problem and several pricing problems (one for each EV). The master problem is a Linear Program (LP) and is initialized with a subset of configurations (columns) that satisfy all the constraints of the master model (a feasible solution is obtained). The problem might have an exponential number of feasible solutions and any one could be taken to initialize the master problem. However, after the initialization, the LP is solved and then the

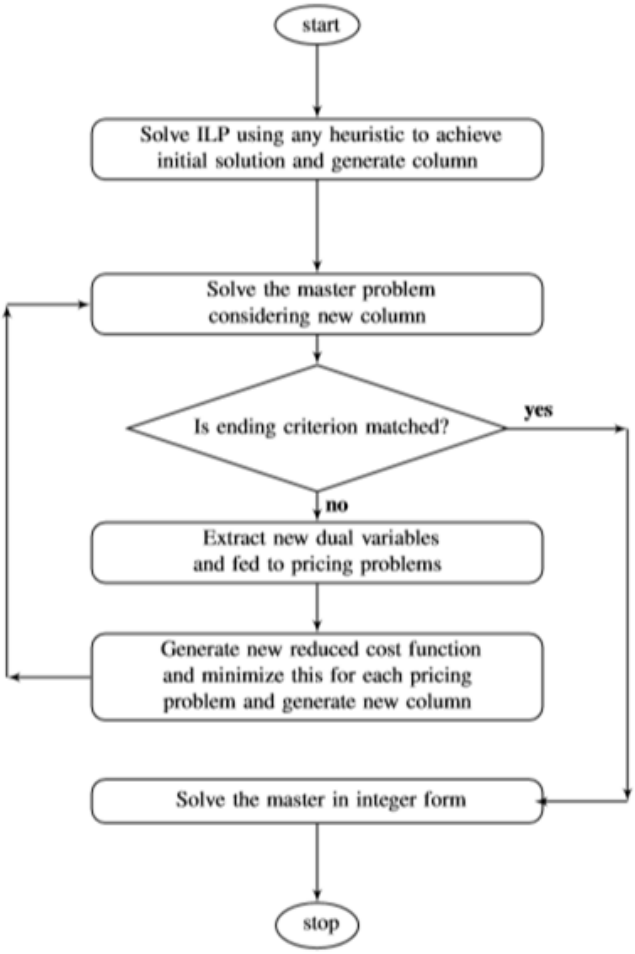

Figure 5.3: Flow diagram for the Dantzig Wolfe decomposition method.

dual values of each constraint are extracted to build the reduced cost function for each pricing problem. The pricing, which is a separate model for the dual LP of the master, tries to optimize the reduced cost function. As our main problem is a maximization problem, each of the pricing problems intends to minimize the respective reduced cost function to generate new columns i.e., new feasible solutions. These new columns are added to the master and the master problem is solved again and generates new values of dual variables. And using these new dual variables, new reduced cost functions are formed and fed to pricing problems to generate new columns. This iteration goes on until a pre-specified criteria is reached. In our problem, the master problem is

solved through the barrier interior point algorithm as it is a pure linear program (LP) and the pricing problems are solved by a greedy heuristic. The overall process of our DWDM are illustrated in Fig. 5.3 and discussed in subsequent subsections.

5.4.1 Master Problem

As we generate a solution for each EV by solving pricing problems, those constraints of the original problem (i.e., ILP), which deals with more than one EV i.e., Eq. (5.5), Eq. (5.9) and Eq. (5.10) should be satisfied by the combined solutions (i.e., by the generated columns) in the master problem. Let, S_v be the feasible solution set, while $s \in S_v$ is a feasible solution i.e., a column and the designed master problem is a LP (linear program). The master problem model is the following:

$$max \sum_{v,t,o} \sum_{s \in S_v} \lambda_s \gamma^s_{vto} \tag{5.12}$$

$$\sum_{s \in S_v} \lambda_s \gamma^s_{vto} \leq \sum_{s \in S_v} \lambda_s \sum_{v'} \gamma^s_{v't(o-1)}; \forall v, v', o \geq 2, t \tag{5.13}$$

$$\sum_{s \in S_v} \lambda_s \sum_{o} (\gamma^s_{vto} \gamma^s_{v't(o-1)})[\tau^s_{v'} + \frac{E_{v'}}{\zeta} + \tau^t_{vv'}] \leq \sum_{s \in S_v} \lambda_s \tau^s_v \; ; \forall t, v, v', o \geq 2 \tag{5.14}$$

$$\sum_{s \in S_v} \lambda_s (\tau^{st}_T me + \sum_{v,o} \gamma^s_{vto}) E_v \leq C; \forall t \tag{5.15}$$

$$\sum_{s \in S_v} \lambda_s = 1, \forall v \tag{5.16}$$

$$\lambda_s \in R^+ \qquad \forall s \in S_v \qquad \forall v \in V \tag{5.17}$$

As discussed in the previous section, the possible number of columns of the master problem is exponential, decision variable, λ_s helps avoid including all the possible columns of a problem in the master model tableau. As the master problem is a LP, before applying constraints (5.14) and (5.15), we have to linearize Eqs. (5.9) and (5.11). The linearized forms are provided in the appendix.

5.4.2 Initial Solution

As we mentioned earlier, at the beginning, the master problem is initialized with a simple solution. To attain this feasible solution, we solve the problem (ILP) using a heuristic approach, where a truck seeks the EV having the shortest deadline. If more than one EV have same deadline, the truck follows the shortest path i.e., the EV nearer to the truck will be served first. After scheduling the first EV, the truck again searches the next EV and so on. A truck can serve an EV only if it has enough energy and time to charge that EV inside the declared charging window and has enough energy to return back to the depot. After determining the route and schedule of one truck, the route and schedule of another truck (if available or if required) is determined in the same fashion. By this way, the algorithm maximizes the number of served EVs using a limited number of trucks.

5.4.3 Pricing Problems

Designing a pricing problem for each truck would create a travelling salesman problem (a well known NP-hard problem); as a ramification, our NP-hard problem would end up as a multiple number of NP-hard problems. Hence, we design a pricing problem for each EV instead of each truck.

Let, α_{ot}, β_g, ϕ_t and σ_s be the dual variables associated with constraints of (5.13),

Algorithm 5.1 Pricing problem Algorithm

procedure PRICING PROBLEM($\boldsymbol{t}, \boldsymbol{v}, \boldsymbol{\Phi}, \Psi_v, \delta_v, \Delta_v, E_v, \zeta$)
  $\boldsymbol{\gamma_{vt}} \leftarrow \mathbf{0}$ ▷ vector of all γ_{vto}
  $\tau_v \leftarrow 0$
  if $\psi_v > 0$ **then**
    $\tau_v \leftarrow \delta_v$
  else
    $\tau_v \leftarrow \Delta_v - E_v/\zeta$
  end if
  $o \leftarrow_o \Phi_{v,t,o} * \gamma_{vto}$
  $\gamma_{vto} \leftarrow 1$
  return $\boldsymbol{\gamma}, \tau_v$
end procedure

(5.14), (5.15) and (5.16) respectively. We assume that $G = \{g = (o, t, v, v') : o \geq 2, \{v, v'\} \in V, v \neq v', t \in T\}$ to represent the subscript of the variables of the linearized constraints and their subsequent dual variables. The objective of the pricing problem is to minimize the reduced cost function which is calculated from the dual variables of the Master problem. The reduced cost function of EV v ($RC_v(t, o)$) for a combination of truck and order (t, o) can be calculated as follows:

$$RC_v(t, o) = \Phi_{vto}\gamma_{vto} + \Psi_v\tau_v - \sum_{t,o} \gamma_{vto} + \Theta_v \tag{5.18}$$

Φ_{vto}, Ψ_v and Θ_v are the summation of corresponding dual values achieved from the master problem. The detailed calculation of Φ_{vto}, Ψ_v and Θ_v is given in the appendix.

Since the pricing sub-problem solves the problem for each single EV, the same parameters and decision variables of the original problem are used in the pricing sub problem. Hence, the pricing problem for EV v can be expressed as:

Objective:

$$\min_{t,o} \; RC_v(t,o) \tag{5.19}$$

such that:

Eqs. (5.3),(5.4) and (5.6)-(5.8) are the constraints.

The direct way of finding the minimum combination is going through all the combinations of (t, o), calculate the reduced cost (through algorithm 5.1 as we will discuss below) and pick up the (t, o) with minimum reduced value. But doing so will give a higher chance for the trucks that appear in the beginning of the trucks list to get assigned vehicles more than the others. This approach will after all end up with the minimum upper bound but as the vehicles have limitations in terms of charging rates, speed and capacity, the integer version of the master model will fail to use the columns generated using this approach to come up with a good integer solution. To overcome this problem, we adopted a round-robin approach where in each iteration of the CG algorithm, we generate columns for only one truck. This will give a better chance for all the trucks to be assigned more EVs.

To attain a quicker solution, instead of solving an ILP for each pricing, a greedy approach is adopted to solve the pricing problem as shown in Algorithm 5.1. This algorithm starts by initializing the output variables. Then it checks whether the term Ψ_v is positive or negative. If it is negative, it assigns τ_v its maximum possible value which is the time window deadline (Δ_v) minus the time to charge the EV (i.e., E_V/ζ). After that, it finds the order that makes the first term of the reduced cost function appears in Eq. (5.18) to be minimum. This is done obviously by finding the minimum Φ_{vto} term.

5.5 Numerical Evaluation and Discussions

To evaluate the performance, we assume a metropolitan city like Montreal having a length of 54 km and a width of 16 km [33]. We randomly choose the positions for the depots and the set of parking lots in the city. We also consider a set of EVs having different charging demands and deadlines (period of charging), and assume the demands and charging windows follow a truncated Gaussian distribution [74]. A set of trucks is considered having each a battery capacity of 250 kWh [41] along with a fast charger having a charging rate of 40 kW [76]. For simplicity, we consider a constant speed of 60 km/h for all trucks and 0.9 kWh energy is required to travel 1 km [89]. Using a C++ platform, IBM Cplex optimizer was run on an Intel(R) Core(TM)i7-6700 CPU having a speed of 3.40 GHz to solve these algorithms.

We examine and compare the computational time of the ILP with our solution, the DWDM model. Since also DWDM is a complex model itself, hence we also seek solutions from two different heuristic approaches to examine the competency of the DWDM model. The heuristic approaches are as follows:

- Strictest Window Shortest Path First (SWSPF): A truck seeks the EV having the strictest charging window. If more than one EV have same widow length, the truck follows the shortest path i.e., the EV nearer to the truck will be served first. After scheduling the first EV, the truck again searches the next EV and so on. A truck can serve an EV only if it has enough energy and time to charge that EV inside the declared charging window and has enough energy to return back to the depot.

- Shortest Demand Shortest Path First (SDSPF): The only difference of SDSPF over SWSPF is to search the EV to charge based on minimum energy demand instead of minimum window length. Similar to SWSPF, SDSPF also follows

the shortest path algorithm when more than one EVs have the same energy demand.

Table 5.2: Performance evaluation of different algorithms

	Efficiency (Served EVs per truck)					Computational time (sec)				
No. of trucks	$\|T\|=1$	$\|T\|=2$	$\|T\|=3$	$\|T\|=4$	$\|T\|=5$	$\|T\|=1$	$\|T\|=2$	$\|T\|=3$	$\|T\|=4$	$\|T\|=5$
ILP	8	7.5	6.66	-	-	38	197	37600	-	-
DWDM	7	6.5	6.33	5.75	5.8	113	213	419	870	1360
SWSPF	3	4	4.3	4.75	4.8	0.01	0.03	0.04	0.06	0.1
SDSPF	3	5	5.33	4.75	4.6	0.01	0.04	0.06	0.07	0.1

We start by first considering a scenario with 40 EVs, each sending its request for charging. The energy demand of each EV follows a truncated Gaussian distribution with a mean of 30 kWh and the width of charging window also follows another truncated Gaussian distribution having a mean of 3 hrs. The number of parking lots is 5 and all EVs select one of these 5 parking lots as their potential location at the beginning of this charging window. To assess the performance, we introduce a term, efficiency which indicates the total number of served EVs by each truck. Table 5.2 indicates that though the ILP provides the optimal solution, the computational time is too large to be applicable in practice especially for a large number of requests. The computational time is more than ten hours for an instance where the number of EVs is 40 and number of trucks is 3. Even for $|T|= 4$, the system runs for too long to achieve a solution and that is why the outcome is not shown here. On the other hand, though the computational time of DWDM is much higher than both heuristics (SWSPF and SDSPF), but much lower than the ILP, the efficiency of DWDM is closer to the optimal one. As an example, when 3 trucks are considered to serve these 40 EVs, DWDM shows an efficiency of 6.33 EVs/truck while this is 5.33 EVs/truck for SDSPF and 4.3 EVs/truck for SWSPF.

Now, recall that the performance of DWDM model is directly influenced by the initial solution (i.e., initial columns to the master problem which is generated from

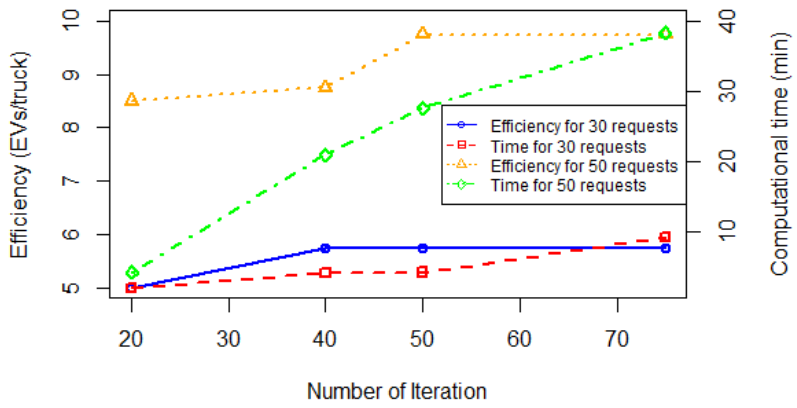

Figure 5.4: Efficiency and required time analysis for DWDM.

a heuristic approach) and the number of iterations (i.e., generated columns from the pricing problems); hence, to attain a better solution, the iterations as we solve should continue till convergence. For larger problem instances, convergence may require too many iterations and consequently, might become of less practical significance. Accordingly, there is a trade-off between achieved performance and computational time of the DWDM model. Fig. 5.4 illustrates the efficiency and required computational time for two different numbers of charging requests while the number of trucks is 4. The efficiency of DWDM increases with the number of iterations for both instances and also takes more time to provide the solution. As an example for 50 charging requests, the efficiency is increased by almost 11.5% when the iteration number is increased from 40 to 50 and requires 5 more minutes to solve, while the efficiency does not improve past iteration 50 even when spending 10 more minutes. On the other side, for 30 charging requests, the efficiency saturates quicker with fewer number of iterations.

Fig. 5.4 also shows that after 40 iterations, DWDM ensures each truck can serve 8.75 EVs while the total number of EVs is 50, but this goes down to 5.5 EVs/truck when the total number of EVs is 30. Hence, the efficiency level is significantly influenced by the number of options i.e., a larger number of EVs provide more options to

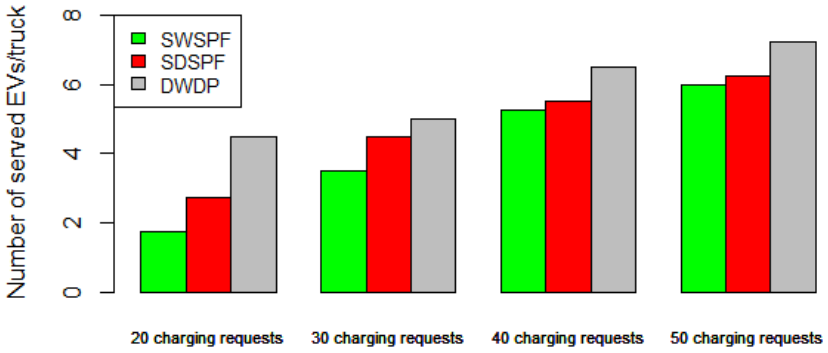

Figure 5.5: Performance comparison with heuristics.

trucks. Fig. 5.5 illustrates that, every algorithm shows higher efficiency for a larger number of EVs. As an example, the efficiency of DWDM is 6.5 EVs/truck for 40 EVs, while it is 7.25 EVs/truck for 50 EVs. And for any instances, DWDM outplays the other two heuristic algorithms (e.g., for 40 EVs, DWDM ensures an efficiency of 6.5 EVs/truck, while its is 5.5 EVs/truck for SDSPF and 5.25 EVs/truck for SWSPF).

Now, since the efficiency is affected by the available options, the variation of average energy demand or the average charging window length should have influence as well. To investigate those influences, we depict a scenario, where 4 trucks are involved to charge a maximum number of 40 EVs at 5 different parking lots. Fig. 5.6 depicts that a smaller average energy demand allows every algorithm to charge higher number of EVs. But as SDSPF seeks to charge smallest demand first, its performance is mostly influenced with the variation of average demand. The efficiency is dropped by 23% for SDSPF while it is 10% for DWDM and 16% for SWSPF when the average energy demand is increased from 20 kWh to 30 kWh.

On the other hand, increasing the charging window length provides more opportunities for trucks to charge more EVs. As SWSPF makes the charging decision depending on the window length, the longer charging window helps improving the performance of SWSPF significantly and its performance is much closer to DWDM

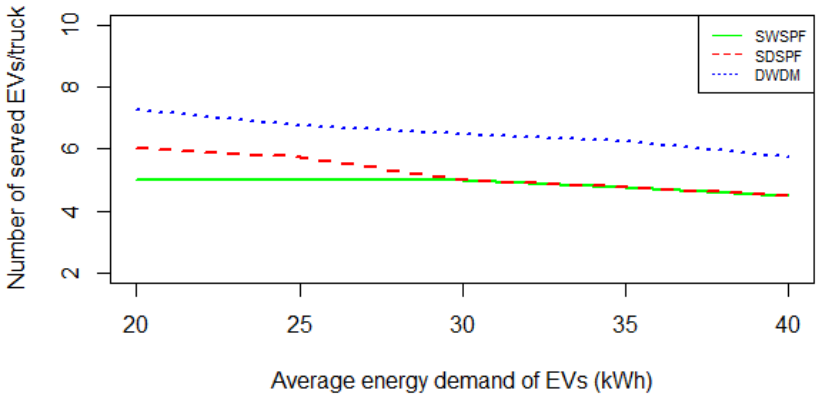

Figure 5.6: Variation in efficiency based on average demand.

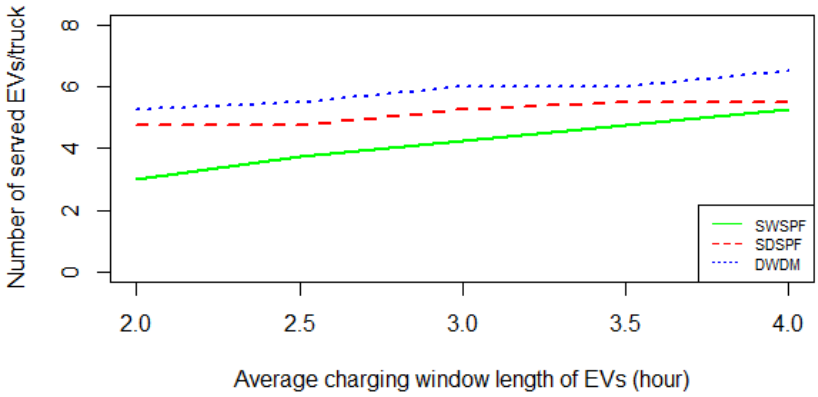

Figure 5.7: Variation in efficiency based on charging window

(shown in Fig. 5.7). DWDM actually shows almost a linear response with the variation of both the average window length as with the average energy demand.

Finally, to determine the required number of trucks to serve a number of charging requests, we assume a constant energy demand by each EV having a constant charging window length for three different number of charging requests. For all three cases, the number of served EVs increases with the number of trucks (Fig.5.8) and initially, this increasing rate is almost linear. After a certain number of trucks, the number of served EVs starts to be saturated since the trucks have reached their serving capacities, which as shown varies with the number of serving requests. In other

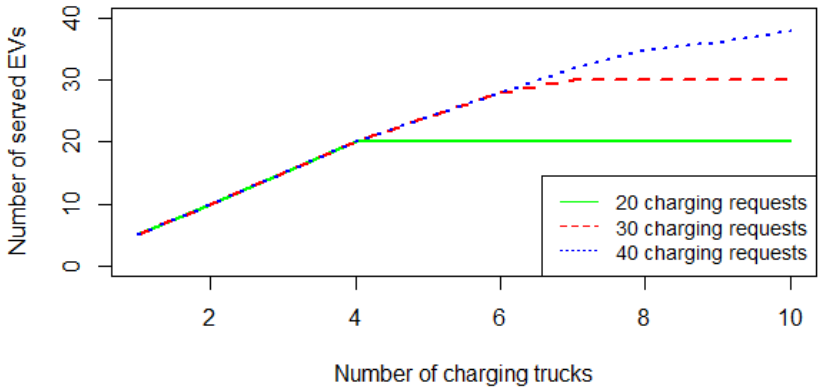

Figure 5.8: Performance evaluation of DWDM with number of trucks.

words, to serve more requests from EVs, more trucks need to be deployed. As an example, the instance where 40 EVs send their charging requests, 8 more EVs can be served by increasing the truck number from 5 to 7, while DWDM model can serve only 3 more EVs by increasing the truck number from 8 to 10. This finding may help determine the required number of trucks for a company to maximize the revenue.

5.6 Conclusion

An offline problem is addressed for a company, which has a number of trucks equipped with a larger battery along with a fast charger to charge EVs through V2V at some predefined parking lots. The objective of the work is to serve as many EVs as possible using this limited number of trucks by determining their trajectories. The problem also considers the energy consumption of trucks during the travelling period and each truck has to return to the depot after serving EVs. All requests are supposed to be available before the time horizon. An ILP was formed to determine the optimal solution and it was formally proven NP-Hard. As the computation time for ILP was too large to be applicable, we decomposed the problem using Dantzig-Wolfe decomposition and its performances were extensively analyzed by varying different parameters

for different scenarios. We also compared its performance with two different heuristic algorithms (SWSPF and SDSPF). Though heuristics are very prompt to provide solutions for any realistic size (i.e., a larger number of charging request will be met by a larger number of trucks) of instance, DWDM shows the highest efficiency in every scenario. Finally, the trade-off between performance of computational time of DWDM is analyzed to determine the iteration number which can ensure a better solution within an acceptable time.

Chapter 6

Attack Model and Detection Methodology for a Coordinated Switching Attack Initiated from EV Charging Ecosystem[1]

Since, the success of EV smart charging relies on the real time data sharing among the entities (e.g., EVs, CSs, grid etc.), IoT enabled charging ecosystem is being popular by everyday and appeared as a new attack surface to the grid. Especially, while the widely used charging protocol, OCPP is still not secured [16], an attacker may take the control of charging/discharging of a large number of EVs to initiate different types of attacks. Hence, we assess the competency of compromised EV charging infrastructures in initiating switching attack to create inter area oscillation. And finally, a neural network based detection mechanism is proposed to detect such attempts before being executed.

[1] A part of this chapter is under review in IEEE Transactions on Industrial Informatics [65], while another portion is submitted in IEEE Transactions on Smart Grid [66]

6.1 Motivation

A major stakeholder of EV interconnected ecosystem is the power grid which can be exploited through the control of EVs or EV charging infrastructures targeting its functional requirements in terms of voltage, frequency or even as transient oscillations, e.g., inter-area oscillations. Sudden transitions from *off* state to *on* state or vice verse of a significant amount of load can create very low-frequency oscillations between two weakly tied power generation areas [78]. These oscillations often represent themselves in the angular speed of generators which also impacts the frequency of the grid. These angular speed are often synchronized together and are kept fixed at the frequency of the grid using various controllers and power system stabilizers (PSSs). Any deviation more than 2.5% in the angular speed of generators is not tolerated and the synchronous machines will be disconnected one by one from the grid by the protection system due to loss of synchronization, and consequently inadequate generation results in cascading failure in the grid [77] and cause a blackout as witnessed on August 10, 1996 where an inter-area oscillation between California and the East zone resulted in a wide area blackout [142]. Similarly, this type of oscillations was also detected on November 29, 2005 in Alberta and September 5, 2015 in Nevada [25]. The threat imposed by this phenomenon is significant since the oscillation frequency is too low to be detected by the practising security mechanism [78].

The consequences of inter-area oscillations are expected to be more tangible due to higher integration level of EVs, especially because, a large-scale charging infrastructure introduces a significant number of rectifiers and hence, the damping ratio might be decreased substantially [56]. Coupling these variations with the connectivity in an IoT-integrated environment, and Information and Communication Technologies (ICT)-empowered smart grids introduces new trends in the management and operation of the power grids. The complexity of the resulting system and the inter

dependency among its components lure attackers to exploit EVs and their charging ecosystem as a new attack surface, devise new attacks, and target the grid's stability and availability. Moreover, EVs and their charging stations are abundant, distributed, connected, remotely accessible, vulnerable to cyber attacks, and equipped with the least of security measures [16]. Those properties favor a coordinated attack to switch a significant portion of the mobile and remotely controlled EV loads on and off to initiate oscillations in the transmission network.

Since, no one has address EV charging ecosystem as a potential source of switching attack as we mentioned in Section 2.2.1, by exploiting the by directional energy transfer capability of EV charging infrastructures, we intend to mimic a similar coordinated attack to assess the consequences and finally propose the corresponding detection framework.

6.2 Problem Definition and Contributions

A coordinated switching attacks on the power grid through the large-scale exploitation of EVs and their charging infrastructure is formulated and as per our best knowledge, no one addressed EVs as a potential switching attack surface before. The threats associated with the EV large-scale charging/discharging functionality, analyzed different attack strategies, determine the inter-area oscillation frequency in each attack strategy, model the grid behavior, and characterize the grid response in the form of inter-area oscillations are identified. This formulation is followed by extensive simulation results that detail the potential impact of those attacks in realistic power systems. Then, a framework based on neural network technique is provided to detect the attack leveraging the available data of the EV ecosystem. As such, the contributions can be outlined as:

- Identification of the EV charging ecosystem as an attack surface for switching attacks.
- Design of two attack strategies to determine the vulnerable frequency and formulation of the switching attack on grids.
- Demonstration of the stealthiness of these attacks through theoretical and numerical analysis.
- Propose detection mechanisms for the EV-based switching attack using neural network techniques and system data.

6.3 System Model

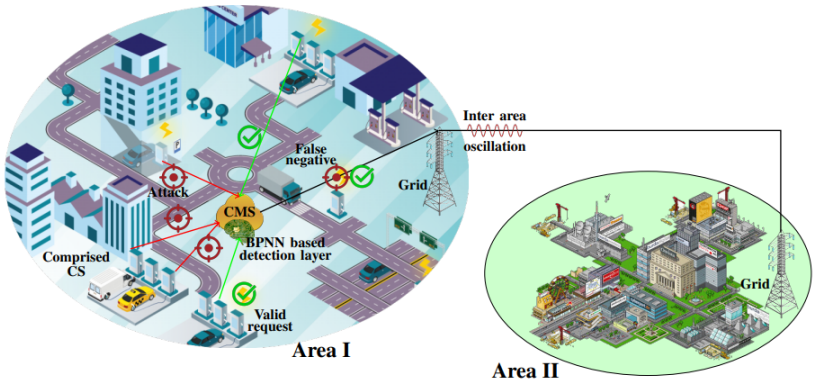

Figure 6.1: A schematic diagram of probable switching attack and its detection.

The considered transmission system consists of several areas, each has power plants, transmission lines, substations and loads as shown in Fig. 6.1. The loads represent IoT-connected, EV-equipped cities with huge consumption of electricity and energy distribution systems. In some transmission systems, the loads and the dense energy consumption areas are far from each other geographically. As a result, several of these areas are connected together by a long weak transmission link for energy sharing. Each of these areas has its own power generation capacity and the capability

of exporting (or importing) energy to (or from) any other connected area through that long weak transmission line. Such a power system can be subjected to various types of stability issues, among which the inter-area oscillation is the most common one. Such condition of instability occurs when a set of synchronous generators, which are scattered in a geographical area, starts to oscillate against the ones in the other areas. A disturbance, such as fault or sudden change in load/generation, may trigger these oscillations. Since this phenomenon may force the system generators to lose synchronization with others and cause a blackout, power utilities deploy several protection and control schemes (e.g., PSSs, supplementary damping controllers associated with flexible alternating current (AC) transmission system (FACTS) devices (e.g., Static Var Compensators), direct current (DC) line modulation, etc. [93]) to remove the oscillations or damp them, respectively. However, those control schemes are designed for specific operating conditions and may not be successful to damp the oscillation especially for a wide area system or consequent to large disturbances and attacks [51]. Additionally, the majority of the existing FACTS devices lacks such a damping scheme for inter-area oscillations.

Now a large number of EVs of area I are assumed to charge their batteries at a significant number of networked public or private CSs which are geographically dispersed as shown in Fig. 6.1, while the public CSs are managed and connected to the power grid through a central management system (CMS). The CMS receives charging/discharging requests from these CSs using the open charge point protocol (OCPP) and these requests are admitted accordingly after a preliminary authentication (e.g., CS ID, SoC level etc.). On the other hand, no authentication is required for private CSs [16]. Now, this is assumed that a sufficient number of both types of CSs in area I are compromised by an attacker having subsequently the ability of controlling the charging/discharging requests. Therefore, the attacker can mimic a

switching attack by commanding those CSs for a quick transition between charging and discharging and create an inter area oscillation between areas I and II. Two different types of attack strategies will be consider to initiate switching attack from EV charging ecosystem and in the first stage of this work, the attack consequences will be observed.

After analyzing the capability of switching attack initiation from EV charging ecosystem, an intelligent detection mechanism is proposed then to detect such adversarial attempts. A back propagation neural network (BPNN) based algorithm is designed and placed at the CMS as shown in Fig. 6.1. This algorithm acts as a filter to detect suspicious requests and hence, instead of an immediate execution of charging or discharging requests, the CMS may discard or create a random delay in the execution (a detailed procedure is discussed in Section 6.7) to disorder the coordination among attackers.

6.4 Threat Model

An attacker is assumed to have the capability of exploiting known and zero-day vulnerabilities in the EV ecosystem to target the power grid. In particular the following assumptions are taken in consideration:

1. The attacker has enough knowledge from public sources about the EV charging infrastructure [6].

2. The attacker has whether the power system data (through insiders or compromising the operator database) or the expertise to perform reconnaissance and intelligence gathering to identify potential attack targets, craft, and execute his attacks [90].

3. The attacker is interested in targeting the power system stability through the EV charging infrastructure.

4. The attacker designs a coordinated multi-site attack and wants to avoid existing detection and protection layers.

5. The attacker whether has the system parameters or is able to inject a chirp signal and observes the system response to determine the inter-area oscillation frequency.

As many CS networks make their status (e.g., number of charging poles, charging rate, poles are occupied or not, etc.) public as a marketing strategy, the attacker can observe some of the inter dependencies using web-services of the EVs, CS vendors and third parties like ChargePoint that aggregate CSs and EVs. The active status of CSs can be accessed and that would help to manipulate the OCPP message which controls the charging/discharging activities via the central agent. As a consequence, the first assumption is inspired from [6], where the authors demonstrated that using publicly available data on electric vehicles, their charging infrastructure and the power grid, an attack to destabilize the power grid can be formulated in the presence of large-scale deployment of electric vehicles. The second assumption is inspired by the analysis of the attack on the Ukrainian power grid and the attacker capabilities, as outlined in [90]. Through this assumption, the attacker is capable of attaining the expertise required to carry out his attack. In the third assumption, we outline the attacker interest and define the scope of his attack. The attacker can exploit the large-scale and distributed deployment of the electric vehicles ecosystem to execute his attack. Moreover, the cyber attack of Black Energy3 trojan on the Supervisory Control and Data Acquisition (SCADA) system of the Ukraine power grid [94] is admonishing for the isolation of the demand side external networks (e.g., CS network) from the smart grid [6]. Such isolation prohibits the grid's inherent detection mechanism from continuous monitoring over these external networks and consequently, imposes difficulty in the detection of a very short duration attack initiated by an external network. Hence, according to the fourth assumption, the attacker will not take any steps that

will trigger deployed control, protection and detection mechanisms that are usually practised by utilities. Through the fifth assumption, we avoid using the assumption that the attacker can always obtain the vulnerable frequency of the system through detailed modeling. Rather than relying on sufficient knowledge about the power system detailed data, which is not practical for a large-scale system, it is assumed that an attacker has the ability to perform a reconnaissance activity benefiting from a small group of compromised EVs. Then, the system measurements and a set of analysis techniques will be used to obtain the vulnerable inter-area frequencies and perform the attack leveraging all the compromised EVs at those frequencies.

6.5 Attack Formulation

Based on the assumptions mentioned in previous subsection, here we model our attack vector. Now, modeling the physical layer of the smart grids requires extensive data about the parameters of the power system which may be even unknown to the operator. Consequently, this is a realistic assumption that even the insiders may not be able to help the adversary to obtain detailed data of the grid. Moreover, due to security concerns, the operator may not keep all the system data in one database to avoid information leakage. As such and to broaden the scopes of the preformed analysis, two different attack models are considered as:

- Attacker $\mathcal{A}$: In this attack, an adversary is considered without having accurate information of the power grid. As such, he/she will use a specifically-tailored and stealthy system identification technique based on eigenvalue realization algorithm (ERA) to gather the required information of the system and calculate the frequency of inter-area modes. Then, the adversary launches the attack by switching the compromised EVs with the calculated frequency.

- Attacker $\mathcal{B}$: Attacker $\mathcal{B}$ can benefit from an insider or a compromised database and obtain the parameters of the system. In such a case, using the detailed modeling of the system, the adversary can calculate the inter-area dominant modes of the grid as explained in Section 6.5.2, and execute the attack accordingly.

The next two subsections discuss the reconnaissance model of attacker $\mathcal{A}$ and the equations that attacker $\mathcal{B}$ will use to obtain the inter-area modes of the smart grid.

6.5.1 Reconnaissance Model of Attacker $\mathcal{A}$

This subsection aims to drive a rigorous attack model for the switching attack (attacker $\mathcal{A}$) to EV infrastructure and targeting the transmission grid stability. In order to launch the switching attack, the adversary needs the frequency of inter-area modes of the grid to switch the EV loads accordingly. Any deviation from the exact value of this inter-area frequency will result in inefficiency of the attack model, stable operation of the grid, and increasing the awareness level of the grid operator. To capture the accurate inter-area mode, the detailed model of the power system is required which is not available for the attacker $\mathcal{A}$. As such, a tailored version of ERA, which initially introduced in [61], is used in this subsection.

Assume that the attacker compromised n_η mass charging EV infrastructure in $m = \{1, ..., \eta\}$ load bus of the power system and aims to target n_ζ synchronous generator whose angular speeds are $n = \{\omega_1, ..., \omega_\zeta\}$. Thus, the transfer function of the power system from attacker point of view can be written as $\omega_{(n_\zeta \times 1)} = G(s)_{(n_\zeta \times n_\eta)} PL_{(n_\eta \times 1)}$, where PL and ω are the vectors of the incremental active power of buses which is compromised by the adversary and angular speed of generators, respectively. Since the detailed parameters of the power system are not known, the main aim of the attacker is to identify a system model $\bar{G}(s)$ using the measured data of the actual system $G(s)$. The use of ERA technique requires to excite the system using an impulse signal in EV

Algorithm 6.1 Calculation of impulse response using chirp signal

Input: Compromised loads and generators η and ζ
Output: Impulse response of the $G(s)$ between load η and generator ζ as $y_{\eta,\zeta}$
for $Cont_L$=1:n_η **do**
    Calculate the Fourier Transform of Chirp signal in each load $\Gamma_\eta(jw) = \mathcal{F}(x_{chirp_\eta}(t))$
end for
for $Cont_G$=1:n_ζ **do**
    Calculate the Fourier Transform of measured angular speed of generator as $\Pi_\zeta(jw) = \mathcal{F}(\omega_\zeta(t))$
end for
for $Cont_L$=1:n_η **do**
    for $Cont_G$=1:n_ζ **do**
        Calculate the impulse response from the η^{th} load to ζ^{th} generator as $y_{\eta,\zeta} = \mathcal{F}^{-1}(\Pi_\eta(jw)/\Gamma_\eta(jw))$
    end for
end for
Apply ERA based on obtained impulse response

charging infrastructure, and gather the system outputs, i.e., $\{\omega_1, ..., \omega_\zeta\}$. However, such an assumption is not realistic in a power system since (i) a huge increase in the EV generation increases the awareness level of the grid operator and reveals the attack, (ii) production of an impulse signal is not physically possible using a limited number of compromised EV charging stations, and (iii) using the impulse signal produces the entire frequency data of the system which is not necessary since the attacker is only interested in the system response in low frequencies (between 0.1 to 1 Hz). As such, we propose to modulate a chirp signal with a limited magnitude and frequency range to the loads of the system in m buses and obtain the impulse response of the system using Algorithm 6.1. Then, the system model can be computed leveraging the obtained impulse response. The use of chirp signal is advantageous since (i) its magnitude can be modified by the adversary and be limited not to alarm the operator, (ii) its frequency range can be modified by the adversary to focus on the range of inter-area mode, as a result, the fast transient and high-frequency dynamics of the

power system will be neglected, and (iii) the duration of the reconnaissance activity can be modified by the adversary as performing a long-term reconnaissance activity results in lower operator awareness. The chirp signal x_{chirp} can be expressed as:

$$x_{chirp} = sin\left(\frac{2\pi f_s(r_f^t - 1)}{ln(r_f)}\right) \quad \text{where} \quad r_f = (\frac{f_e}{f_s})^{(\frac{1}{T})} \tag{6.1}$$

In this equation, f_s, f_e, and T are the starting frequency, ending frequency, and duration of the signal, respectively. By applying this signal to the system, gathering the measurements and applying Algorithm 6.1, the impulse response of the grid will be available to the attacker. Having the impulse response of the system, a modified ERA technique can be used to obtain the system model. The linearized state-space representation of the $G(s)$ can be written as:

$$\dot{\mathbf{x}} = \mathbf{Ax} + \mathbf{Bu} \tag{6.2a}$$

$$\mathbf{y} = \mathbf{Cx} + \mathbf{Du} \tag{6.2b}$$

where x, u, and y are system states, inputs, and outputs, respectively, and matrices A, B, C, and D represent the small signal behavior of the system. Since these matrices are not known, the main aim here is to obtain the identified values of these matrices, i.e., $\bar{A}$, $\bar{B}$, $\bar{C}$, and $\bar{D}$, by giving a known input and measure the system response. Assume that the obtained impulse response of the system is rearranged as a time series of k measurements, i.e., $y_I = \{y_I^0, y_I^1, y_I^2, ..., y_I^{k-1}, y_I^k\}$, where each y_I^i represent a block matrix obtained from $y_{\eta,\zeta}$ in Algorithm 6.1. It is worth mentioning that the number of the k should be large enough to show the damped response of the system; moreover, the time steps between k and $k+1$ should be small enough to capture the frequency of the under study modes of the system, i.e., inter-area-modes. This response is corresponded to the Markov parameters of the system as

$\{\bar{D}, \bar{C}\bar{B}, \bar{C}\bar{A}\bar{B}, \bar{C}\bar{A}^2\bar{B}, \ldots, \bar{C}\bar{A}^{k-1}\bar{B}, \bar{C}\bar{A}^k\bar{B}\}$ [46]. This expression easily identifies the $\bar{D} = y_I^0$. Also, note that the system is assumed to be stable, which also matches the attacker objective since (i) he/she is still in reconnaissance mode and doesn't have enough information to make the system unstable, (ii) the number of leveraged EV chargers for reconnaissance is low, and (iii) the attacker aims to keep the operating point of the system fixed so that the gathered data remains useful for the attack objective. Then, using the measured data, Hankel matrices can be developed as:

$$H = \begin{bmatrix} y_I^1 & y_I^2 & \cdots & y_I^L \\ y_I^2 & y_I^3 & \cdots & y_I^{L+1} \\ \vdots & \vdots & \ddots & \vdots \\ y_I^{k-L+1} & y_I^{k-L+2} & \ddots & y_I^k \end{bmatrix} = \begin{bmatrix} \bar{C}\bar{B} & \bar{C}\bar{A}\bar{B} & \ldots & \bar{C}\bar{A}^{L-1}\bar{B} \\ \bar{C}\bar{A}\bar{B} & \bar{C}\bar{A}^2\bar{B} & \ldots & \bar{C}\bar{A}^L\bar{B} \\ \vdots & \vdots & \ddots & \vdots \\ \bar{C}\bar{A}^{k-L}\bar{B} & \bar{C}\bar{A}^{k-L+1}\bar{B} & \ddots & \bar{C}\bar{A}^{k-1}\bar{B} \end{bmatrix} = \mathcal{O}\mathcal{C} \quad (6.3a)$$

$$H' = \begin{bmatrix} y_I^2 & y_I^3 & \cdots & y_I^{L+1} \\ y_I^3 & y_I^4 & \cdots & y_I^{L+2} \\ \vdots & \vdots & \ddots & \vdots \\ y_I^{k-L+2} & y_I^{k-L+3} & \ddots & y_I^{k+1} \end{bmatrix} = \begin{bmatrix} \bar{C}\bar{A}\bar{B} & \bar{C}\bar{A}^2\bar{B} & \ldots & \bar{C}\bar{A}^L\bar{B} \\ \bar{C}\bar{A}^2\bar{B} & \bar{C}\bar{A}^3\bar{B} & \ldots & \bar{C}\bar{A}^{L+1}\bar{B} \\ \vdots & \vdots & \ddots & \vdots \\ \bar{C}\bar{A}^{k-L+1}\bar{B} & \bar{C}\bar{A}^{k-L+2}\bar{B} & \ddots & \bar{C}\bar{A}^k\bar{B} \end{bmatrix} = \mathcal{O}A\mathcal{C} \quad (6.3b)$$

where $\mathcal{O}$ and $\mathcal{C}$ are the observability and controlability matrices. Then, the singular value decomposition (SVD) of Hankel matrices can be written as:

$$H = U\Sigma V^T = [\tilde{U}U^+] \begin{bmatrix} \overbrace{\tilde{\Sigma}}^{\in\mathcal{I}} & \mathbf{0} \\ \mathbf{0} & \underbrace{\Sigma^+}_{\notin\mathcal{I}} \end{bmatrix} \begin{bmatrix} \tilde{V}^T \\ V^{+T} \end{bmatrix} \tag{6.4}$$

where $\tilde{}$ and $^+$ indicate the inter-area modes and the rest of system dynamics, respectively, and $\mathcal{I}$ represent the set of all inter-area modes. In such a case, the predicted matrices of the system modes can be written as:

$$\bar{A} = \tilde{\Sigma}^{-1/2}\tilde{U}^T H' \tilde{V}\tilde{\Sigma}^{-1/2} \tag{6.5}$$

Assuming the inter-area modes of the matrix $\bar{A}$ to be $\lambda_q = \sigma_q + j\theta_q, \forall q \in \mathcal{I}$, the inter-area frequency can be obtained using the frequency of these modes, i.e., $\theta_q/2\pi$. Despite the efficiency of the proposed technique, the size of the Hankel matrix can significantly increase, and consequently makes it computationally difficult for the adversary to calculate the SVD of the Hankel matrices. As such, we simplify the attack procedure by applying a chirp signal in the input of the system and observing the fast Fourier transform (FFT) of the system response. In such a case and based on the discussed techniques, the observed output of the power system to the injected chirp signal will help the adversary to calculate the inter-area modes of the system.

As the attack will be initiated from CS or from a number of CSs to bus $i \in \{1, ..., \eta\}$, after injecting the chirp signal, the active power flow to bus i can be expressed as:

$$P_{Li} = P^0_{Li} + P_{ch} = P^0_{Li} + \alpha_i x_{chirp} \tag{6.6}$$

where P^0_{Li} is the initial load value, α_i is the load escalating factor, which is a function

of the total power rating of comprised CSs that can be calculated as $\alpha_i = \sum_l n_{li}\rho_l$, where, n_{li} indicates the number of comprised level l chargers connected with bus i and ρ_l indicates the respective power rating. In practice, three types of chargers are used and we assume that an attacker has access to publicly available data about the power rating of these chargers.

The proposed attack reconnaissance phase is stealthy, since (i) the attacker will use only a small part of the compromised EV infrastructure (less than 5% of load in several buses of the grid) to explore the power system and find the inter-area modes, this will ensure that the power system operator misses the attacker reconnaissance phase since such small load variation is normal in a grid, and (ii) the start and end frequency of chirp signal is matched with the frequency of inter-area modes of the system in low frequency range, often less than 1 Hz, which may assist this to be stealthy from the operator point of view again due to large period of the signal. As such, the attacker will alter the power consumption of the EV loads smoothly by modulating a specific pre-known signal to the power consumption of the loads and monitoring the consequences through PMU data installed at generators. Such PMUs with data about the rotor angle of generators are already deployed in many power system plants [24],[156].

6.5.2 State-space Representation of Attacker $\mathcal{B}$

On the other hand, for attacker $\mathcal{B}$, we assume that the system data is available and hence to conclude on the frequency of oscillations and stability condition of the system, , small signal stability of the multi-machine power system needs to be studied. The fourth-order model of synchronous generator as well as the algebraic equations describing the power transmission system are combined to attain the state-space model. Then, the eigenvalues of the system are calculated from state-space

representation to identify the inter-area modes. The obtained state-space modeling of the system can be used to determine the stability condition of the linearized system, and also for design and sensitivity analysis purposes.

The following differential equations describe the fourth-order model of i^{th} synchronous machine:

$$\frac{d\delta_i}{dt} = \omega_i - \omega_s \tag{6.7a}$$

$$\frac{d\omega_i}{dt} = \frac{(T_{mi} - \acute{E}_{di}I_{di} - \acute{E}_{qi}I_{qi} - (\acute{X}_{qi} - \acute{X}_{di})I_{di}I_{qi})}{M_i} \tag{6.7b}$$

$$\frac{d\acute{E}_{qi}}{dt} = \frac{-\acute{E}_{qi} + (X_{di} - \acute{X}_{di})I_{di} + E_{fdi}}{\acute{T}_d} \tag{6.7c}$$

$$\frac{d\acute{E}_{di}}{dt} = \frac{-\acute{E}_{di} + (X_{qi} - \acute{X}_{qi})I_{qi}}{\acute{T}_q} \tag{6.7d}$$

where, T_{mi}, δ_i, ω_i are the input mechanical torque, rotor angle, and rotational speed of ith synchronous machine, respectively. $\acute{E}_{qi}$ and $\acute{E}_{di}$ also represent the internal machine voltages. X_{qi} and X_{di} represent q- and d- axis synchronous reactances, $\acute{X}_{qi}$ and $\acute{X}_{di}$ are q- and d-axis transient reactances, and $\acute{T}_q$ and $\acute{T}_d$ are open-circuit time constants in q- and d-axis. In summary, the synchronous machine equations can be described as:

$$\dot{\mathbf{x}} = f(\mathbf{x}, \mathbf{z}, \mathbf{w}) \tag{6.8}$$

where

$$\mathbf{x} = \{\delta_i, \omega_i, \acute{E}_{di}, \acute{E}_{qi}\} \quad \mathbf{z} = \{T_{mi}, E_{fdi}\} \quad \mathbf{w} = \{I_{qi}, I_{di}\} \tag{6.9}$$

Then the synchronous machine stator can be represented as:

$$E_{di} - V_i sin(\delta_i - \theta_i) - R_{si}I_{di} + \acute{X}_{qi}I_{qi} = 0 \tag{6.10a}$$

$$E_{qi} - V_i cos(\delta_i - \theta_i) - R_{si} I_{qi} - \acute{X}_{di} I_{di} = 0 \tag{6.10b}$$

where θ_i and V_i represent the voltage angle and magnitude at ith machine stator, respectively, and R_{si} represents stator resistance. These equations link the synchronous generator to the power system whose behaviour in generator and load buses can be described in Eqs. (6.11)-(6.12), and Eqs. (6.13)-(6.14), respectively.

$$I_{di} V_i sin(\delta_i - \theta_i) + I_{qi} V_i cos(\delta_i - \theta_i) + P_{Li} - \sum_{k=1}^{n} V_i V_k Y_{ik} cos(\theta_i - \theta_k - \Delta_{ik}) = 0 \tag{6.11}$$

$$I_{di} V_i cos(\delta_i - \theta_i) - I_{qi} V_i sin(\delta_i - \theta_i) + Q_{Li} - \sum_{k=1}^{n} V_i V_k Y_{ik} sin(\theta_i - \theta_k - \Delta_{ik}) = 0 \tag{6.12}$$

$$P_{Li} - \sum_{k=1}^{n} V_i V_k Y_{ik} cos(\theta_i - \theta_k - \Delta_{ik}) = 0 \tag{6.13}$$

$$Q_{Li} - \sum_{k=1}^{n} V_i V_k Y_{ik} sin(\theta_i - \theta_k - \Delta_{ik}) = 0 \tag{6.14}$$

In these equations, P_{Li} and Q_{Li} are the active and reactive power consumption in bus i, respectively. The magnitude and angle of the admittance between buses i and k are also represented by Y_{ik} and Δ_{ik}, respectively. In order to obtain the linearized model of the system, the equilibrium point of the system is obtained from the power flow solution of the system. It is worth mentioning that this solution can be obtained by solving algebraic equations (6.11)-(6.14) using conventional Newton-based techniques. This equilibrium point demonstrates the system parameters (V_i and θ_i) in steady-state

operating condition. Then, the internal parameters of the synchronous generator will be obtained assuming the differential terms of (6.7) to be zero, and solving the resulted algebraic equations of the synchronous machine, i.e., $\dot{\mathbf{x}} = 0 \rightarrow \mathbf{x}_0$.

The linearized model of the system then can be obtained by augmenting all the equations obtained from the linearization of separate parts of the system. As I_{qi} and I_{di} are not the system states, as a result, they can be replaced in the system equations by equivalent terms obtained from synchronous machine stator equations. Then, the system can be represented as

$$\dot{\mathbf{x}} = f(\mathbf{x}, \mathbf{y}) \quad \text{and} \quad g(\mathbf{x}, \mathbf{y}) = 0 \tag{6.15}$$

where

$$\mathbf{y} = \{V_1, V_2, ..., V_n, \theta_1, \theta_2, ..., \theta_n\} \tag{6.16}$$

The small signal model then can be represented as a descriptor system as:

$$\begin{bmatrix} \frac{d}{dt}\Delta\mathbf{x} \\ 0 \end{bmatrix} = \begin{bmatrix} \mathbf{A} & \mathbf{B} \\ \mathbf{C} & \mathbf{D} \end{bmatrix} \begin{bmatrix} \Delta\mathbf{x} \\ \Delta\mathbf{y} \end{bmatrix} \tag{6.17}$$

where

$$a_{ij} = J(\frac{dx_i}{dt}, x_j)|_{x_0,y_0} \quad b_{ij} = J(\frac{dx_i}{dt}, y_j)|_{x_0,y_0} \tag{6.18a}$$

$$c_{ij} = J(g_i, x_j)|_{x_0,y_0} \quad d_{ij} = J(g_i, y_j)|_{x_0,y_0} \tag{6.18b}$$

In these equations, $J(\alpha, \beta)$ represents the Jacobian of function α with respect to set of variables β. Consequently, the closed-loop system can be obtained as:

$$\frac{d}{dt}\Delta\mathbf{x} = \mathbf{A}_{sys}\mathbf{x}, \quad \mathbf{A}_{sys} = \mathbf{A} - \mathbf{B}\mathbf{D}^{-1}\mathbf{C} \tag{6.19}$$

Then, the eigenvalues of matrix $\mathbf{A}_{sys}$ provide the modes of the system, where the

damping of inter-area mode and its frequency are observable. The arrays of matrix $\mathbf{A}_{sys}$ are dependent on $\frac{\partial P_{Li}}{\partial V_j}$, which represents the voltage-dependent nature of the load.

Having the state-space model of the system, the eigenvalues of the system, and consequently, the inter-area modes can be obtained. The summary of two attack strategies are presented in Fig. 6.2.

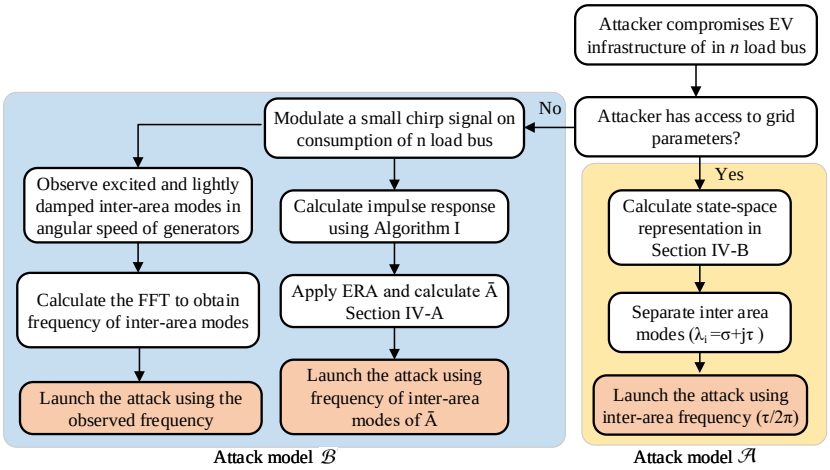

Figure 6.2: A flowchart of the attack strategies.

6.6 Numerical Analysis for Switching Attacks

To evaluate the performance of the grid in the presence of attack, three different power systems are considered as test cases, i.e., two-area Kundur system, 39-bus New England power system, and 5-area Australian power grid.

Two types of switching attack scenarios are also evaluated; 1) sudden termination of EV charging (i.e., drop in load) and 2) sudden supply from EVs (i.e., spike in generation). The two-area Kundur system is attacked leveraging the grid parameters (attacker $\mathcal{B}$) due to its small size, whereas the other two systems are under attack without available data (attacker $\mathcal{A}$) since they mimic realistic systems. The state-space model and stability analyses are preformed using MATLAB, whereas the

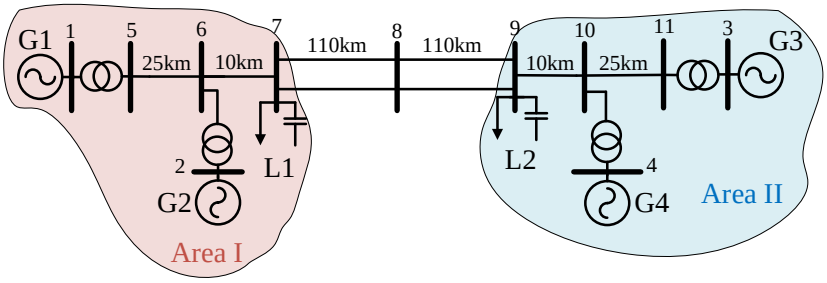

Figure 6.3: The two area Kundur system.

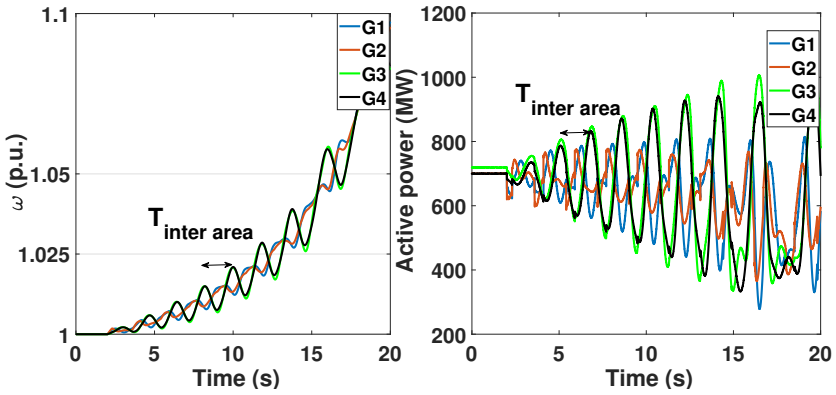

Figure 6.4: Angular speed and active power output of the generators following a discharging attack at bus 7.

EMTP-RV and Simulink software packages are used to obtain the time-domain results.

6.6.1 Two-Area Kundur System

The two-area Kundur system [55] is shown in Fig. 6.3. We assume that the attacker uses the system parameters to calculate the inter-area mode (attack $\mathcal{B}$) and launch a switching attack at bus 7 of area I with duty cycle of 50% and 1.87 s period based on the mode specification. The instability of the generators and the effectiveness of the attack over the angular speeds of all four generators are depicted in Fig. 6.4 to depict that the speed of generators in similar areas reacts to the attack almost with similar manners, while Fig. 6.5 shows the corresponding active and reactive power of the tie-lines.

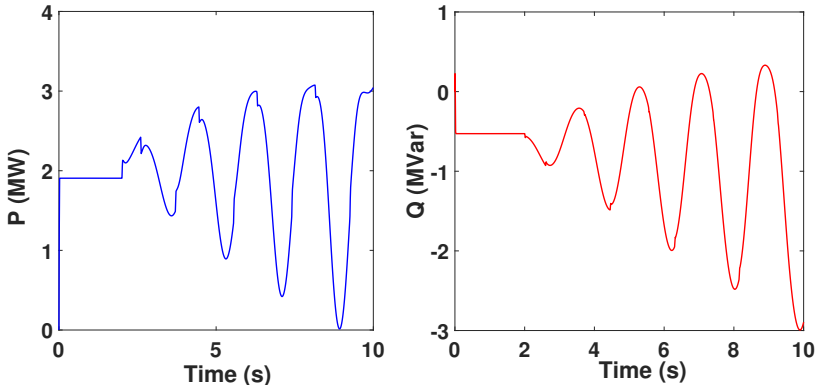

Figure 6.5: Active and reactive power flowing in one of the tie-lines between area I and II.

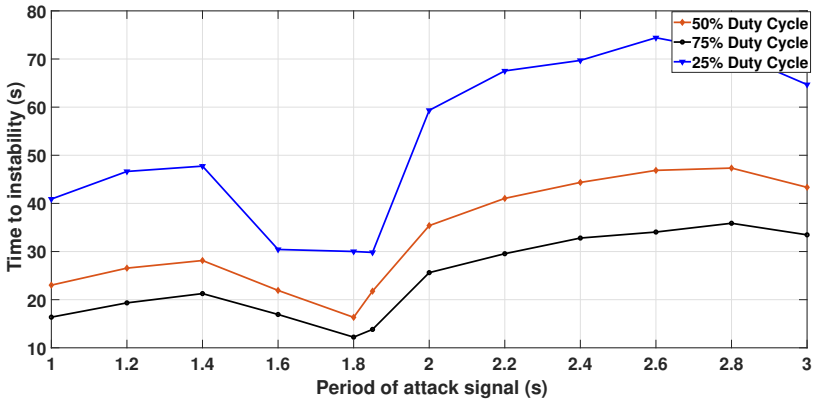

Figure 6.6: The dependency of duty cycle of charge/discharge, switching signal, and time to instability at load 7.

To assess the consequences of such attack, another parameter, Time of Instability (ToI) is analyzed. ToI is defined as the time required for at least one of generator's angular speed to pass 2.5% deviation. Fig. 6.6 depicts the influence of attack period on the parameter of ToI for different values of duty cycle. It can be observed that near the frequency of the inter-area mode, ToI decreases significantly for all three scenarios. Moreover, for a higher duty cycle, the ToI is lower.

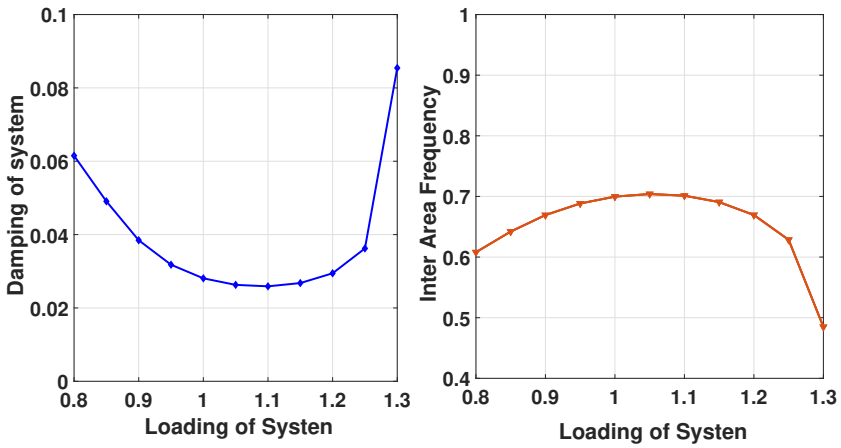

Figure 6.7: Variation of damping ratio and frequency of inter-area mode following the change of system loading.

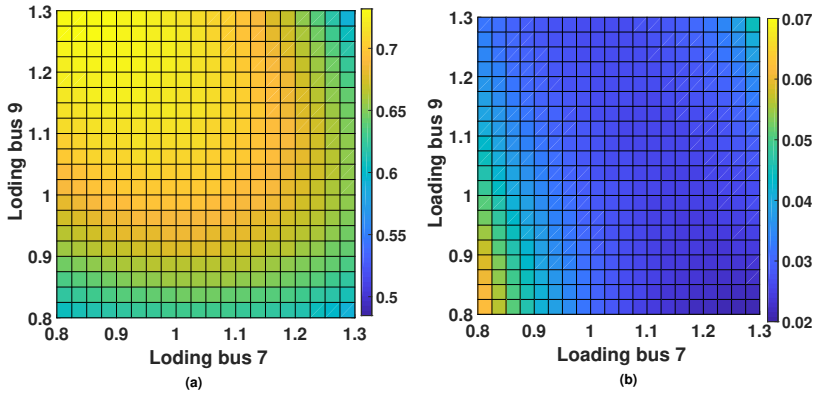

Figure 6.8: The frequency and damping ratio of inter-area mode following a coordinated attack to bus 7 and 9, a) frequency, b) damping.

To investigate the impact of system loading on the damping ratio and assess the vulnerability state of the system, the damping ratio and frequency of inter-area mode in different loading conditions of bus 7 are shown in Fig. 6.7. It is evident that when the system is under stress, i.e., highly loaded, the damping of system increased around 70% which indicates that more CSs need to be compromised to achieve instability. In this condition, the frequency of inter-area mode also decreases by around 0.2Hz which shows attacker can use low-variation attack signals and reduce its visibility. In contrary, when the system is lightly loaded, the damping increases and frequency

decreases. To obtain the impact of loading, which also corresponds to the time of the day, on the system vulnerability, the variation of damping ratio and frequency of system for simultaneous different loading conditions in each area (bus 7 and 9) is shown in Fig. 6.8.

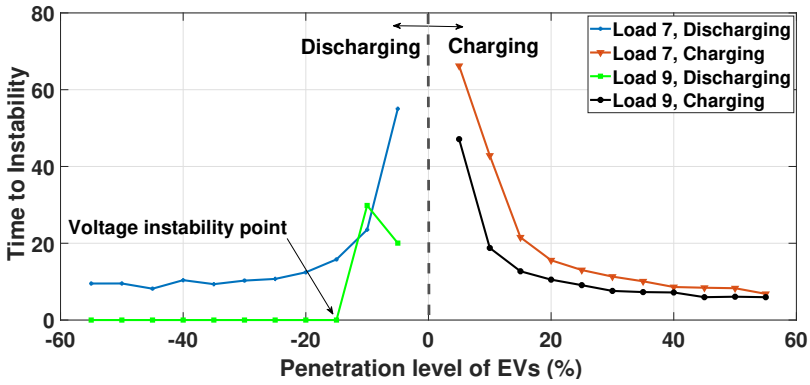

Figure 6.9: ToI versus the penetration level of EVs in two-area Kundur system.

The major impact of having EVs in the system is that they can also charge or discharge depending on the number of compromised CSs. Fig. 6.9 shows the impact of the different number of compromised CSs in the ToI parameter. It can be observed that the discharging attack on bus 9 has a more severe impact on stability compared to bus 7. Moreover, bus 9 is also sensitive to voltage stability issue when the number of charging stations increases. The voltage stability can often be prevented using the injection of reactive power in various levels of grid operation. If the adversary also targets the voltage stability, he/she can benefit from the ability of charging stations to absorb a high amount of reactive power and intensify the voltage stability issue in the grid. In such a case, the system operator will perform several load shedding remedial actions to save the system. The use of FACTS devices can also improve the system response in terms of voltage stability since these devices can inject reactive power using the power electronic-based switches and their control schemes, and consequently improve the voltage profile. The control scheme of these devices can also be used to

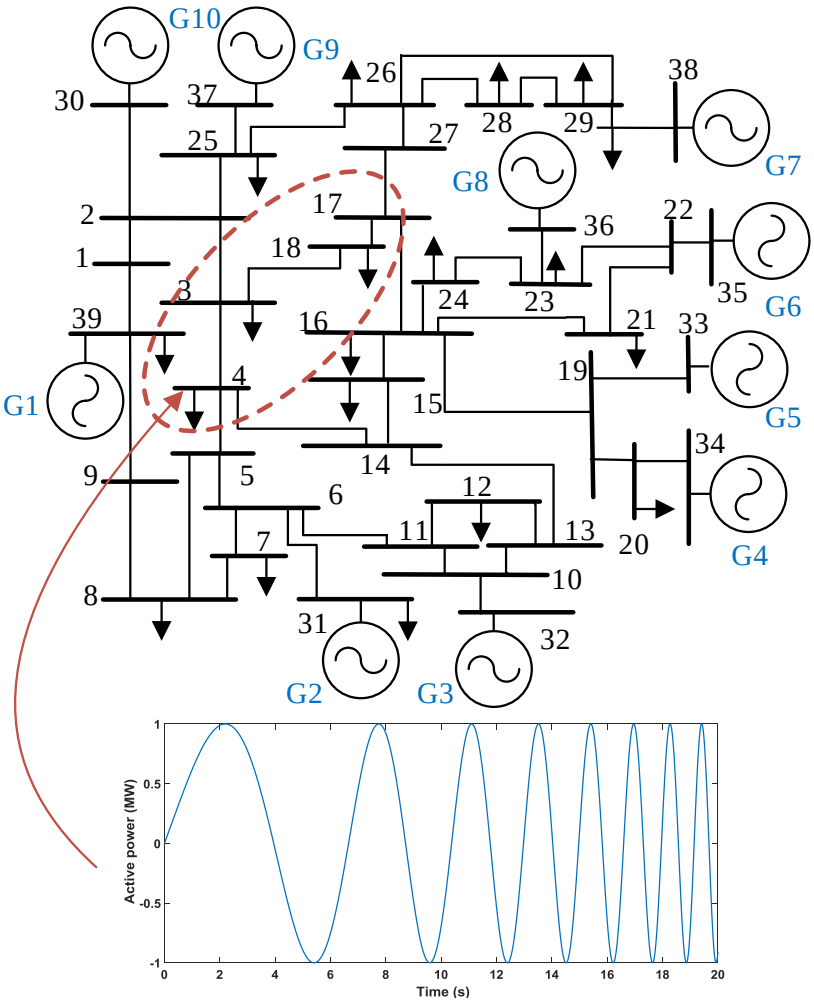

Figure 6.10: 39-bus New England System.

improve the stability margin of the system, however, they can not solve the instability problem permanently.

6.6.2 39-Bus New England Power System

Fig. 6.10 depicts the 39-bus new England power system with 10 synchronous generators modeled in details with IEEE ST1 excitation system, IEEE G1 turbine governor model, and automatic Voltage Regulator (AVR). Generator 1 has an aggregated model that represents the US/Canada interconnections.

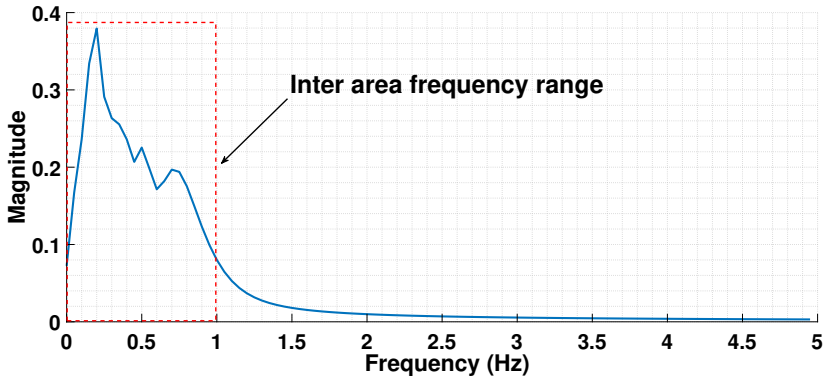

Figure 6.11: Frequency content of chirp signal.

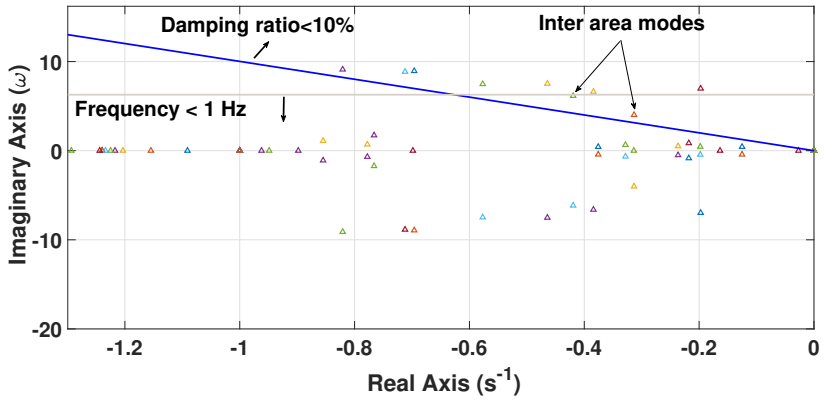

Figure 6.12: The modal analysis of the 39-bus system with identification of inter-area modes.

To investigate the frequency of inter-area mode, a chirp signal is applied (stated in subsection 6.5.1) to the load 4, 18, 3, and 39 with only 10 MW of load which is 2% of the load at those buses as shown in Fig. 6.10. Since we are interested in inter-area modes of the system, starting and ending frequencies are assumed to be 0.1 Hz and 1 Hz, respectively, and the reconnaissance is taking place in 20 s to mislead the grid operator. The frequency content of this signal is depicted in Fig. 6.11. It can be observed that most of the energy of the signal is in the specified range i.e., 0.1 Hz to 1.0 Hz.

The modal analysis of the system reveals two critical inter-area modes with frequency and damping ratio less than 1 Hz and 10%, respectively, as shown in Fig. 6.12.

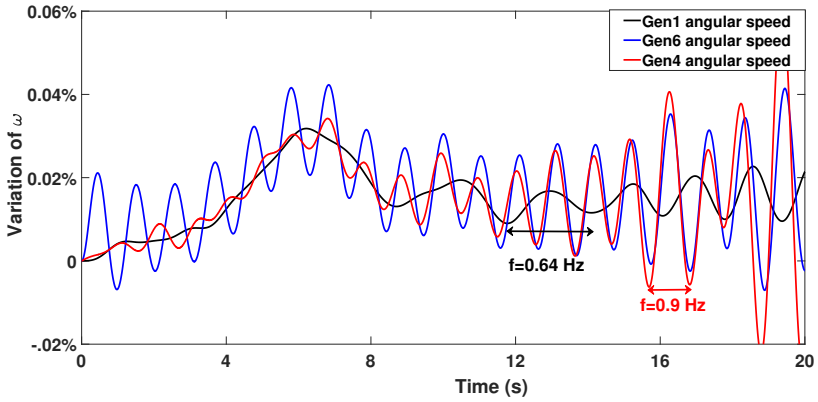

Figure 6.13: The angular speed of generators G1, G6 and G4 following the reconnaissance activity of attacker.

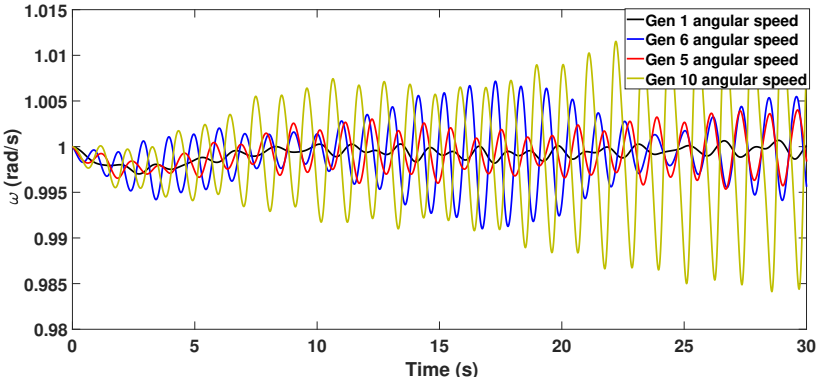

Figure 6.14: Reaction of system generators to 20% of attack (0.9 Hz mode excitation) to the compromised area (loads 18, 3, 39, and 4).

The response of the system in terms of generator angular frequency is demonstrated in Fig. 6.13. It can be observed from this figure that the amount of system response is less than 0.05% of nominal system frequency, therefore, this will remain hidden from the system operator. Fig. 6.13 also shows that the obtained signals from three generators have two poorly damped inter-area oscillation modes with frequency of 0.64 Hz and 0.9 Hz. It also can be observed that in low frequency mode (0.64 Hz), Generator G1 is oscillating against other ones in the system, while in the other, G4 and G6 are in the same area since their response becomes almost similar in such a case.

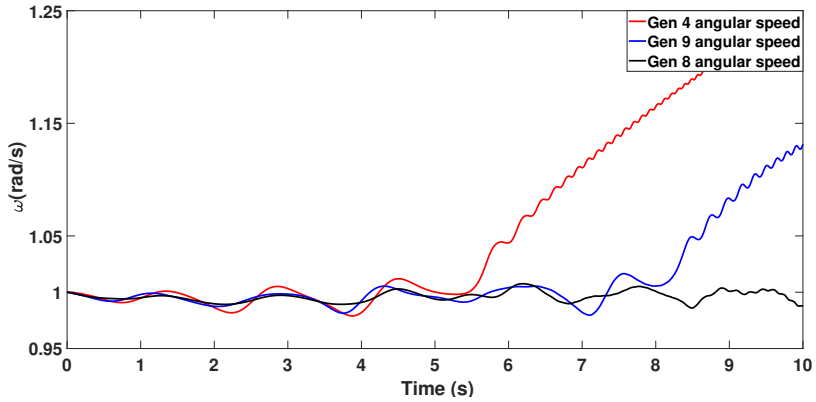

Figure 6.15: Reaction of system generators to 47 MW switching attack in all the load buses of the system.

To demonstrate how attacker can benefit from the knowledge obtained from reconnaissance activity, 20% of the loads in a compromised area (shown in Fig. 6.10) are altered with a sinusoidal waveform of 0.9 Hz obtained from high-frequency inter-area mode. Fig. 6.14 shows the angular speed of the generators 1, 6, 5, and 10. It can be observed that the angular speed of generator 10 is becoming unstable as the most sensitive generator. When 47 MW of all the system loads are changed as a result of attack to EVs with frequency of 0.64 Hz, the collected results depicted in Fig. 6.15 shows a fast instability of system (around 10s) due to a huge number of compromised EV charging stations.

6.6.3 Australian Power System

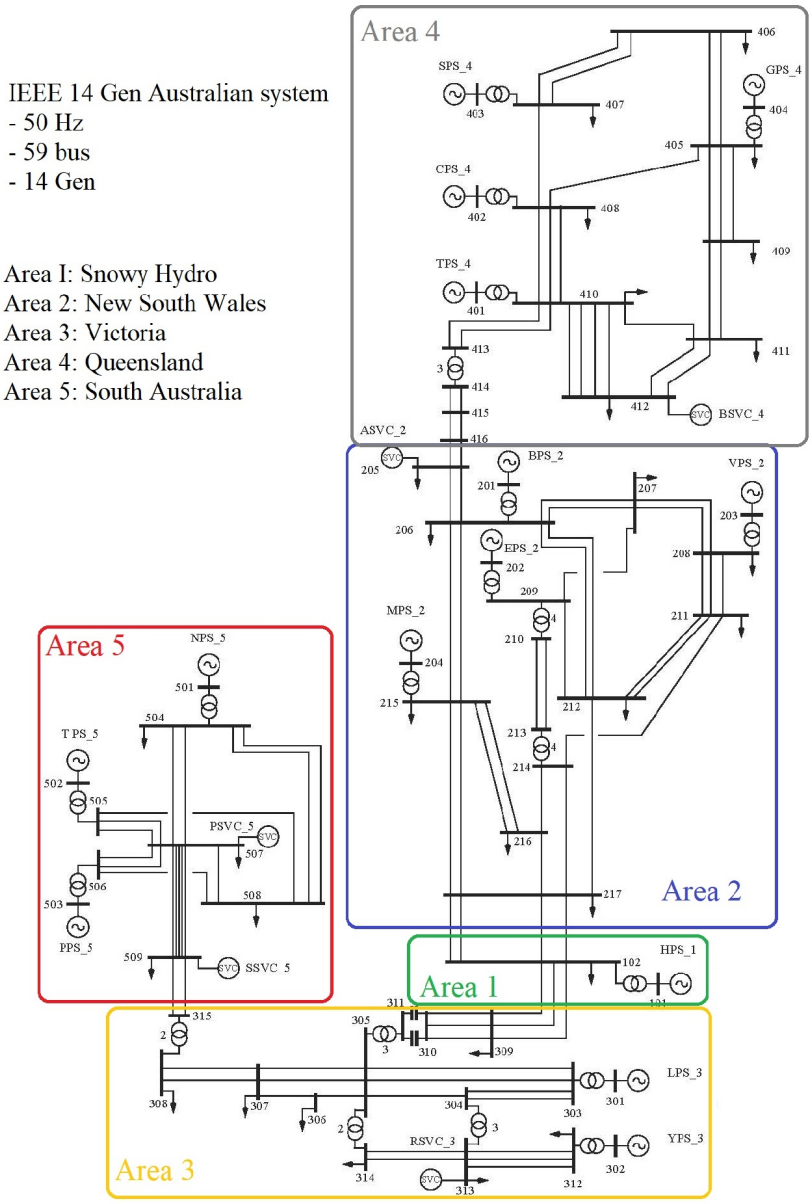

Figure 6.16: IEEE Australian power system [40].

The Australian power system is used, as a realistic test system, to show the impact of the switching attack. The single-line diagram of this system is depicted in Fig. 6.16. This system has 5 areas, 59 buses, and 14 generators that operate at 50 Hz. Depending on the loading condition of the system, different inter-area modes can be excited in

Table 6.1: The inter-area modes of system in scenarios 1 and 2.

	Scenario 1			Scenario 2		
	Eig.	Freq.	Damping	Eig.	Freq.	Damping
λ_1	$-0.089 \pm 3.578i$	0.5695	-0.025	$-0.175 + 4.447i$	0.707	-0.039
λ_2	$-0.052 \pm 2.459i$	0.3915	-0.021	$-0.061 + 2.846i$	0.453	-0.021
λ_3	$-0.152 \pm 2.098i$	0.334	-0.072	$-0.137 + 2.391i$	0.380	-0.057
λ_4	$-0.843 \pm 2.411i$	0.384	-0.330	$-0.679 + 1.928i$	0.306	-0.332
λ_5	$-0.440 \pm 1.406i$	0.224	-0.298	$-0.450 + 1.375i$	0.218	-0.311

this grid. As a result, this system is often used in study of power grid stability issues in low frequencies [31]. Two different loading condition scenarios are considered here. In the first one, the power flows from north to south of the grid and the system loading is heavy (peak time), i.e., total load is considered to be 22,300 MW. In the second scenario, the transfer between different parts of the system is almost zero since the system lightly loaded (off peak time), i.e., total load is considered as 14,630 MW.

For both of the considered scenarios, initially, the eigenvalues of the system in both scenarios are shown in Fig. 6.17. It can be observed that in both scenarios, the system has 5 inter-area modes, with frequencies $\{0.5695, 0.3915, 0.3339, 0.3837, 0.2238\}$ Hz and $\{0.7078, 0.4530, 0.3806, 0.3068, 0.2189\}$ Hz for scenarios 1 and 2, respectively. The variation between inter-area modes of two different loaded conditions indicates that an attacker requires different attack procedure on different time of the day.

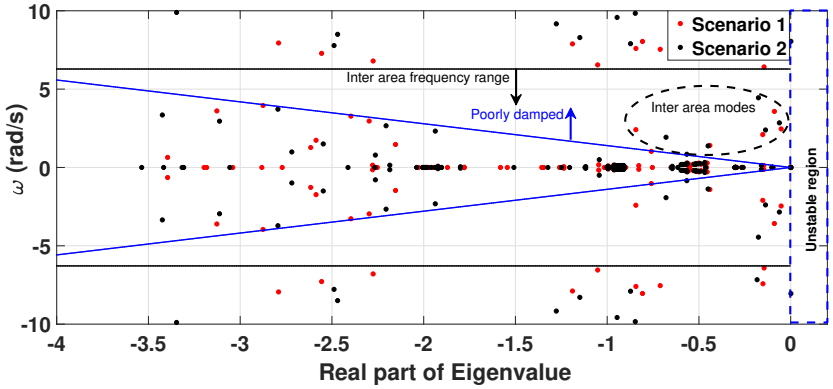

Figure 6.17: System eigenvalues and inter-area modes for Australian system in both peak and off-peak time.

Table 6.1 shows the details of each mode for both of the scenarios. It is worth mentioning that modes with damping close to zero represent a more vulnerable condition in the system. Thus, we focus on the first three modes. Assuming an adversary without significant information about the system parameters, the chirp signal can provide the required data of the system to the adversary. Fig. 6.18 shows the system response and the estimation of the inter-area oscillation frequencies following a 10% change in load 508 in area 5. It can be observed that the adversary obtains almost similar frequencies by observing the system measurements. It needs to be mentioned that the identification of the inter-area modes are done without significant change in the system angular speeds, i.e., less than 0.2%, as a result, the adversary could be remain stealthy.

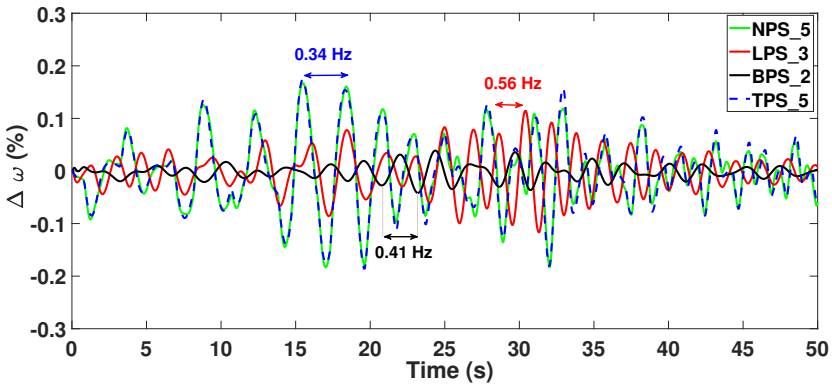

Figure 6.18: The angular speeds of synchronous generators following a 10% change in load 508 in area 5.

In the next step, based on the acquired knowledge, we investigate the impact of two types of attack scenarios (i.e., drop in load by stop EV charging or spike in generation by discharging EVs). We assume that the adversary uses the obtained knowledge and charges the compromised set of EVs in the system, i.e., 10% of load in area 5 of system. Fig. 6.19 illustrates the angular speed of 5 generators from 5 areas of the system following the attack at t=10 s on heavy loaded condition. Fig. 6.19 depicts that the system becomes unstable in almost 35 seconds after the attack initiation.

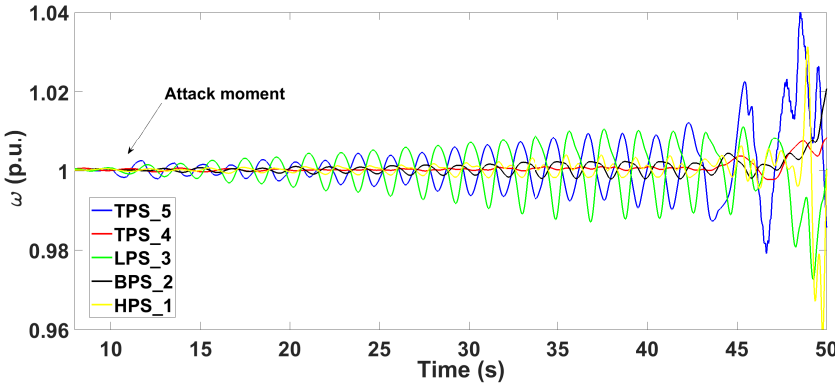

Figure 6.19: The angular speed of 5 generators form 5 areas of system following charging of EVs in area 5 equal to 10% of load in this area.

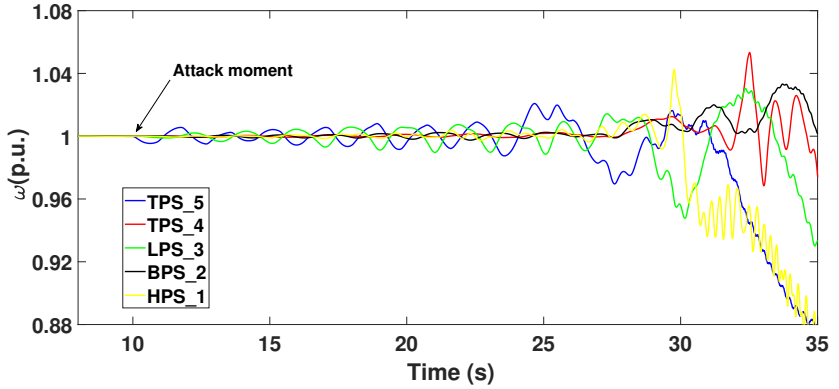

Figure 6.20: The angular speed of 5 generators form 5 areas of system following discharging of EVs in area 5 equal to 20% of load in this area.

Besides, generator at area 5 suffers with slightly worse instability condition.

Since in the considered scenario the system is heavily loaded, it is expected that discharging the huge amount of EVs significantly decreases the time required to meet instability. Fig. 6.20 illustrates the angular speeds of synchronous generators in such a condition, where the EVs start to inject their power (discharging EVs) equal to 20% of total load in area 5. As expected, the system becomes unstable quickly after 22 seconds following the attack moment. In both of these attacks, the adversary uses the 0.54 Hz inter-area mode of system. Moreover, to demonstrate a scenario where the adversary has the ability to compromise several areas of system, a new attack scenario is considered in which instead of comprising CSs only from one area, the

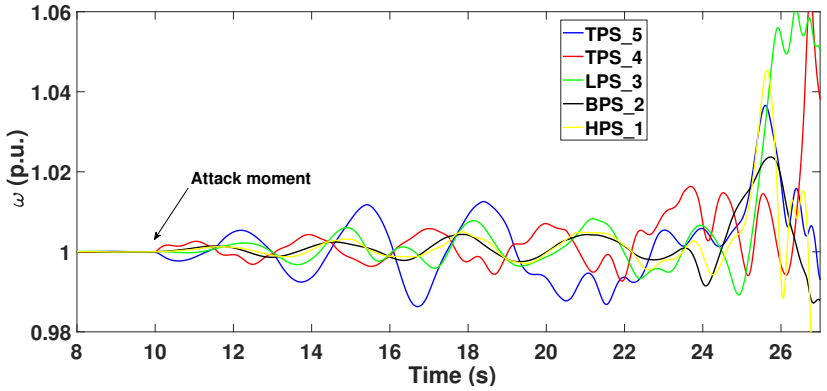

Figure 6.21: The angular speed of 5 generators from 5 areas of system following charging/discharging of EVs in area 5/area 4 equal to 10% of area load.

adversary drops 10% of loads in area 5 and increase 10% generation by discharging in area 4. The attack is launched using 0.334 Hz inter-area mode since it affects both of these areas. Fig. 6.21 shows the angular speeds of generators and depicts their instability. It can be observed that the system becomes quickly unstable for such more dispersed but coordinated attack.

6.7 Attack Detection Mechanism

The above-presented challenges call for a formulation of the threats associated with the EV large scale charging/discharging functionality, modeling the grid behavior, and characterizing the grid response. This formulation is a first step towards designing proactive and reactive strategies to prevent the impact of those attacks on the power grid. Hence, we propose a detection method to assist the grid to be protected from the dire consequences of inter-area oscillation initiated from EV charging ecosystem. Since, EV charging and discharging is executed through a pre-defined message exchange as in OCPP [12], for switching attack, a set of messages need to be exchanged and approved. Hence, a neural network based anomaly detection engine can be designed to monitor message exchanges to detect the switching attack. The

built engine will leverage historical patterns of charging and/or discharging behavior of EV users. This engine will be deployed by the central management system (CMS) of EV charging to detect malicious messages and to protect the grid from the EV-based coordinated switching attack, instead of immediate execution, the malicious requests might be discarded or delayed. For a detailed description, we explain the attack scenarios to understand the features needed to be monitored by the CMS to detect a malicious attempt. Then, we depict the detection algorithm based on back propagation neural network (BPNN) and finally the competency of this detection mechanism is elaborated.

6.7.1 Coordinated Switching Attack Vector

To initiate a switching attack from the CS surface, a number of CSs have to alter their action of charging to not charging/discharging and again back to the previous state within a very short period of time. The required compromised EV load (either public or private or both) and duration of the attack duration are dependent on the loaded condition of the grid. These also depend on the attack pattern, such as surge in load (i.e., sudden change in charging/not charging) or spike in generation (i.e., sudden increment by EV discharging). The simulation of different attack scenarios over three different power systems (i.e., two area kundur bench mark, 39-Bus New England power system and Australian power system) for different loaded situations (e.g., peak time, off-peak time) provide the attack vector containing amount of comprised load; i.e., number of comprised CSs and their charging rate, the duration of the attack, the oscillation frequency, etc. The features of this attack vector are studied during the training period of our proposed detection algorithm to detect malicious attempts when they exist.

Our attack simulation reveals that a number of CSs alter their actions within a

short period of time. Hence, along with observing the activity of a single public CS, the algorithm will monitor or scan the activities of other active public CSs over a certain period of time. Active CSs indicate those CSs which are in service during the monitored time period. This period of time represents the duration required to perform a switching attack.

As a consequence, to detect a switching attack motive of an CS, two important features of the data need to be studied: i) the duration between two successive charging or discharging sessions and ii) the load variation for a certain period of time. The threshold value of these features should be varied with different load conditions of the grid and the proposed detection algorithm has to study these from the given training set.

6.7.2 BPNN Based Detection Mechanism

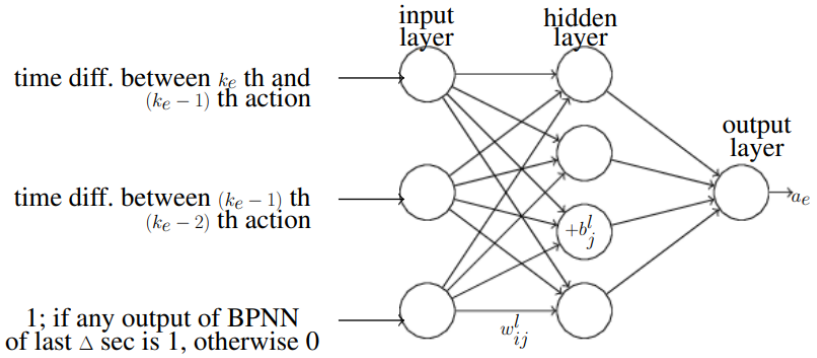

Figure 6.22: A back propagation neural network to detect malicious requests.

After simulating different attack scenarios, a BPNN is designed to assess the features of the data set to identify the switching attack attempt initiated from a connected CS. As the BPNN is hosted by the CMS as depicted in Fig. 6.1, this can only detect the switching attack initiated from public CSs. Since, all public CSs are assumed to be connected through a CMS, a CMS can exploit this BPNN to detect switching attacks.

The designed BPNN consists of one input, one or multiple hidden layers and an output layer. Each node of each layer is connected with all the nodes of adjacent layers with a weighted link. $\mathcal{W}$ is the vector of the weighted link, while $w_{ij}^{l} \in \mathcal{W}$ is the link between node j of layer l with the node i of layer $(l-1)$ as depicted in Fig. 6.22 and $w_{ij}^{l} = w_{ji}^{l}$. The bias vector is represented as $\bar{\mathcal{B}}$, while $b_{j}^{l} \in \bar{\mathcal{B}}$ would be added to the j^{th} node of any layer l except the input layer to reduce the variance and hence introduce flexibility and better generalisation to the BPNN. Finally, as the activation function, we utilize ReLU function in hidden layer to avoid vanishing gradient problem and the softmax function is utilized in output layer to generate the binary output (e.g., output 1 indicates an attack attempt, while 0 is for non-malicious request).

The CMS is assumed to manage a set of CS E. Whenever an action request (charging/stop charging/discharging) arrives to the CMS, this request is passed to the designed BPNN to determine whether this request is malicious or not. As an example, while the k_eth action arrives from CS $e \in E$, the first node of input layer measures the time difference between k_eth and $(k_e - 1)$th action request. On the other hand, the input to the second node of input layer is the time difference between $(k_e - 1)$th and $(k_e - 2)$th action. These two inputs help to identify the anomaly in the action behavior of CS e. The input to the third node of the input layer is a binary one. As we investigate a coordinated attack, the third input is considered as 1 while any other malicious attempt was detected in last Δ time; otherwise, this input is considered as 0. The value Δ is determined from the simulation and varied from grid to grid and even from time to time.

To train the BPNN, a large data set is required for different switching attack scenarios initiated from public CSs. As a consequence, we simulate different attack scenarios for different load conditions over different grids. However, at the beginning, arbitrary values are chosen for $w_{ij}^{l} \in \mathcal{W}$, $b_{j}^{l} \in \bar{\mathcal{B}}$ and the binary output a_{e}^{k} for the k_{e}^{th}

request from CS e is known for the training set. Now, utilizing these arbitrary values and the activation function, the BPNN calculates the output $\bar{a}_e^k$ as:

$$\bar{a}_e^k = softmax(b_o + \sum_j y_j) \tag{6.20}$$

here, b_o is the bias of output node and y_j is the output of the hidden node j as expressed in the following:

$$y_j = ReLU(b_j + \sum_i x_i); \forall j \tag{6.21}$$

b_j is the bias of node j of the hidden layer, while x_i is the input from node i from the input layer. Then, $\bar{a}_e^k$ will be compared with the known a_e^k. If these two values do not match, a back propagation approach is introduced to set the values for $\mathcal{W}$ and $\bar{\mathcal{B}}$ for the whole training set to attain the objective of $\bar{a}_e^k = a_e^k$. Finally, the BPNN tests and evaluates these values.

Though conventionally an OCPP request is immediately executed just after an authentication (e.g., CS ID, EV ID etc.), our designed algorithm can act as a filter to assess those messages before execution. Since, the actual intention of detecting such adversary attempts is to prevent the grid from the switching attack, whenever, the CMS would suspect a request as an adversary one, the request might be discarded or a random delay δ would be generated instead of the immediate execution to disrupt the anticipated coordination of attacks. The overall process is depicted in Fig.6.23.

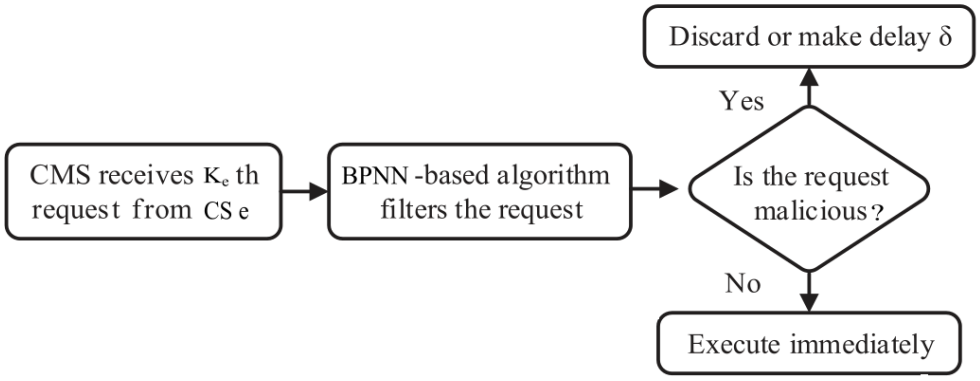

Figure 6.23: Flow diagram of BPNN based detection and mitigation process.

6.7.3 Performance Evaluation of BPNN

Now, in order to evaluate the effectiveness of the proposed detection method, first, we have simulated switching attacks for different load conditions to attain the training and testing data set. These simulations assist to map the respective charging/discharging requests, e.g., each charging/discharging session starting time, duration, charging rate, etc.

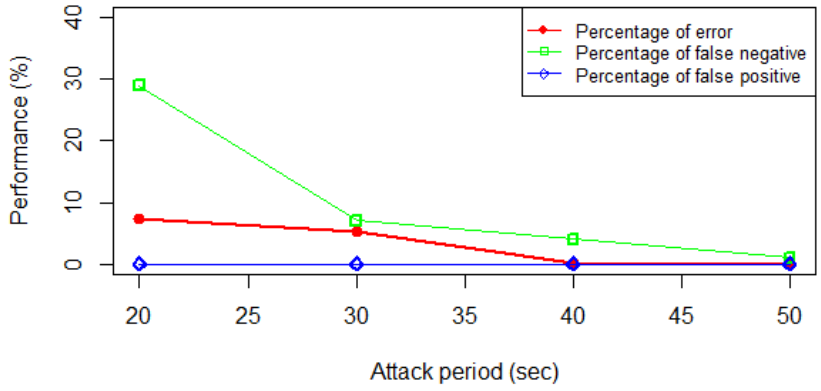

Figure 6.24: Performance analysis of the designed perception.

To evaluate the performance, we consider three different performance parameters; percentage of error, percentage of false negative and percentage of false positive decisions. Percentage of error considers the overall error rate based on the total data length, while false negative indicates those decisions which show attack attempts as

non-attack. As a ramification, a higher ratio of false negative decisions may allow attack attempts, even when applying a BPNN having a higher accuracy. On the other hand, a higher ratio of false positive (i.e., non attack attempt is detected as attack) may deprive legitimate EV users from obtaining their service and consequently, degrade the quality of service (QoS) of the CSs.

Fig. 6.24 depicts the performance of a perception (i.e., the BPNN having a single hidden layer) for different attack duration, while the performance metric is actually the average value after running 10 time for each data set. The figure depicts that the percentage of error decreases with the attack duration; for instance, the percentage of error decreased from 8% to 5% when the attack duration increased from 20sec to 30sec and this perception is almost 100% accurate for those attacks whose duration is more than 40sec. As a consequence, an attacker having smaller period to carry its attack, i.e., a prompt attack, is stealthier and more difficult to detect. However, though almost 92% accuracy is shown for attacks having 20sec duration, the ratio of false negative decision is almost 30%, which indicates that even after a higher accuracy, the BPNN is not able to detect all attempts. However, as our intention is to prevent the grid from an anticipated switching attack and since such attack is actually attempted from a set of CSs, even this amount of accuracy could be sufficient to disrupt the mutual coordination among those comprised CSs and pacify their desired consequences (i.e., the rest false negative requests would not be large enough to create the instability).

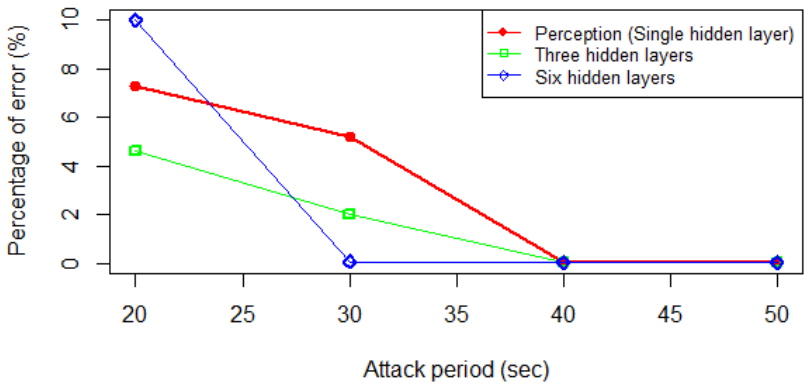

Figure 6.25: Accuracy variation with number of hidden layers.

The accuracy is also evaluated with the number of hidden layers as shown in Fig. 6.25 and this depicts that there is no consistency in accuracy with the number of hidden layers. As an example, a BPNN having six hidden layers shows the worst performance for the attack set having a duration of 20sec, while this becomes almost accurate for an attack duration of 30sec. This observation imposes a challenge to set a global design for different attack scenarios.

6.8 Conclusion

The increased popularity of EVs and their charging infrastructure has opened new windows for rogue actors to attack the power grid. Through the exploit of large-scale deployment of EV charging systems and EV functionalities, we presented a coordinated switching attack to initiate inter-area oscillations in the power grid. Our switching attack was formulated in two forms: a decrease in load through the termination of EV charging, and an increase in power supply through EV ancillary services which is a unique functionality of EVs. The consequences of the attack were presented through a state-space model, and tested on the two-area Kundur system, 39-Bus New England system, and on the Australian 5-area power grid. Two attack strategies are

considered to demonstrate the impact of attacker knowledge on the performed attack. We have shown that using the reconnaissance method by altering a very small amount of load, the adversary can observe and determine the inter-area mode. After gathering the knowledge for different loaded systems, we examined different attack scenarios i.e., only drop in load or only spike in generation or a combination between both. Finally, we provided a framework to detect these attack attempts by implementing a BPNN based algorithm hosted by the CMS.

Chapter 7

Discussion and Future work

7.1 Discussion

To ameliorate the consequences of global warming, a prompt transportation electrification is inevitable and fortunately, the global EV market was burgeoning. But the sudden impact of the Global pandemic, COVID-19 is jeopardizing the anticipated growth and lowering the EV sale by 17% in Europe [88]. However, IEA makes an interesting observation that while EV growth is declining by 17%, then this declining rate is 80% for combustion engine vehicle [88] and hence, that can be taken as an indication that this pandemic is making people more environment conscious. Consequently, in the post pandemic market, the EV growth may surpass the previous anticipation and consequently, ongoing research needs to be continued and accelerated to ensure their graceful penetration. In this thesis, our main objective was to accelerate this EV penetration by developing the EV charging scheme more smart and secured. However, among with other causes, the range anxiety was identified as the major obstacle that make people reluctant in switching to EVs. The smaller battery size, frequent charging requirement, longer charging and waiting time, inadequate charging facility etc. originate such anxiety. Since, an abrupt change in battery

technology (i.e., larger battery in cheaper price with lighter weight) is not possible, the strategical placement and dimension of a fast charging network might be a major key to mitigate the range anxiety, while a prolific CS network should offer a minimum QoS to encourage people in using public CSs and should not degrade the power quality of the grid. On the other hand, to attain the goal of carbon reduction, the grid dependency for EV charging also requires to be curtailed and hence, auxiliary green charging sources have to be stimulated. Though introducing RE based standalone CSs or implementing bidirectional energy transfer capability of EVs (especially V2V) could be potential solutions for curtailing the dependency on the grid, we addressed the intermittent behavior of RE production as the major challenge of managing a RE based standalone CS, while the trajectory and scheduling selections of V2V enabled charging trucks are required for an efficient strategy of charging EVs to maximize the revenue. However, to attain such smart charging solutions, a successful information sharing communication platform is inevitable and fortunately is now reality. But unfortunately, this communication link introduces different types of attack possibilities especially to the grid stability. Accounting this in our consideration, as per our best knowledge, we are the first who investigated the competency of EV charging ecosystem as a potential surface for initiating switching attack to create an inter area oscillation between two weakly tied power generation areas. After simulating a detailed attack scenarios and observed the dire consequences, we also proposed a neural network based detection algorithm which has a high accuracy of detection before the attack being executed.

First, a two stage model was proposed to tackle a charging infrastructure network design problem, while the first stage determined the optimal locations and the second one decided the capacity (i.e., the required number of poles) to minimize the deployment cost. Assuring a minimum QoS in terms of tolerable waiting time and

detour distance might make the design appealing to EV users. Given that the mass deployment of CSs may degrade the voltage level at any bus of the power distribution network. Hence, to make it stable, we considered installing voltage regulators (if required) and determined the respective tap positions. The strategical CS deployment was capable of reducing the required number of voltage regulators to minimize the cost. We also determined the transformer capacity to support the installed CSs and the capacity of distribution grid was also considered to avoid load congestion. Finally, We examined two different designs of expanding CSs facility to meet the increasing anticipated demand and suggested to consider the anticipated future load during the present installation for being more compatible and cost efficient at the long run.

However, users' satisfaction should get most priority to promote the EV market. Getting required energy inside targeted deadlines at minimum price, rather than the cleanliness of the energy source, is a major key to satisfy EV owners. On the other hand, green energy sources need to be incorporated for achieving the anticipated benefits of EVs in mitigating global warming and energy scarcity. Hence, in the second project, we assumed a smart CS, which used a PV system integrated with an ESS to charge EVs at variable rates. A quadratic price function was proposed, that ensured the equity among the EVs, i.e., an EV could enjoy a higher charging rate only by paying more. As PV was the only energy source, when few EVs were charging at higher rates, others had to charge slowly at lower price. This load shifting mechanism together with an ESS helped accommodate the EV charging using the limited amount of energy. To handle the uncertain behavior of both the load request and PV generation, a frequent prediction was made. The model was examined in both centralized (ILP based model) and decentralized methods (game theoretic model). Though the centralized method was capable of providing optimal solution, it took a very long time in making a decision especially for a large number of EVs. On

the other hand, the game theoretic model was prompt and capable of providing optimal solution, while this considered the upcoming load requests during the strategy selection.

Next, an offline problem was addressed for a company having a number of trucks equipped with a larger battery along with a fast charger to charge EVs through V2V at some predefined parking lots. The objective of the work was to serve as many EVs as possible using this limited number of trucks by determining their trajectories and schedules. An EV was considered served only when its demand would be fulfilled inside its given charging window. The problem also considered the energy consumption of trucks during the travelling period and each truck had to return to the depot after serving EVs. An ILP was formed to determine the optimal solution and it was formally proven NP-Hard. As the computation time for ILP was too large to be applicable, we decomposed the problem using Dantzig-Wolfe decomposition and its performances were extensively analyzed by varying different parameters for different scenarios and compared with two other proposed greedy algorithms. We also discussed the trade-off between performance and computational time of this decomposition model to determine the iteration number which can ensure a better solution within an acceptable time.

Since, the inter connected EV charging infrastructure has opened new windows for rogue actors to attack the power grid, through the exploit of large-scale deployment of EV charging systems and EV functionalities, we presented a coordinated switching attack to initiate inter-area oscillations in the power grid. Our switching attack was formulated in two forms: a decrease in load through the termination of EV charging, and an increase in power supply through EV ancillary services which is a unique functionality of EVs. The consequences of the attack were presented through a state-space model, and tested on the two-area Kundur system, 39-Bus New England system,

and on the Australian 5-area power grid. Two attack strategies were considered to demonstrate the impact of attacker knowledge on the performed attack. We had shown that using the reconnaissance method by altering a very small amount of load, the adversary can observe and determine the inter-area mode. After gathering the knowledge for different loaded systems, we examined different attack scenarios i.e., only drop in load or only spike in generation or a combination between both.Finally, we provided a BPNN based framework to detect the attack attempts and attained a high accuracy of detection before the attack execution.

7.2 Future Work

The work presented in the thesis provided considerable effort to identify the challenges that hinder the EV adoption and hence, obstruct to attain the carbon emission reduction goal from the transportation sector. We designed a strategical placement, dimension and expansion methodology for the DC fast charger in an urban area to mitigate the range anxiety. After that we proposed a smart management system for a PV based standalone CS to propel the RE integration in EV charging, while V2V energy sharing was also considered to curtail the dependency on traditional CSs. Finally, the competency of compromised CSs as switching attack surface was tested and a BPNN based detection algorithm was presented. However, there remains several future research directions as extensions of these addressed problems which may add extra benefits to ensure a smooth penetration of mass number of EVs.

As an example, our proposed method suggested to deploy a large number of CSs to mitigate the range anxiety and hence integrate a remarkable load with the grid, which may cause a significant power loss and introduce a new peak on load profile and as a ramification, a set of strategies need to be taken from the power generation and transmission end. Hence, we are aiming to do a detailed investigation regarding

the possible negative consequences of large scale fast CSs penetration to determine the possible mitigation for the power operators.

In both our second and third contributions, we addressed two scheduling problem, while the problems were solved in an offline fashion. However, in real life, that might not be always possible to attain all information prior the decision making process and sometimes, an instantaneous decision is required to be made. As a consequence, as an extension of those works, we are planning to solve the problems in an online fashion. On the other hand, instead of handling a single PV powered CS as our second project, this could be worthy to handle a multiple number of standalone CSs, where the scheduler will also solve the CS selection for an EV to minimize its charging price and time. Moreover, other renewable energy sources also could be incorporated and handled for such standalone CSs. On the other hand, as an extension of the third work, where we determined the routing and scheduling of a set of V2V enabled trucks, instead of considering pre-assigned parking lot, we could optimize the charging locations to serve more number of EVs. We can also consider multiple number of depots, while one truck may start its journey from one depot and finish at the most convenient one to maximize the objective. To attain a more realistic scenario, we will consider different battery sizes of charging trucks as well.

The Internet of Things (IoT) enabled CS network was successfully investigated as a potential switching attack surface to the grid in this thesis and we devised a BPNN based detection mechanism having sufficient accuracy to derange the coordination of attacks attempts. However, other machine learning (ML) algorithms also can be implemented and tested. On the other hand, for mitigation purpose, we are aiming to design a wide area controller. However, beside initiating switching attacks, attackers may compromise CSs or manipulate OCPP messages to control the charging/discharging operations to create different types of attack and creates substantial

losses to EVs, CSs and grid. Hence, monitoring CS networks from the CMS end for detecting any type of malicious activities becomes noteworthy for taking mitigation initiatives. However, for developing such a detection mechanism, a detailed simulation will be required which should consider EV charging ecosystem, OCPP protocol and the smart grid. Since, a test bed might be too expensive and complex to test such scenarios, we are also planning to develop a co-simulator to serve these purposes.

Bibliography

[1] 81% of electric vehicle charging is done at home. Available at https://insideevs.com/most-electric-vehicle-owners-charge-at-home-in-other-news-the-sky-is-blue/.

[2] History of the electric vehicle. Available at https://en.wikipedia.org/wiki/History_of_the_electric_vehicle.

[3] List of rooftop photovoltaic installations. Available at https://en.wikipedia.org/wiki/List_of_rooftop_photovoltaic_installations.

[4] Ikea to install electric car-charging stations at all canadian stores, July 2015. Available at http://www.cbc.ca/news/business/ikea-to-install-electric-car-charging-stations-at-all-canadian-stores-1.3144670.

[5] Canada's largest commercial rooftop solar system unveiled, June 2016. Available at https://www.enmax.com/news-events/news/largest-rooftop-solar-system-unveiled.

[6] S. Acharya, Y. Dvorkin, and R. Karri. Public plug-in electric vehicles+ grid data: Is a new cyberattack vector viable? *arXiv preprint arXiv:1907.08283*, 2019.

[7] F. Ahmad, M. S. Alam, and S. M. Shariff. A cost-efficient energy management

system for battery swapping station. *IEEE Systems Journal*, 13(4):4355–4364, Dec 2019.

[8] F. Ahmad, M. S. Alam, S. M. Shariff, and M. Krishnamurthy. A cost-efficient approach to ev charging station integrated community microgrid: A case study of indian power market. *IEEE Transactions on Transportation Electrification*, 5(1):200–214, March 2019.

[9] E. Akhavan-Rezai, M. F. Shaaban, E. F. El-Saadany, and F. Karray. Online intelligent demand management of plug-in electric vehicles in future smart parking lots. *IEEE Systems Journal*, 10(2), 2016.

[10] C. Alcaraz and et al. OCPP protocol: Security threats and challenges. *IEEE Transactions on Smart Grid*, 8(5), 2017.

[11] M. Alizadeh, H. Wai, M. Chowdhury, A. Goldsmith, A. Scaglione, and T. Javidi. Optimal pricing to manage electric vehicles in coupled power and transportation networks. *IEEE Transactions on Control of Network Systems*, 4(4):863–875, Dec 2017.

[12] O. C. Alliance. Open charge point protocol 2.0, 2018, 2018.

[13] R. Alvaro, J. González, C. Gamallo, J. Fraile-Ardanuy, and D. L. Knapen. Vehicle to vehicle energy exchange in smart grid applications. In *Connected Vehicles and Expo (ICCVE), 2014 International Conference on*, pages 178–184. IEEE, 2014.

[14] M. H. Amini, J. Mohammadi, and S. Kar. Distributed holistic framework for smart city infrastructures: Tale of interdependent electrified transportation network and power grid. *IEEE Access*, 7:157535–157554, 2019.

[15] S. Amini, H. Mohsenian-Rad, and F. Pasqualetti. Dynamic load altering attacks in smart grid. In *2015 IEEE Power Energy Society Innovative Smart Grid Technologies Conference (ISGT)*, pages 1–5, Feb 2015.

[16] J. Antoun and et al. A detailed security assessment of the ev charging ecosystem. *IEEE Network*, 2020.

[17] J. Arbib and T. Seba. Rethinking transportation 2020-2030. *RethinkX, May*, 2017.

[18] R. Atallah, C. Assi, W. Fawaz, M. H. K. Tushar, and M. J. Khabbaz. Optimal supercharge scheduling of electric vehicles: Centralized vs. decentralized methods. *IEEE Transactions on Vehicular Technology*, 2018.

[19] S. Bae and A. Kwasinski. Spatial and temporal model of electric vehicle charging demand. *IEEE Transactions on Smart Grid*, 3(1):394–403, March 2012.

[20] M. Baran and F. F. Wu. Optimal sizing of capacitors placed on a radial distribution system. *IEEE Transactions on Power Delivery*, 4(1):735–743, Jan 1989.

[21] M. E. Baran and F. F. Wu. Network reconfiguration in distribution systems for loss reduction and load balancing. *IEEE Transactions on Power delivery*, 4(2):1401–1407, 1989.

[22] S. Barghi-Nia. *Managing Stress of Electric Vehicles on Smart Grids*. PhD thesis, École Polytechnique de Montréal, 2017.

[23] I. S. Bayram, G. Michailidis, M. Devetsikiotis, and F. Granelli. Electric power allocation in a network of fast charging stations. *IEEE Journal on Selected Areas in Communications*, 31(7), 2013.

[24] T. Bi, J. Guo, K. Xu, L. Zhang, and Q. Yang. The Impact of Time Synchronization Deviation on the Performance of Synchrophasor Measurements and Wide Area Damping Control. *IEEE Transactions on Smart Grid*, 8(4):1545–1552, July 2017.

[25] Z. Bo, O. Shaojie, Z. Jianhua, S. Hui, W. Geng, and Z. Ming. An analysis of previous blackouts in the world: Lessons for China's power industry. *Renewable and Sustainable Energy Reviews*, 42:1151–1163, 2015.

[26] E. Bulut and M. C. Kisacikoglu. Mitigating range anxiety via vehicle-to-vehicle social charging system. In *Vehicular Technology Conference (VTC Spring), 2017 IEEE 85th*, pages 1–5. IEEE, 2017.

[27] H. Cai, X. Jia, A. S. Chiu, X. Hu, and M. Xu. Siting public electric vehicle charging stations in beijing using big-data informed travel patterns of the taxi fleet. *Transportation Research Part D: Transport and Environment*, 33:39–46, 2014.

[28] B. Canis. Battery manufacturing for hybrid and electric vehicles: Policy issues. Congressional Research Service, Library of Congress, 2011.

[29] Q. Chen, F. Wang, B. M. Hodge, J. Zhang, Z. Li, M. Shafie-Khah, and J. P. S. Catalão. Dynamic price vector formation model-based automatic demand response strategy for pv-assisted ev charging stations. *IEEE Transactions on Smart Grid*, 8(6):2903–2915, Nov 2017.

[30] A. Chesterton. Bmw: Electric cars will never be as cheap as a combustion engine, October 2018. Available at `https://www.carsguide.com.au/car-news/bmw-electric-cars-will-never-be-as-cheap-as-a-combustion-engine-71326`.

[31] R. Christie. Power systems test case archive. *Electrical Engineering dept., University of Washington*, page 108, 2000.

[32] P. Coelho. Linearization of the product of two variables. *Canada Research Chair in Integrated Logistics*, 2013.

[33] J.-P. Collin and M. Robertson. The borough system of consolidated montreal: revisiting urban governance in a composite metropolis. *Journal of Urban Affairs*, 27(3):307–330, 2005.

[34] Q. Cui, Y. Weng, and C. Tan. Electric vehicle charging station placement method for urban areas. *IEEE Transactions on Smart Grid*, pages 1–1, 2019.

[35] N. Daina, A. Sivakumar, and J. W. Polak. Electric vehicle charging choices: Modelling and implications for smart charging services. *Transportation Research Part C: Emerging Technologies*, 81:36 – 56, 2017.

[36] G. Desaulniers, J. Desrosiers, Y. Dumas, M. M. Solomon, and F. Soumis. Daily aircraft routing and scheduling. *Management Science*, 43(6):841–855, 1997.

[37] J. Desrosiers, Y. Dumas, M. M. Solomon, and F. Soumis. Time constrained routing and scheduling. *Handbooks in operations research and management science*, 8:35–139, 1995.

[38] J. Desrosiers, M. Sauvé, and F. Soumis. Lagrangian relaxation methods for solving the minimum fleet size multiple traveling salesman problem with time windows. *Management Science*, 34(8):1005–1022, 1988.

[39] C. Dharmakeerthi, N. Mithulananthan, and T. Saha. A comprehensive planning framework for electric vehicle charging infrastructure deployment in the power grid with enhanced voltage stability. *International Transactions on Electrical Energy Systems*, 25(6), 2015.

[40] A. Dwivedi and X. Yu. A maximum-flow-based complex network approach for power system vulnerability analysis. *IEEE Transactions on Industrial Informatics*, 9(1):81–88, Feb 2013.

[41] T. Earl, L. Mathieu, S. Cornelis, S. Kenny, C. C. Ambel, and J. Nix. Analysis of long haul battery electric trucks in eu. In *Commercial Vehicle Workshop, Graz*, 2018.

[42] O. Edenhofer. *Climate change 2014: mitigation of climate change*, volume 3. Cambridge University Press, 2015.

[43] A. El Desouky and M. El Kateb. Hybrid adaptive techniques for electric-load forecast using ann and arima. *IEE Proceedings-Generation, Transmission and Distribution*, 147(4), 2000.

[44] M. Erol-Kantarci, J. H. Sarker, and H. T. Mouftah. Quality of service in plug-in electric vehicle charging infrastructure. In *2012 IEEE International Electric Vehicle Conference*, pages 1–5. IEEE, 2012.

[45] F. Fakhrmoosavi, M. Kavianipour, M. Shojaei, A. Zockaie, M. Ghamami, J. Wang, and R. Jackson. Electric vehicle charger placement optimization in michigan considering monthly traffic demand and battery performance variations. *Transportation Research Record*, page 0361198120981958, 2020.

[46] L. Fan and Z. Miao. Time-domain measurements-based dq-frame admittance model identification of inverter-based resources. *IEEE Trans. on Power Systems*, pages 1–1, 2020.

[47] A. Farraj, E. Hammad, A. A. Daoud, and D. Kundur. A Game-Theoretic Analysis of Cyber Switching Attacks and Mitigation in Smart Grid Systems. *IEEE Transactions on Smart Grid*, 7(4):1846–1855, July 2016.

[48] J. M. Foster, G. Trevino, M. Kuss, and M. C. Caramanis. Plug-in electric vehicle and voltage support for distributed solar: theory and application. *IEEE Systems Journal*, 7(4):881–888, 2013.

[49] Y. Fraiji and et al. Cyber security issues of Internet of electric vehicles. In *2018 IEEE Wireless Communications and Networking Conference*.

[50] A. Gagarin and P. Corcoran. Multiple domination models for placement of electric vehicle charging stations in road networks. *Computers & Operations Research*, 96:69–79, 2018.

[51] S. Ghosh, M. S. El Moursi, E. El-Saadany, and K. Al Hosani. Online Coherency Based Adaptive Wide Area Damping Controller for Transient Stability Enhancement. *IEEE Transactions on Power Systems*, pages 1–1, 2019.

[52] R. Gottumukkala and et al. Cyber-physical System Security of Vehicle Charging Stations. In *2019 IEEE Green Technologies Conference*.

[53] S. Guo and H. Zhao. Optimal site selection of electric vehicle charging station by using fuzzy topsis based on sustainability perspective. *Applied Energy*, 158:390–402, 2015.

[54] O. Hafez and K. Bhattacharya. Optimal design of electric vehicle charging stations considering various energy resources. *Renewable energy*, 107:576–589, 2017.

[55] E. Hammad and et al. A Class of Switching Exploits Based on Inter-Area Oscillations. *IEEE Transactions on Smart Grid*, 9(5):4659–4668, Sep. 2018.

[56] H. Huang, C. Y. Chung, K. W. Chan, and H. Chen. Quasi-Monte Carlo Based Probabilistic Small Signal Stability Analysis for Power Systems With Plug-In

Electric Vehicle and Wind Power Integration. *IEEE Transactions on Power Systems*, 28(3):3335–3343, Aug 2013.

[57] C. Isidore. Tesla has a problem. maybe a big problem. Available at `https://money.cnn.com/2018/03/28/news/companies/tesla-model-3-cash-crunch/index.html`, March 2018.

[58] M. S. Islam, N. Mithulananthan, and K. Bhumkittipich. Feasibility of pv and battery energy storage based ev charging in different charging stations. In *2016 13th International Conference on Electrical Engineering/Electronics, Computer, Telecommunications and Information Technology (ECTI-CON)*, pages 1–6, June 2016.

[59] L. Jia, Z. Hu, Y. Song, and Z. Luo. Optimal siting and sizing of electric vehicle charging stations. In *Electric Vehicle Conference (IEVC), 2012 IEEE International*, pages 1–6. IEEE, 2012.

[60] L. Jia, Z. Hu, Y. Song, and Z. Luo. Optimal siting and sizing of electric vehicle charging stations. In *2012 IEEE International Electric Vehicle Conference*, pages 1–6. IEEE, 2012.

[61] J.-N. Juang and R. Pappa. An eigensystem realization algorithm for modal parameter identification and model reduction. *Journal of Guidance Control and Dynamics*, 8, 11 1985.

[62] M. E. Kabir, C. Assi, H. Alameddine, J. Antoun, and J. Yan. Demand aware deployment and expansion method for an electric vehicles fast charging network. In *2019 IEEE International Conference on Communications, Control, and Computing Technologies for Smart Grids (SmartGridComm)*, pages 1–7, 2019.

[63] M. E. Kabir, C. Assi, H. Alameddine, J. Antoun, and J. Yan. Demand-aware provisioning of electric vehicles fast charging infrastructure. *IEEE Transactions on Vehicular Technology*, 69(7):6952–6963, 2020.

[64] M. E. Kabir, C. Assi, M. H. K. Tushar, and J. Yan. Optimal scheduling of ev charging at a solar power-based charging station. *IEEE Systems Journal*, 14(3):4221–4231, 2020.

[65] M. E. Kabir, M. Ghafouri, B. Moussa, and C. Assi. Coordinated charging and discharging of electric vehicles: A new class of switching attacks. *IEEE Transactions on Industrial Informatics*, 2020 (under review).

[66] M. E. Kabir, M. Ghafouri, B. Moussa, and C. Assi. A two-stage protection method for detection and mitigation of coordinated evse switching attacks. *IEEE Transactions on Smart Grid*, 2021 (under review).

[67] M. E. Kabir, I. Sorkhoh, B. Moussa, and C. Assi. Routing and scheduling of mobile ev chargers for vehicle to vehicle (v2v) energy transfer. In *2020 IEEE Power Energy Society General Meeting (PESGM)*, pages 1–5, 2020.

[68] M. E. Kabir, I. Sorkhoh, B. Moussa, and C. Assi. Joint routing and scheduling of mobile charging infrastructure for v2v energy transfer. *IEEE Transactions on Intelligent Vehicles*, 2021 (accepted).

[69] M. N. Kabir, Y. Mishra, G. Ledwich, Z. Y. Dong, and K. P. Wong. Coordinated control of grid-connected photovoltaic reactive power and battery energy storage systems to improve the voltage profile of a residential distribution feeder. *IEEE Transactions on industrial Informatics*, 10(2):967–977, 2014.

[70] O. G. M. Khan, E. El-Saadany, A. Youssef, and M. Shaaban. Impact of Electric

Vehicles Botnets on the Power Grid. In *IEEE Canada Electrical Power and Energy Conference*, 2019.

[71] W. Khan, A. Ahmad, F. Ahmad, and M. Saad Alam. A comprehensive review of fast charging infrastructure for electric vehicles. *Smart Science*, 6(3):256–270, 2018.

[72] W. Khan, F. Ahmad, and M. S. Alam. Fast ev charging station integration with grid ensuring optimal and quality power exchange. *Engineering Science and Technology, an International Journal*, 22(1):143–152, 2019.

[73] M. Khodari and et al. Decentralized firmware attestation for in-vehicle networks. In *Proceedings of the 5th on Cyber-Physical System Security Workshop*, pages 47–56, 2019.

[74] M. E. Khodayar, L. Wu, M. Shahidehpour, et al. Hourly coordination of electric vehicle operation and volatile wind power generation in scuc. *IEEE Trans. Smart Grid*, 3(3):1271–1279, 2012.

[75] O. T. T. Kim, N. H. Tran, V. Nguyen, S. M. Kang, and C. S. Hong. Cooperative between v2c and v2v charging: Less range anxiety and more charged evs. In *Information Networking (ICOIN), 2018 International Conference on*, pages 679–683. IEEE, 2018.

[76] S. Kim, H. Jung, J. Hwang, S. Lee, and K. Song. A study on the construction of ev charging infrastructures in highway rest area. In *4th International Conference on Power Engineering, Energy and Electrical Drives*, pages 396–400, 2013.

[77] B. Kirby et al. Frequency control concerns in the north american electric power system. *Washington, DC, USA: U.S. Dept. Energy*, 2003.

[78] M. Klein, G. J. Rogers, and P. Kundur. A fundamental study of inter-area oscillations in power systems. *IEEE Transactions on power systems*, 6(3):914–921, 1991.

[79] L. Kojovic. Impact DG on voltage regulation. In *IEEE Power Engineering Society Summer Meeting,*, volume 1, pages 97–102. IEEE, 2002.

[80] P. Kong. Autonomous robot-like mobile chargers for electric vehicles at public parking facilities. *IEEE Transactions on Smart Grid*, pages 1–1, 2019.

[81] A.-M. Koufakis, E. S. Rigas, N. Bassiliades, and S. D. Ramchurn. Towards an optimal ev charging scheduling scheme with v2g and v2v energy transfer. In *Smart Grid Communications (SmartGridComm), 2016 IEEE International Conference on*, pages 302–307. IEEE, 2016.

[82] S. Krishnan. Vehicle to vehicle (v2v) charging: Ev as a power source, August 2018. Available at `https://getelectricvehicle.com/vehicle-to-vehicle-charging/`.

[83] R. Kumar, A. Jha, A. Damodaran, D. Bangwal, and A. Dwivedi. Addressing the challenges to electric vehicle adoption via sharing economy: an indian perspective. *Management of Environmental Quality: An International Journal*, 2020.

[84] E. Künle and C. Minke. Macro-environmental comparative analysis of e-mobility adoption pathways in france, germany and norway. *Transport Policy*, 2020.

[85] A. Y. S. Lam, Y. Leung, and X. Chu. Electric vehicle charging station placement: Formulation, complexity, and solutions. *IEEE Transactions on Smart Grid*, 5(6):2846–2856, Nov 2014.

[86] F. Lambert. Median electric car range increased by 56% over the last 6 years. *Electrek*, December 2017. Available at `https://electrek.co/2017/12/26/average-electric-car-range/`.

[87] F. Lambert. Chevy bolt ev sales are slumping in the us, gm says production going to canada and south korea. *electrek*, October 2018. Available at `https://electrek.co/2018/10/03/chevy-bolt-ev-sales-slumping-us/`.

[88] F. Lambert. As the covid-19 crisis hammers the auto industry, electric cars remain a bright spot, May 2020. Available at `https://www.iea.org/commentaries/as-the-covid-19-crisis-hammers-the-auto-industry-electric-cars-remain-a-bright-spot`.

[89] A. Łebkowski. Studies of energy consumption by a city bus powered by a hybrid energy storage system in variable road conditions. *Energies*, 12(5):951, 2019.

[90] R. M. Lee, M. J. Assante, and T. Conway. Analysis of the Cyber Attack on the Ukrainian Power Grid. *SANS ICS Report*, 2016.

[91] S. Lee, S. Iyengar, D. Irwin, and P. Shenoy. Shared solar-powered ev charging stations: Feasibility and benefits. In *Green and Sustainable Computing Conference (IGSC0¡ 2016 Seventh International*, pages 1–8. IEEE, 2016.

[92] G. Li, L. Boukhatem, L. Zhao, and J. Wu. Direct vehicle-to-vehicle charging strategy in vehicular ad-hoc networks. In *New Technologies, Mobility and Security (NTMS), 2018 9th IFIP International Conference on*, pages 1–5. IEEE, 2018.

[93] J. Lian and et al. Universal wide-area damping control for mitigating inter-area oscillations in power systems. Technical report, Pacific Northwest National Lab.(PNNL), Richland, WA (United States), 2017.

[94] G. Liang and et al. The 2015 ukraine blackout: Implications for false data injection attacks. *IEEE Transactions on Power Systems*, 32(4):3317–3318, 2016.

[95] C. Liu, K. Chau, D. Wu, and S. Gao. Opportunities and challenges of vehicle-to-home, vehicle-to-vehicle, and vehicle-to-grid technologies. *Proceedings of the IEEE*, 101(11):2409–2427, 2013.

[96] S. Liu and et al. A Framework for Modeling Cyber-Physical Switching Attacks in Smart Grid. *IEEE Transactions on Emerging Topics in Computing*, 1(2):273–285, Dec 2013.

[97] S. Liu, X. Feng, D. Kundur, T. Zourntos, and K. L. Butler-Purry. Switched system models for coordinated cyber-physical attack construction and simulation. In *2011 IEEE First International Workshop on Smart Grid Modeling and Simulation (SGMS)*, pages 49–54, Oct 2011.

[98] S. Liu, D. Kundur, T. Zourntos, and K. L. Butler-Purry. Coordinated variable structure switching attack in the presence of model error and state estimation. In *2012 IEEE Third International Conference on Smart Grid Communications (SmartGridComm)*, pages 318–323, Nov 2012.

[99] Z.-f. Liu, W. Zhang, X. Ji, and K. Li. Optimal planning of charging station for electric vehicle based on particle swarm optimization. In *Innovative Smart Grid Technologies-Asia (ISGT Asia), 2012 IEEE*, pages 1–5. IEEE, 2012.

[100] J. A. P. Lopes, F. J. Soares, and P. M. R. Almeida. Integration of electric vehicles in the electric power system. *Proceedings of the IEEE*, 99(1):168–183, 2011.

[101] E. Loveday. Plug-in vehicles to represent 3% of global automotive market by 2020; phev sales to easily outnumber sales of bevs in us. Available at `https:`

//insideevs.com/news/318120/plug-in-vehicles-to-represent-3-of-global-automotive-market-by-2020-phev-sales-to-easily-outnumber/.

[102] C. Luo, Y. F. Huang, and V. Gupta. Stochastic dynamic pricing for ev charging stations with renewables integration and energy storage. *IEEE Transactions on Smart Grid*, PP(99):1–1, 2017.

[103] S. Lv, Z. Wei, G. Sun, S. Chen, and H. Zang. Optimal power and semi-dynamic traffic flow in urban electrified transportation networks. *IEEE Transactions on Smart Grid*, pages 1–1, 2019.

[104] Maigha and M. L. Crow. Cost-constrained dynamic optimal electric vehicle charging. *IEEE Transactions on Sustainable Energy*, 8(2):716–724, April 2017.

[105] T. Mao, X. Zhang, and B. Zhou. Modeling and solving method for supporting 'vehicle-to-anything'ev charging mode. *Applied Sciences*, 8(7):1048, 2018.

[106] G. P. McCormick. Computability of global solutions to factorable nonconvex programs: Part i—convex underestimating problems. *Mathematical programming*, 10(1):147–175, 1976.

[107] S. Mehar and S. M. Senouci. An optimization location scheme for electric charging stations. *IEEE SaCoNet*, pages 1–5, 2013.

[108] Z. Miljanic, V. Radulovic, and B. Lutovac. Efficient placement of electric vehicles charging stations using integer linear programming. *Advances in Electrical and Computer Engineering*, 18(2):11–17, 2018.

[109] S. Mishra, X. Li, A. Kuhnle, M. T. Thai, and J. Seo. Rate alteration attacks in smart grid. In *2015 IEEE Conference on Computer Communications (INFOCOM)*, pages 2353–2361, April 2015.

[110] A. G. Morosan and et al. Ocpp security-neural network for detecting malicious traffic. In *Proceedings of the International Conference on Research in Adaptive and Convergent Systems*, pages 190–195, 2017.

[111] M. Nasr, K. Gupta, C. da Silva, C. H. Amon, and O. Trescases. Sic based on-board ev power-hub with high-efficiency dc transfer mode through ac port for vehicle-to-vehicle charging. In *Applied Power Electronics Conference and Exposition (APEC), 2018 IEEE*, pages 3398–3404. IEEE, 2018.

[112] Niclas. Solar charging station: types and applications, November 2016. Available at `https://sinovoltaics.com/technology/solar-charging-station-types-and-applications/`.

[113] D. Niyato, E. Hossain, and A. Fallahi. Sleep and wakeup strategies in solar-powered wireless sensor/mesh networks: Performance analysis and optimization. *IEEE Transactions on Mobile Computing*, 6(2):221–236, Feb 2007.

[114] J. Pontes. 30% plugin vehicle market share in the netherlands!, December 2020. Available at `https://cleantechnica.com/2020/12/19/30-plugin-vehicle-market-share-in-the-netherlands/`.

[115] H. Quebec. Electric vehicle charging stations technical installation guide, 2015.

[116] R. Rana and S. Mishra. Day-ahead scheduling of electric vehicles for overloading management in active distribution system via web-based application. *IEEE Systems Journal*, pages 1–11, 2018.

[117] B. Roberts, K. Akkaya, E. Bulut, and M. Kisacikoglu. An authentication framework for electric vehicle-to-electric vehicle charging applications. In *Mobile Ad Hoc and Sensor Systems (MASS), 2017 IEEE 14th International Conference on*, pages 565–569. IEEE, 2017.

[118] D. Ronanki, A. Kelkar, and S. S. Williamson. Extreme fast charging technology—prospects to enhance sustainable electric transportation. *Energies*, 12(19):3721, 2019.

[119] J. E. Rubio and et al. Addressing security in ocpp: Protection against man-in-the-middle attacks. In *2018 9th IFIP International Conference on New Technologies, Mobility and Security (NTMS)*.

[120] A. S. Safigianni and G. J. Salis. Optimum voltage regulator placement in a radial power distribution network. *IEEE Transactions on Power Systems*, 15(2):879–886, 2000.

[121] D. Said and H. T. Mouftah. Novel communication protocol for the ev charging/discharging service based on vanets. *IEEE Transactions on Intelligent Vehicles*, 2(1):25–37, 2017.

[122] D. Said and H. T. Mouftah. A novel electric vehicles charging/discharging management protocol based on queuing model. *IEEE Transactions on Intelligent Vehicles*, 5(1):100–111, 2020.

[123] E. Schmidt. Electric vehicles sales update q2 2018, canada, August 2018. Available at `https://www.fleetcarma.com/electric-vehicles-sales-update-q2-2018-canada/`.

[124] E. Schmidt. The key to increasing ev adoption is hidden in ev driving and charging data, January 2018. Available at `https://www.fleetcarma.com/key-increasing-ev-adoption-hidden-ev-driving-charging-data/`.

[125] J. B. SNYDER. Rivian confirms v2v charging, auxiliary batteries, June 2019. Available at `https://www.autoblog.com/2019/06/08/rivian-confirms-v2v-charging-auxiliary-batteries/`.

[126] P. Solar. In africa: Costs and markets. *International Renewable Energy Agency (IRENA) report*, 2016.

[127] M. M. Solomon and J. Desrosiers. Survey paper—time window constrained routing and scheduling problems. *Transportation science*, 22(1):1–13, 1988.

[128] S. Soltan, P. Mittal, and H. V. Poor. BlackIoT: IoT Botnet of high wattage devices can disrupt the power grid. In *27th {USENIX} Security Symposium ({USENIX} Security 18)*, pages 15–32, 2018.

[129] T. J. C. Sousa, V. Monteiro, J. C. A. Fernandes, C. Couto, A. A. N. Meléndez, and J. L. Afonso. New perspectives for vehicle-to-vehicle (v2v) power transfer. In *IECON 2018 - 44th Annual Conference of the IEEE Industrial Electronics Society*, pages 5183–5188, 2018.

[130] V. L. Statistics. Transport statistics bulletin, available online, 2008.

[131] T. Sweda and D. Klabjan. An agent-based decision support system for electric vehicle charging infrastructure deployment. In *Vehicle Power and Propulsion Conference (VPPC), 2011 IEEE*, pages 1–5. IEEE, 2011.

[132] S. Taghizadeh, P. Jamborsalamati, M. Hossain, and J. Lu. Design and implementation of an advanced vehicle-to-vehicle (v2v) power transfer operation using communications. In *2018 IEEE International Conference on Environment and Electrical Engineering and 2018 IEEE Industrial and Commercial Power Systems Europe (EEEIC/I&CPS Europe)*, pages 1–6. IEEE, 2018.

[133] Y. Tao, M. Huang, and L. Yang. Data-driven optimized layout of battery electric vehicle charging infrastructure. *Energy*, 150:735–744, 2018.

[134] H. C. Tijms and H. C. Tijms. *Stochastic models: an algorithmic approach*, volume 994. John Wiley & Sons Chichester, 1994.

[135] M. H. K. Tushar, C. Assi, M. Maier, and M. F. Uddin. Smart microgrids: Optimal joint scheduling for electric vehicles and home appliances. *IEEE Transactions on Smart Grid*, 5(1):239–250, Jan 2014.

[136] W. Tushar, W. Saad, H. V. Poor, and D. B. Smith. Economics of electric vehicle charging: A game theoretic approach. *IEEE Transactions on Smart Grid*, 3(4):1767–1778, Dec 2012.

[137] E. Ucer, R. Buckreus, M. C. Kisacikoglu, E. Bulut, M. Guven, Y. Sozer, and L. Giubbolini. A flexible v2v charger as a new layer of vehicle-grid integration framework. In *2019 IEEE Transportation Electrification Conference and Expo (ITEC)*, pages 1–7. IEEE, 2019.

[138] E. Ucer, I. Koyuncu, M. C. Kisacikoglu, M. Yavuz, A. Meintz, and C. Rames. Modeling and analysis of a fast charging station and evaluation of service quality for electric vehicles. *IEEE Transactions on Transportation Electrification*, 5(1):215–225, 2019.

[139] B. Vaidya and et al. Deployment of secure ev charging system using open charge point protocol. In *2018 14th International Wireless Communications Mobile Computing Conference (IWCMC)*.

[140] F. van Gool. Lower semicontinous functions with values in a continous lattice. *Comment, Math, Univ, Carolin*, 33(3):505–523, 1992.

[141] A. B. van Groenou, H. Lovell, and E. Franklin. Household decision-making for home batteries.

[142] V. Venkatasubramanian and et al. Analysis of 1996 western american electric blackouts. *Bulk Power System Dynamics and Control-VI, Cortina d'Ampezzo, Italy*, pages 22–27, 2004.

[143] G. Wang, Z. Xu, F. Wen, and K. P. Wong. Traffic-constrained multiobjective planning of electric-vehicle charging stations. *IEEE Transactions on Power Delivery*, 28(4):2363–2372, 2013.

[144] H. Wang, Q. Huang, C. Zhang, and A. Xia. A novel approach for the layout of electric vehicle charging station. In *Apperceiving Computing and Intelligence Analysis (ICACIA), 2010 International Conference on*, pages 64–70. IEEE, 2010.

[145] M. Wang, M. Ismail, X. Shen, E. Serpedin, and K. Qaraqe. Spatial and temporal online charging/discharging coordination for mobile pevs. *IEEE Wireless Communications*, 22(1):112–121, February 2015.

[146] M. Wang, M. Ismail, R. Zhang, X. Shen, E. Serpedin, and K. Qaraqe. Spatio-temporal coordinated v2v fast charging strategy for mobile gevs via price control. *IEEE Transactions on Smart Grid*, PP(99):1–1, 2017.

[147] M. Wang, M. Ismail, R. Zhang, X. Shen, E. Serpedin, and K. Qaraqe. Spatio-temporal coordinated v2v energy swapping strategy for mobile pevs. *IEEE Transactions on Smart Grid*, 9(3):1566–1579, 2018.

[148] M. Wang, M. Ismail, R. Zhang, X. S. Shen, E. Serpedin, and K. Qaraqe. A semi-distributed v2v fast charging strategy based on price control. In *Global Communications Conference (GLOBECOM), 2014 IEEE*, pages 4550–4555. IEEE, 2014.

[149] M. Wang, H. Liang, R. Zhang, R. Deng, and X. Shen. Mobility-aware coordinated charging for electric vehicles in vanet-enhanced smart grid. *IEEE Journal on Selected Areas in Communications*, 32(7):1344–1360, July 2014.

[150] M. Wang and H. Wang. Deployment of plug-in electric vehicles in china and the usa: issues and opportunities, foreword. *Mitigation and Adaptation Strategies for Global Change*, 25:285–288, 2020.

[151] Q. Wang, X. Liu, J. Du, and F. Kong. Smart Charging for Electric Vehicles: A Survey From the Algorithmic Perspective. *IEEE Communications Surveys Tutorials*, 18(2):1500–1517, Secondquarter 2016.

[152] Y. Wang, Z. Su, N. Zhang, and A. Benslimane. Sweet: Secure wireless energy transfer with electric vehicles in vehicular energy networks. In *2020 IEEE Conference on Communications and Network Security (CNS)*, pages 1–9. IEEE, 2020.

[153] Z. Wang and S. Wang. Grid power peak shaving and valley filling using vehicle-to-grid systems. *IEEE Transactions on power delivery*, 28(3):1822–1829, 2013.

[154] Z. Wei, Y. Li, and L. Cai. Electric vehicle charging scheme for a park-and-charge system considering battery degradation costs. *IEEE Transactions on Intelligent Vehicles*, 3(3), Sept 2018.

[155] Z. Wei, Y. Li, Y. Zhang, and L. Cai. Intelligent parking garage ev charging scheduling considering battery charging characteristic. *IEEE Transactions on Industrial Electronics*, 65(3), March 2018.

[156] F. Wilches-Bernal, R. H. Byrne, and J. Lian. Damping of Inter-Area Oscillations via Modulation of Aggregated Loads. *IEEE Transactions on Power Systems*, pages 1–1, 2019.

[157] D. Wu, H. Zeng, C. Lu, and B. Boulet. Two-stage energy management for office buildings with workplace ev charging and renewable energy. *IEEE Transactions on Transportation Electrification*, 3(1):225–237, March 2017.

[158] X. Xi, R. Sioshansi, and V. Marano. Simulation–optimization model for location of a public electric vehicle charging infrastructure. *Transportation Research Part D: Transport and Environment*, 22, 2013.

[159] T. Xia, Y. Zhang, L. Chen, Z. Yuan, P. N. Markham, Y. Ye, and Y. Liu. Phase angle-based power system inter-area oscillation detection and modal analysis. *European Transactions on Electrical Power*, 21(4):1629–1639, 2011.

[160] Y. Xiang, J. Liu, R. Li, F. Li, C. Gu, and S. Tang. Economic planning of electric vehicle charging stations considering traffic constraints and load profile templates. *Applied Energy*, 178:647–659, 2016.

[161] Q. Yan, I. Manickam, M. Kezunovic, and L. Xie. A multi-tiered real-time pricing algorithm for electric vehicle charging stations. In *2014 IEEE Transportation Electrification Conference and Expo (ITEC)*, pages 1–6, June 2014.

[162] Y. Yang, Q. S. Jia, G. Deconinck, X. Guan, Z. Qiu, and Z. Hu. Distributed coordination of ev charging with renewable energy in a microgrid of buildings. *IEEE Transactions on Smart Grid*, PP(99):1–1, 2017.

[163] B. Ye, J. Jiang, L. Miao, P. Yang, J. Li, and B. Shen. Feasibility study of a solar-powered electric vehicle charging station model. *Energies*, 8(11):13265–13283, 2015.

[164] H.-G. Yeh, D. F. Gayme, and S. H. Low. Adaptive var control for distribution circuits with photovoltaic generators. *IEEE Transactions on Power Systems*, 27(3):1656–1663, 2012.

[165] P. You and Z. Yang. Efficient optimal scheduling of charging station with multiple electric vehicles via v2v. In *Smart Grid Communications (SmartGridComm), 2014 IEEE International Conference on*, pages 716–721. IEEE, 2014.

[166] P. You, Z. Yang, M.-Y. Chow, and Y. Sun. Optimal cooperative charging strategy for a smart charging station of electric vehicles. *IEEE Trans. Power Syst*, 31(4):2946–2956, 2016.

[167] K. Young, C. Wang, L. Y. Wang, and K. Strunz. Electric vehicle battery technologies. In *Electric vehicle integration into modern power networks*, pages 15–56. Springer, 2013.

[168] H. Yu, J. Chen, and C. Sun. *N-Person Noncooperative Game with Infinite Strategic Space*, pages 77–84. Springer Berlin Heidelberg, Berlin, Heidelberg, 2005.

[169] L. Zhang and et al. A two-stage deep learning approach for can intrusion detection. In *Proc. Ground Vehicle Syst. Eng. Technol. Symp.(GVSETS)*, pages 1–11, 2018.

[170] R. Zhang, X. Cheng, and L. Yang. Flexible energy management protocol for cooperative ev-to-ev charging. *IEEE Transactions on Intelligent Transportation Systems*, 2018.

[171] Y. Zhang and L. Cai. Dynamic charging scheduling for ev parking lots with photovoltaic power system. *IEEE Access*, 6:56995–57005, 2018.

[172] G. Zhou, X. Ou, and X. Zhang. Development of electric vehicles use in china: A study from the perspective of life-cycle energy consumption and greenhouse gas emissions. *Energy Policy*, 59:875–884, 2013.

[173] H. Zhou, W. Xu, Y. Bi, J. Chen, Q. Yu, and X. S. Shen. Toward 5g spectrum sharing for immersive-experience-driven vehicular communications. *IEEE Wireless Communications*, 24(6):30–37, Dec 2017.

[174] Y. Zhou, D. Yau, P. You, and P. Cheng. Optimal-cost scheduling of electrical vehicle charging under uncertainty. *IEEE Transactions on Smart Grid*, PP(99):1–1, 2017.

[175] L. Zhu, F. R. Yu, B. Ning, and T. Tang. Stochastic charging management for plug-in electric vehicles in smart microgrids fueled by renewable energy sources. In *2011 IEEE Online Conference on Green Communications*, pages 7–12. IEEE, 2011.

Appendix A

Appendix

Linearization:

The linearized form of Eq. (5.9) is as follows:

$$\sum_{o}(\Lambda_{vv't}^{o(o-1)} + \Gamma_{vv't}^{o(o-1)}\frac{E_{v'}}{\zeta} + \Lambda_{vv't}^{o(o-1)}\tau_{vv'}^{t}) \leq \tau_v; \forall v, v', t \tag{A.1a}$$

$$\Lambda_{vv't}^{o(o-1)} \leq \Delta_{v'}\Gamma_{vv't}^{o(o-1)}; \forall v, v', o, t \tag{A.1b}$$

$$\Lambda_{vv't}^{o(o-1)} \leq \tau_{v'}; \forall v, v', o, t \tag{A.1c}$$

$$\Lambda_{vv't}^{o(o-1)} \geq \tau_{v'} - \Delta_{v'}(1 - \Gamma_{vv't}^{o(o-1)}); \forall v, v', o, t \tag{A.1d}$$

$$\Lambda_{vv't}^{o(o-1)} \geq 0; \forall v, v', o, t \tag{A.1e}$$

$$\Gamma_{vv't}^{o(o-1)} \leq \gamma_{vto}; \forall v, v', o, t \tag{A.1f}$$

$$\Gamma_{vv't}^{o(o-1)} \leq \gamma_{v't(o-1)}; \forall v, v', o, t \tag{A.1g}$$

$$\Gamma_{vv't}^{o(o-1)} \geq \gamma_{vto} + \gamma_{v't(o-1)} - 1; \forall v, v', o, t \tag{A.1h}$$

Eqs. (A.1f) - (A.1h) also can be utilized to linearize Eq. (5.11).

Reduced cost function:

To calculate the reduced cost function for any EV v, Φ_{vto}, Ψ_v and Θ_v are calculated as follows:

$$\begin{aligned}\Phi_{vto} = \sum_{|v|\geq o\geq 2,t} \alpha_{ot}\gamma_{vto} - \sum_{|v|-1\geq o\geq 1,t} \alpha_{ot}\gamma_{vto} + \sum_{g_3} \beta_g^{20f}\gamma_{vto} \\ + \sum_{g_4} \beta_g^{20g}\gamma_{v'to} - \sum_{g_3} \beta_g^{20h}\gamma_{vto} + \sum_t E_v\phi_t \sum_o \gamma_{vto} + \\ \sum_t \omega_t\tau_{dv}^t\gamma_{vt1} + \sum_t \omega_t\tau_{v't}^t\gamma_{v'to}; \forall v\end{aligned} \tag{A.2}$$

$$\Psi_v = \sum_{g_4} \beta_g^{20d}\tau_{v'} - \sum_{g_4} \beta_g^{20c}\tau_{v'}; \forall v \tag{A.3}$$

$$\Theta_v = \sum_{s\in S_v} \sigma_s; \forall v \tag{A.4}$$

$G = \{g = (o, t, v, v') : v, v' \in V, v \neq v', t \in T, o \geq 2\}$ represents the subscript of the variables of the linearized constraints and their subsequent dual variables. And β_g^{20c}, β_g^{20d}, β_g^{20f},β_g^{20g} and β_g^{20h} are the dual values come from constraints (A.1c), (A.1d), (A1.f), (A1.g) and (A1.h) respectively.